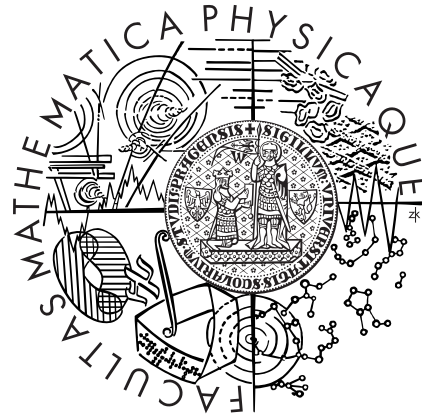


Charles University in Prague
Faculty of Mathematics and Physics

DOCTORAL THESIS



Martin Lanzendörfer

**Flows of incompressible fluids with pressure-dependent viscosity
(and their application to modelling the flow in journal bearing)**

Mathematical Institute of Charles University

Supervisor of the doctoral thesis: prof. RNDr. Josef Málek, DSc.

Study programme: Physics

Specialization: Mathematical and Computer Modelling

Prague, 2011

My deepest gratitude goes to precious teachers.

I would like to express my thanks to my supervisor, Josef Málek, for all his guidance and support and, in particular, for the encouragement, inspiration and enthusiasm he passes on to all his students. My gratitude belongs to Jaroslav Hron, among others for the way he implemented his software and for his constant readiness to give advice. My co-authors, Jan Stebel and Adrian Hirn, are greatly acknowledged.

I greatly appreciate the opportunity to be a part of two groups with many friendly people and the most pleasant and relaxed atmosphere, the group of Mathematical modeling in the Mathematical Institute of Charles University and the Department of Computational Methods in the Institute of Computer Science. My thanks belongs in particular to Milan Pokorný, Miroslav Rozložník, Zdeněk Strakoš and Miroslav Tůma. My special thanks go to the dear ladies in the Library of ICS and to Hanka Bílková.

*To those who can benefit.
To my dear Ema.*

I declare that I carried out this doctoral thesis independently, and only with the cited sources, literature and other professional sources.

I understand that my work relates to the rights and obligations under the Act No. 121/2000 Coll., the Copyright Act, as amended, in particular the fact that the Charles University of Prague has the right to conclude a license agreement on the use of this work as a school work pursuant to Section 60 paragraph 1 of the Copyright Act.

In Prague, May 2, 2011.

Název práce: Proudění nestlačitelných tekutin s viskozitou závislou na tlaku
(a jejich aplikace při modelování proudění v ložisku)

Autor: Martin Lanzendörfer

Pracoviště: Matematický ústav Univerzity Karlovy

Školitel: prof. RNDr. Josef Málek, DSc.

Abstrakt: Viskozita tekutin při hydrodynamickém mazání zpravidla závisí na tlaku a rychlosti smyku. Práce se zabývá ustáleným izotermálním prouděním právě takových tekutin. Naváže na nedávné výsledky dosažené pro případ homogenních Dirichletových okrajových podmínek a ukáže existenci a jednoznačnost slabého řešení pro okrajové podmínky používané v praktických aplikacích. Druhá část je pak věnována numerickým simulacím. Experimenty naznačí úspěšnost použité metody konečných prvků dokud konstitutivní model splňuje jistá omezení. Jak omezení potřebná v teoretických výsledcích, tak ta naznačovaná numerickými experimenty umožňují používat přesné modely maziv v jistém rozsahu tlaku a rychlosti smyku. Poslední část práce charakterizuje tento rozsah v případě třech typických reprezentantů maziv.

Klíčová slova: existence a jednoznačnost slabého řešení, metoda konečných prvků, viskozita závislá na tlaku a rychlosti smyku, nestlačitelné tekutiny, hydrodynamické mazání

Title: Flows of incompressible fluids with pressure-dependent viscosity
(and their application to modelling the flow in journal bearing)

Author: Martin Lanzendörfer

Department: Mathematical Institute of Charles University

Supervisor: prof. RNDr. Josef Málek, DSc.

Abstract: The viscosity of the fluids involved in hydrodynamic lubrication typically depends on pressure and shear rate. The thesis is concerned with steady isothermal flows of such fluids. Generalizing the recent results achieved in the case of homogeneous Dirichlet boundary conditions, the existence and uniqueness of weak solutions subject to the boundary conditions employed in practical applications will be established. The second part is concerned with numerical simulations of the lubrication flow. The experiments indicate that the presented finite element method is successful as long as certain restrictions on the constitutive model are met. Both the restrictions involved in the theoretical results and those indicated by the numerical experiments allow to accurately model real-world lubricants in certain ranges of pressures and shear rates. The last part quantifies those ranges for three representative lubricants.

Keywords: existence and uniqueness of weak solutions, finite element method, pressure-thickening, shear-thinning, incompressible fluids, hydrodynamic lubrication

Contents

1	Introduction	1
1.1	Some open problems in hydrodynamic lubrication	2
1.2	Governing equations	8
1.3	Constitutive equations	9
1.4	Boundary conditions	15
2	Well-posedness of the mathematical problem	19
2.1	Definition of the problem	20
2.2	Central features and discrete approximation	25
2.3	Well-posedness results	31
2.4	Auxiliary tools	38
3	Numerical method	40
3.1	Description of the numerical method	41
3.2	Observed behavior of the numerical method	42
3.3	Condition (A4) seems to determine the numerical stability	43
4	Numerical simulations	47
4.1	Planar Poiseuille flow	48
4.2	Sliding converging surfaces	49
4.3	Planar steady flow in journal bearing	56
5	Relation between the assumed and real-world rheologies	72
5.1	Relevance of conditions (A1) – (A3) for the reference lubricants	74
5.2	“Well-posed” constitutive model approximation	75
5.3	Relevance of condition (A4) for the reference lubricants	80
6	Conclusion	87
	Bibliography	89

Notation

\mathbb{N}, \mathbb{R}	set of all positive integers, all real numbers
\mathbb{R}^d	Euclidean space of dimension d
$\mathbb{R}_{sym}^{d \times d}$	space of real (symmetric) square matrices
$\mathbf{y} \cdot \mathbf{z}$	the scalar-product of vectors $\mathbf{y}, \mathbf{z} \in \mathbb{R}^d$
$\mathbf{P} : \mathbf{Q}$	$= \sum_{i,j=1}^d P_{ij} Q_{ij}$, the scalar-product of tensors, $\mathbf{P}, \mathbf{Q} \in \mathbb{R}^{d \times d}$
$ \mathbf{Q} $	$= \sqrt{\mathbf{Q} : \mathbf{Q}}$
$\Omega \subset \mathbb{R}^d$	bounded domain in \mathbb{R}^d
$\partial\Omega \in \mathcal{C}^{0,1}$	its boundary, which is Lipschitz continuous
\mathbf{n}	a unit outward normal vector to $\partial\Omega$
\mathbf{y}_τ	$= \mathbf{y} - (\mathbf{y} \cdot \mathbf{n})\mathbf{n}$, the tangential part of vector \mathbf{y} on $\partial\Omega$
$ \Omega $	d -dimensional Lebesgue measure of $\Omega \subset \mathbb{R}^d$
$ \Gamma $	$(d-1)$ -dimensional measure of $\Gamma \subset \partial\Omega$, $\Omega \subset \mathbb{R}^d$
$L^p(\Omega), \ \cdot\ _p$	space of Lebesgue integrable functions in Ω , $p \in \langle 1, \infty \rangle$
$W^{k,p}(\Omega), \ \cdot\ _{k,p}$	standard Sobolev space
\mathbf{X}	$= X^d = X \times \cdots \times X$, for a function space X
$(\xi, \eta)_\Omega$	$= \int_\Omega \xi \eta \, d\mathbf{x}$
$(\mathbf{S}, \mathbf{D})_\Omega$	$= \int_\Omega \mathbf{S} : \mathbf{D} \, d\mathbf{x}$
$\langle \mathbf{b}, \mathbf{w} \rangle_\Gamma$	$= \int_\Gamma \mathbf{b} \cdot \mathbf{w} \, d\mathbf{x}$
$\langle \mathbf{f}, \mathbf{w} \rangle$	$= \langle \mathbf{f}, \mathbf{w} \rangle_{\mathbf{W}^{1,r}(\Omega)^*, \mathbf{W}^{1,r}(\Omega)}$
$\mathcal{X}^{r,\gamma}, \mathcal{Q}^r$	are defined on page 23
$\overline{\mathcal{X}}^{r,\gamma}, \overline{\mathcal{Q}}_{\Omega^*}^r$	defined on page 26
$\mathcal{X}_h^{r,\gamma}, \mathcal{Q}_h^r$	defined on page 29
$\ \cdot\ _{(r,\gamma)}$	$= \max\{\ \cdot\ _{1,r}, \ \cdot\ _{\gamma;\Gamma}\}$, see page 23
$\overline{C}_{\text{div}}(s), C_{\text{div}}(s, \nu), C_{\text{reg}}(s)$	defined on page 26, see also (2.13)
$\beta_{\Omega^*}(s, \nu), \beta(s, \nu)$	see (2.14)–(2.17)
$\tilde{\beta}_{\Omega}(s, \nu), \tilde{\beta}(s, \nu)$	see $(\mathbf{IS}_{\Omega}^{s,\nu})$ and $(\mathbf{IS}^{s,\nu})$ on page 30, see also (2.22)

Chapter 1

Introduction

Contents

1.1	Some open problems in hydrodynamic lubrication	2
1.1.1	Journal bearings	5
1.1.2	Features neglected	7
1.2	Governing equations	8
1.3	Constitutive equations	9
1.3.1	On the (in)compressibility	10
1.3.2	On the viscosity dependence on pressure	11
1.3.3	On the viscosity dependence on shear rate	13
1.3.4	Three reference lubricants characterization	14
1.4	Boundary conditions	15
1.4.1	The fluid–solid interface	15
1.4.2	The requirement to determine the level of pressure	16
1.4.3	Permeable interfaces, artificial boundaries	17

1.1 Some open problems in hydrodynamic lubrication

The age of all kinds of powered machinery started with the Industrial Revolution about two centuries ago, and it is not yet to pass away. By every movement in any machine a part of the consumed energy is wasted due to the relative motion of its solid components, being dissipated partly to the generated heat and vibrations and partly to the degradation of the solid surfaces. The very purpose of lubrication is to reduce the friction and wear by introducing a fluid medium in between the solid surfaces. The most desirable kind of lubrication is *thick-film* lubrication, where the surfaces are completely separated by the fluid film, the friction is minimal and there is no wear. In *hydrodynamic lubrication* the fluid film is generated and maintained by the relative motion of the surfaces and due to viscous drag.

To understand the basic operation, consider an incompressible fluid introduced in between (infinite) parallel rigid plates. The distance between the plates is h and one of them is sliding relative to the other with the velocity V . The fluid adheres to the solid surfaces and no external pressure gradient is imposed. Thus, a simple shear flow is generated, with the flow rate $Q = Vh/2$ and no pressure gradient. Once the surfaces are not parallel but slightly inclined towards one another, so that h is decreasing in the direction of the sliding, such simple shear flow is not possible, because Q is constant due to the principle of mass conservation, while h varies. The incompressibility constraint then induces a pressure flow adding to the shear flow where h is small and lessening it where h is large. Thus, a positive (in case of converging surfaces) pressure peak is generated, which allows the fluid film separating the surfaces to bear a considerable load.

In contrast to the simple shear flow, the flow involved in hydrodynamic lubrication is more complex. The resulting flow rate and the pressure and velocity profiles depend on various additional parameters, in particular on material properties of the fluid. The generated flow is essential for the operational properties of the hydrodynamical bearings. The ability of the mathematical models and numerical results to provide reliable predictions is of great importance to engineering decisions. Despite the tremendous progress during the past decades, this ability and understanding is not complete^a.

The processes involved in lubrication have been studied for centuries, and the lubricants, the surfaces, the geometries and the mechanics involved have been developed and optimized. This thesis will not attempt to give a complete survey of what has been achieved in the field. The reader can find the essentials and further references in many up-to-date books; to select one we refer to Szeri (1998). Instead, we will concentrate on some of the questions left open. Recent achievements in the mathematical theory allow us to revisit some fundamental issues while the growing availability of computer power draws our attention to new questions.

The foundations of the theoretical treatment of lubrication have been laid already by Rayleigh and Stokes, and in particular by the excellent work by Reynolds (1886). Let us briefly survey the basic chain of assumptions involved in deriving the standard Reynolds equation (see Rajagopal and Szeri, 2003; Szeri, 1998, for more details). Starting from the principles of continuum mechanics, the conservation of mass and balances of linear and angular momenta, one assumes that the Cauchy stress tensor of a compressible homogeneous fluid depends only on

^a "...there has been relatively little progress since the classic Newtonian film thickness solutions toward relating film thickness and traction to the properties of individual liquid lubricants and it is not clear at this time that full numerical solutions can even be obtained for heavily loaded contacts using accurate models." (Bair and Gordon, 2006)

the density and the velocity gradient. The requirement of frame indifference then implies that the dependence on the velocity gradient can be only through its symmetric part, while the isotropy and the assumption that the stress be linear in the velocity gradient leads to the compressible Navier–Stokes model. Assuming that the fluid is incompressible (and consequently the unspecified spherical stress enters the framework) and that the viscosity is constant, one obtains the incompressible Navier–Stokes equations. Assuming that the body forces and the inertial forces are negligible, and comprising further that the lubrication flow takes place in a thin film between almost parallel surfaces, one concludes that the pressures can be treated as being constant across the film, and the velocities as being parallel to the surfaces. By integrating the equations across the film one arrives to a single equation for the pressure: the Reynolds equation.

While the above assumptions are reasonable for a large class of applications, outside this class they could lead to serious discrepancy. In particular, this thesis will be concerned with the instance where the pressures generated in the lubrication flow exceed the range where the viscosity can be considered independent of the pressure. This case is essential for—but not restricted to—*elastohydrodynamic lubrication*, where the pressures are extremely high and the viscosity can increase by several orders of magnitude. (For simplicity, though, we will address rather the *rigid–piezoviscous regime* (see Szeri, 1998), occurring in applications that exhibit pressures high enough to effectively change the lubricant’s viscosity from its inlet value, yet not so high as to initiate significant elastic deformation in the bearing material.) Similarly, the viscosity can decrease once the shear rate is large enough, whereas the limit where the shear-thinning appears can be rather small for some technologically important fluids, or rather high for other lubricants. The fluid properties under consideration will be specified in Section 1.3 in more detail.

Once the dependence of the viscosity on the pressure is taken into account, several other attributes of the above procedure have to be reconsidered as well. We will stick to the assumption that the fluid is incompressible, which can be justified even under extreme pressures, since the density of the liquids under consideration varies only slightly. However, an interesting question concerning the derivation of the governing equations from the principles of continuum mechanics appears: whether the viscosity of an incompressible fluid can depend on the pressure; in Section 1.2, we merely refer to a recent discussion by Málek and Rajagopal on this topic.

Having formulated a consistent constitutive relation, the subsequent important question is concerned with the mathematical self-consistency of the resulting system of equations and with suitable choices of boundary conditions. The existence of weak solutions for certain subclass of the considered fluids has been established only recently. For steady flows, which we will be concerned with, the first existence result has been formulated by Franta et al. (2005) for the case of homogeneous Dirichlet boundary conditions. The main results of our study, presented in Chapter 2, incorporate the boundary conditions applicable to lubrication flow problems (see Section 1.4). In this text we neglect the inertia of the fluid, such that we can focus more on the issues related to the constitutive relation; however, the results presented has been achieved with the convective term included, see Lanzendörfer (2009); Lanzendörfer and Stebel (2011a,b).

There is one particular distinction of piezoviscous models that is related to the level of pressure in the flow. In the case that the Dirichlet boundary conditions are prescribed on the entire boundary, the solution of the system is not determined unless an additional condition on the

pressure is given. As long as the viscosity is independent of the pressure, only the gradient of pressure is present in the governing equations and the pressure field is determined up to a constant: one can shift the pressure solution arbitrarily without otherwise affecting the solution. However, once the viscosity depends on the pressure, the pressure level affects the whole solution and has to be determined by an additional constraint (see Section 1.4 and Chapter 2). We will show^b that the boundary conditions allowing for free inflow and outflow while prescribing the traction determine the pressure level.

While in the case of a Newtonian fluid the assumption of the flow being in a thin film between almost parallel surfaces (together with neglecting the body and inertial forces) has led to the conclusion that the pressure can be treated as being constant across the film and allowed to derive the Reynolds equation, one has to be careful once the viscosity depends on the pressure. Rajagopal and Szeri (2003) have pointed out that the pressure dependence of viscosity in the derivation of the governing equations for EHL cannot be only recognized *a posteriori*, i.e., after the Reynolds equation has been stated under the assumption of constant viscosity. If, instead, the equation is derived consistently by taking into account the pressure dependence of the viscosity from the outset, then one has to involve additional simplifying assumptions and derives a modified Reynolds equation with an additional term present. In particular, once the viscosity varies rapidly with the pressure, it is no more obvious during the process whether the assumption of the pressure being constant across the field remains valid. Presumably, the full numerical simulation of such flows could shed some light upon this uncertainty. In general, full numerical simulations of lubrication flow, using accurate constitutive relations, may be of great aid to the validation of the (modified) Reynolds equations when non-Newtonian lubricants are involved.

In Chapters 3 and 4, we will employ a numerical approach based on the finite element discretization (in two space dimensions) successfully used for flow problems with different kinds of generalized Navier–Stokes models (and for other problems). It will allow us to illustrate the basic features of some steady flows, including the flow between converging surfaces or in the journal bearing. In particular, the possible sensitivity of the major characteristics on the pressure level (and on the related boundary conditions) will be demonstrated. The significant departures of the flow features when compared to the Newtonian fluid will be apparent.

We emphasize that the currently available theoretical framework allows to establish the mathematical well-posedness only for certain subclass of fluids under consideration. Strictly speaking, the current theory does *not* cover the constitutive relations of pressure-thickening fluids within the entire range of pressures where the experimental data from physical measurements are available. Once the derivative of the viscous stress tensor with respect to the pressure exceeds a certain bound, the governing equations lose their elliptic structure and there have been no theoretical results beyond that limit so far. One of the aims of the thesis is to examine the behavior of the numerical simulations in this respect. The observations are summarized in Chapter 3. No change in the behavior of the numerical solutions or of the numerical method has been found, which could be related directly to the theoretical assumptions of Chapter 2. However, (as expected) once the variations of the viscosity with pressure are large enough, the numerical method fails. A reasonably tight relation of the failure to a condition on the derivative of the viscous stress with respect to pressure has been identified. The condition found by numerical experiments seems identical to the assumption required for the pressure field to be uniquely determined by the velocity field.

^b The result concerning the existence and uniqueness of a weak solution subject to such boundary conditions has been a joint work with J. Stebel.

Qualitatively, the limitations of the mathematical theory with respect to the real-world relations between the viscosity and the pressure have been obvious by the very establishment of the first results. Examples of the viscosity formulae fulfilling the theoretical assumptions have been provided, showing that the realistic lubricants can be approximated in some range of pressures and shear rates. It has not been clear quantitatively, however, how large the ranges of parameters in question can be. We do not provide a systematic study on this matter; in Chapter 5 we examine only the three reference lubricants presented by Bair (2006) and we specify the ranges of pressures and shear rates where the well-posedness has been proved, and the ranges (somewhat larger), where successful numerical solution might be expected (based on our experience).

Note that the results presented in the thesis concern the flow of an incompressible homogeneous pressure-thickening and shear-thinning fluid in general, and they are not restricted to the lubrication problems only. Such fluid models may be applied also in other scientific areas, for example in the modeling of the Earth's mantle, glaciers or avalanches.

1.1.1 Journal bearings

Among the many mechanisms based on hydrodynamic lubrication, we will illustrate the presented ideas on a simple model of the flow in a journal bearing. We will not discuss any details or particular engineering aspects, our goal is merely to motivate the more general issues by a practical example. Note that we will stay far from the full complexity of the journal bearing lubrication problem; see the next subsection for a list of the most important features excluded from our consideration.

The journal bearing, in the simple form we are going to look at, consists of two cylinders of parallel eccentric axes, the outer cylinder (the bearing) being held steady while the inner (the journal) rotates about its own axis. The lubricant is introduced into the gap between the surfaces and is driven by the journal rotation and the viscous drag to a shearing flow. Since the distance between the surfaces is (due to the eccentricity) not uniform, a pressure profile is induced and a reaction force is generated, allowing the rotating journal to sustain certain load while the solid surfaces are separated by the fluid film.

A three-dimensional setting is illustrated in Figure 1.1a. The bearing can be immersed in a lubricant pool or exposed to open air, for example. One usually assumes that the lubricant is subject to an ambient pressure at the bearing ends; note in particular that some inflow and outflow of the lubricant may occur. Various techniques are used to supply the lubricant in between the surfaces and avoid draining of the bearing, supply channels in the bearing body being one example, as indicated in Figure 1.1b. The body of the bearing and/or the journal can also be made of a porous material (see Figure 1.1c), which leads to a complex flow problem involving the lubrication flow, the flow in the porous media and at their interface. Note that in all the above mentioned settings, the inflow/outflow through (a part of) the domain boundary is naturally present in the problem, see Subsection 1.4.3 for further discussion of the boundary conditions.

Steady flow. In this thesis, we confine ourselves to studying steady flows in a fixed geometry; which in this context means within the geometry with a prescribed position of the journal axis. In real world, the rotating journal (when working in the hydrodynamic regime) "floats" in the

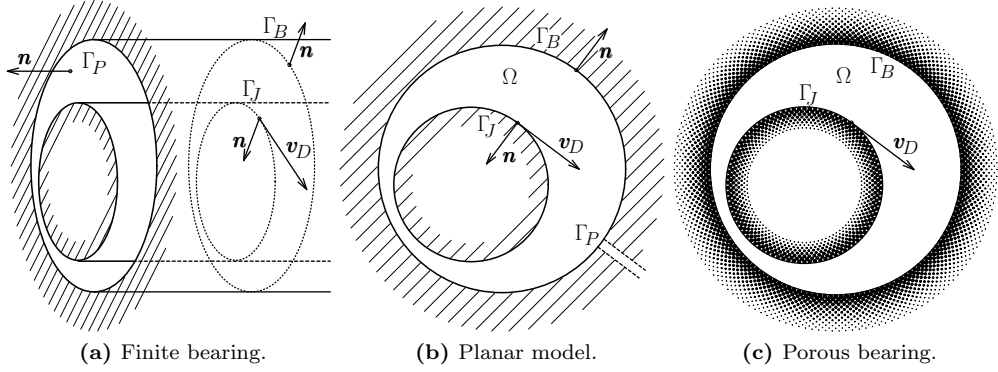


Figure 1.1: Three examples of the journal bearing problem setting.

lubricant, being actuated by the resultant of applied load and of the forces due to the lubricant flow. Assuming that the motion of the journal axis is slow compared to the rotation speed, one can interpret the steady flow problem as a quasi-steady approximation to the unsteady flow at certain time and position of the journal axis. In particular, if the applied load is constant in time, the journal axis can eventually reach a steady state, where the applied load is in balance with the force exerted by the fluid. Note that such a stable equilibrium may or may not be reached; for example, it is well-documented in the literature (e.g., see Brindley et al., 1983; Li et al., 2000b) that under the assumptions of full-film and constant viscosity lubricant, the journal exhibits a half-speed whirl: the trajectory of the journal spirals towards the bearing while the angular velocity of its path approaches $\omega/2$, where ω denotes the angular velocity of the journal rotation. On the other hand, steady equilibria can be reached if cavitation and/or pressure-dependent viscosity is present in the model (see Gwynllwy et al., 1996b). We will not address questions of the dynamical behavior of the journal bearing system in this thesis.

Planar flow. If the bearing is “infinitely” long, there is no pressure relief in the axial direction. Axial flow is therefore absent and changes in shear flow must be balanced by changes in circumferential pressure flow alone. The same conditions apply in first approximation to finite bearings of sufficient length, leading to the *long-bearing* approximation (see Szeri, 1998), usually applied if the length/diameter ratio $L/D > 2$. We remark that the aspect ratio of industrial bearings is customarily in the range $0.25 < L/D < 1.5$, neither the short-bearing (see *ibidem*) nor the long-bearing approximation being applicable to such bearings. The numerical examples in Chapter 4 will follow the long-bearing assumption and we will be concerned with the planar flow in an eccentric annulus, see Figure 1.1b. Note that the full three-dimensional setting would substantially increase the CPU and memory demands, or in other words, it would decrease the accuracy (in the sense of the size of mesh elements) accessible in our numerical experiments.

By taking the long-bearing approximation, one immediately loses the information about the level of pressure (unless there is a supply channel modelled in the bearing body or the solid walls are modelled as being porous, etc.) hitherto present in the finite-length bearing due to the open ends. Indeed, if the flow between infinite cylinders is considered then the level of pressure can be arbitrary. As mentioned already, this does not deserve any special treatment as long as the viscosity does not depend on the pressure (or, similarly, as long as cavitation of the lubricant is not considered); while in the case with a piezoviscous lubricant an additional

requirement on the pressure level has to be included into the model. In the literature concerned with the numerical simulations this deficiency of the long-bearing approximation is not always emphasized. Either the mean value of the pressure over the entire domain is usually prescribed (which is not justified by the application), or the ambient pressure is prescribed at the point of the largest gap. In Subsection 4.3.4 (see the references therein), we will illustrate on a few numerical experiments that the particular appearance of this requirement can affect the solution of the problem considerably.

1.1.2 Features neglected

Let us emphasize the most blatant simplifications (some of them having been mentioned already) which are not justifiable, but we take them nevertheless, merely for the sake of easier explanation. See Szeri (1998) for more details concerning each of the following points.

- Isothermal flows will be considered (at elevated temperature, possibly). In the majority of journal bearings, in particular in the regimes where the viscosity considerably depends on pressure, this is not a valid assumption. Note that all the energy lost by viscous forces is dissipated into heat, which implies a significant heat production within the flow. The viscosity depends strongly on temperature. In fact, its dependence on temperature may affect the solution more than its dependence on pressure.
- The entire domain is considered to be filled by the lubricant (the *full-film* conditions) and no cavitation nor free boundary is involved; the incompressible fluid sustains arbitrary negative pressures. This assumption is not realistic either; the real liquids can withstand some tensile stresses, but below certain pressure either gaseous or vapor cavitation occurs. “Under normal operating conditions a lubricant film ... is expected to cavitate within the diverging part of the clearance, where, on the assumption of a continuous lubricant film, theory predicts negative pressures. This much is clear. Still, the subject of considerable discussion, however, are (1) the exact position of the film-cavity interface and (2) the boundary conditions that apply at that interface.” (Szeri, 1998, page 98).
- The inertial forces will be neglected in this text. Concerning results on the mathematical well-posedness see Lanzendörfer (2009); Lanzendörfer and Stebel (2011a,b), where the convective term is included in the governing equations. Some of the numerical simulations presented in Section 4.3 would not differ significantly, were the inertial forces included in the model. Note, however, that in some journal bearing applications their inclusion can have substantial effect.
- No effects of surface roughness are considered; we consider the solid surfaces as being perfectly smooth. Moreover, in Chapter 4, we will assume that the fluid adheres to the boundary, i.e., we will prescribe the Dirichlet boundary conditions. The theoretical results in Chapter 2 include also Navier’s slip boundary conditions.
- The solid parts are considered to be rigid (the rigid–piezoviscous regime is assumed). This may be a valid assumption if the pressures are not too large (while the elastic moduli of the solid parts are large enough), but this condition is never verified in the thesis.
- The lubricant is pressure-thickening and shear-thinning only. In fact, one can observe other non-Newtonian phenomena apparent in the lubrication flow, such as the visco-

elasticity or the normal stress differences effects, to name two. These are out of the scope of the thesis, however.

- The fluid is taken as incompressible; see Subsection 1.3.1.

1.2 Governing equations

The mathematical description of the flow is based on the following considerations. Let $I \subset \mathbb{R}$ be a time interval and $\Omega \subset \mathbb{R}^d$ be a spatial domain occupied by the fluid. The principle of *mass conservation* may be expressed in the form

$$\frac{d}{dt} \int_B \rho \, d\mathbf{x} + \int_{\partial B} \rho \mathbf{v} \cdot \mathbf{n} \, d\mathbf{x} = 0 \quad (1.1)$$

for any bounded subset B of Ω with the boundary ∂B sufficiently smooth so that the outward normal vector \mathbf{n} may be defined. Here the time $t \in I$ and the spatial position $\mathbf{x} \in \Omega$ are independent variables, and the density $\rho = \rho(t, \mathbf{x})$ and the velocity $\mathbf{v} = \mathbf{v}(t, \mathbf{x})$ of the fluid are state functions. The balance of *linear momentum* leads to

$$\frac{d}{dt} \int_B \rho \mathbf{v} \, d\mathbf{x} + \int_{\partial B} (\rho \mathbf{v} (\mathbf{v} \cdot \mathbf{n}) - \mathbf{T}^T \mathbf{n}) \, d\mathbf{x} = \int_B \rho \tilde{\mathbf{f}} \, d\mathbf{x}, \quad (1.2)$$

where $\tilde{\mathbf{f}} = \tilde{\mathbf{f}}(t, \mathbf{x})$ is the density of an external force and $\mathbf{T} = \mathbf{T}(t, \mathbf{x})$ is the Cauchy stress tensor, $\mathbf{T} = \mathbf{T}^T$ due to the balance of *angular momentum* (assuming that there are no internal couples).

If all the quantities are sufficiently smooth, one can apply Green's theorem to (1.1)–(1.2) and obtain

$$\left. \begin{aligned} \partial_t \rho + \operatorname{div}(\rho \mathbf{v}) &= 0 \\ \partial_t(\rho \mathbf{v}) + \operatorname{div}(\rho \mathbf{v} \otimes \mathbf{v}) - \operatorname{div} \mathbf{T} &= \rho \tilde{\mathbf{f}} \end{aligned} \right\} \quad \text{in } I \times \Omega,$$

where $(\mathbf{u} \otimes \mathbf{u})_{ij} = u_i u_j$ and $(\operatorname{div} \mathbf{T})_i = \sum_{j=1}^d \partial_{x_j} T_{ij}$.

We confine ourselves to *isothermal flows* only; therefore, we do not mention the balance of energy. In what follows, all parameters or variables are considered at a given temperature, though this is not denoted explicitly.

For *incompressible* fluid we require in addition that

$$\operatorname{div} \mathbf{v} = 0 \quad \text{in } I \times \Omega. \quad (1.3)$$

If the fluid is also *homogeneous* then the density is a positive constant $\rho \equiv \rho_0 > 0$ and (1.3) replaces (1.1).

We shall consider only *steady flows* of incompressible homogeneous fluids in the thesis and, for simplicity, we will neglect the inertial forces. Therefore, we rewrite (1.2) as

$$- \int_{\partial B} \mathbf{T} \mathbf{n} \, d\mathbf{x} = \int_B \mathbf{f} \, d\mathbf{x}, \quad (1.4)$$

where $\mathbf{f} = \rho_0 \tilde{\mathbf{f}}$. Provided that \mathbf{T} and \mathbf{f} are smooth enough, we write

$$\boxed{\begin{array}{l} \operatorname{div} \mathbf{v} = 0 \\ -\operatorname{div} \mathbf{T} = \mathbf{f} \end{array}} \quad \text{in } \Omega. \quad (1.5)$$

However, instead of (1.5) which involves the derivatives of \mathbf{T} , we will later consider rather the *weak solutions* of the problem, that will be properly defined in Subsection 2.1.3. Note that the notion of a weak solution derives directly from the integral formulation (1.4), as has been proposed^c already by Oseen (1927), see also Feireisl (2004, 2007).

1.3 Constitutive equations

For the *Newtonian* fluids, a linear relation between the stress and the symmetric part of the velocity gradient $\mathbf{D} = \frac{1}{2}(\nabla \mathbf{v} + \nabla \mathbf{v}^T)$ is required, which yields (note that $\operatorname{tr} \mathbf{D} = \operatorname{div} \mathbf{v}$)

$$\mathbf{T} = -p\mathbf{I} + 2\mu\mathbf{D}, \quad \operatorname{tr} \mathbf{D} = 0, \quad (1.6)$$

in the case of homogeneous incompressible fluid, and

$$\mathbf{T} = -p(\rho)\mathbf{I} + \lambda(\rho)(\operatorname{tr} \mathbf{D})\mathbf{I} + 2\mu(\rho)\mathbf{D}^\delta, \quad \mathbf{D}^\delta := \mathbf{D} - \left(\frac{1}{3} \operatorname{tr} \mathbf{D}\right)\mathbf{I}$$

in the case of homogeneous compressible fluid. Here λ and μ are the bulk and shear moduli of viscosity. The corresponding equations of motion for Newtonian fluids are referred to as the *Navier–Stokes* equations. Fluids, however, display a variety of relations between the stress and the other state variables. For a brief overview of the most frequent *non-Newtonian* phenomena and the corresponding fluid models see, e.g., Málek and Rajagopal (2006, 2007) and the references given there.

In this thesis, we will be concerned with the generalization of (1.6), where the viscosity depends on the pressure and the shear rate, in particular with the pressure-thickening and shear-thinning fluids. Namely, we will consider a class of incompressible fluids whose Cauchy stress is given by

$$\boxed{\mathbf{T} = -p\mathbf{I} + 2\eta(p, |\mathbf{D}|)\mathbf{D}}, \quad \operatorname{tr} \mathbf{D} = 0, \quad (1.7)$$

where $|\mathbf{Q}|^2 = \sum_{i,j=1}^d Q_{ij}^2$. To avoid confusion in what follows, we will denote the above generalized viscosity of an incompressible fluid by $\eta = \eta(p, |\mathbf{D}|)$. Note that the above class of fluids excludes some phenomena that may appear in applications and will not be considered, such as the normal stress differences or viscoelastic behavior.

Note that p is the mean normal stress here, $p = -\frac{1}{3} \operatorname{tr} \mathbf{T}$, the reaction force due to the constraint that the fluid is incompressible. For the derivation of the above and other constitutive relations and for the related thermodynamic considerations see Málek and Rajagopal (2006, 2007). We mention that (1.7) may be viewed as an implicit constitutive equation,

$$\mathbf{T} - \frac{1}{3}(\operatorname{tr} \mathbf{T})\mathbf{I} - 2\eta\left(-\frac{1}{3} \operatorname{tr} \mathbf{T}, |\mathbf{D}|\right)\mathbf{D} = 0,$$

^c Oseen (1927) only treats Navier–Stokes fluids and their linearizations. Note that the notion of solution was not called “weak”.

see *ibidem* and Rajagopal (2006) for a detailed discussion.

The counterpart of (1.7) in the case of a compressible fluid would be

$$\mathbf{T} = -p(\rho)\mathbf{I} + \lambda(\rho, \operatorname{tr} \mathbf{D}, |\mathbf{D}^\delta|)(\operatorname{tr} \mathbf{D})\mathbf{I} + 2\mu(\rho, \operatorname{tr} \mathbf{D}, |\mathbf{D}^\delta|)\mathbf{D}^\delta,$$

(see Málek and Rajagopal, 2010). In this case $p \neq -\frac{1}{3} \operatorname{tr} \mathbf{T}$; but p is the thermodynamical pressure related to ρ by the equation of state. If this relation is invertible then the viscosity naturally depends on the thermodynamical pressure:

$$\mathbf{T} = -p(\rho)\mathbf{I} + \lambda(\rho(p), \operatorname{tr} \mathbf{D}, |\mathbf{D}^\delta|)(\operatorname{tr} \mathbf{D})\mathbf{I} + 2\mu(\rho(p), \operatorname{tr} \mathbf{D}, |\mathbf{D}^\delta|)\mathbf{D}^\delta.$$

If one considers a simple shear flow (e.g., between infinite parallel plates), then the (compressible) fluid undergoes an isochoric motion, both the pressure and density are constant within the flow, $p(\rho) = -\frac{1}{3} \operatorname{tr} \mathbf{T}$, and one observes (cf. (1.7))

$$\mathbf{T} = -p\mathbf{I} + 2\mu(\rho(p), |\mathbf{D}|)\mathbf{D}. \tag{1.8}$$

A natural question arises, whether it is reasonable to consider the viscosity to depend on the pressure, while considering an incompressible fluid. The answer advocated in this thesis is twofold:

First, as will be documented in this section for liquids such as lubricants, when the fluid is subject to a sufficiently large range of pressures, while the density may vary by a few percent, the viscosity can vary by several orders of magnitude. Moreover, the relative density variations with pressure decrease with the increasing pressure; on the contrary, the relative changes of viscosity due to the pressure are larger at larger pressures. Therefore, it is well justified to suppose the liquid to be incompressible while at the same moment to consider its viscosity to be pressure dependent.

Second, although this thesis considers the incompressible fluids only, we remark that an investigation of compressible models related to liquid lubricants is of importance as well. In order to provide a reliable comparison of the two (compressible and incompressible) models in the context of the real-world applications, a natural prerequisite is to be able to provide reliable predictions of the flow for either of them. The theoretical results for incompressible fluids (presented in Chapter 2) as well as our numerical experiments (see Chapter 3) suffer from certain limitations and are applicable to real-world liquids only in a limited range of pressures (this will be documented in Chapter 5). Whether these limitations are due to insufficiency of the current theoretical approach only, or whether they are inherent with the assumption of incompressibility, is not clear. Note, however, as far as concerns the rigorous analysis, that so far there has been no results for compressible liquids analogous to those presented in Chapter 2 for incompressible models (e.g., see Novotný and Straškraba, 2004).

1.3.1 On the (in)compressibility

Many experimental works on the variation of the density of liquids subject to a wide range of pressures are reported in the 1931 book by Bridgman. We mention an empirical expression

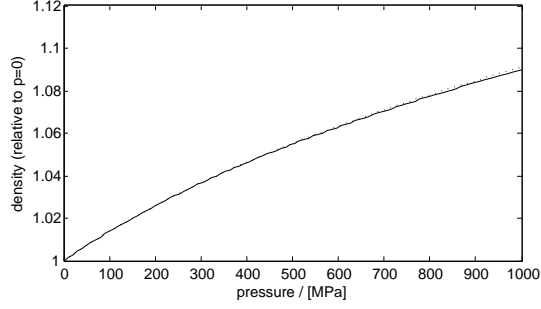


Figure 1.2: The relative density $\rho(p)/\rho(0)$ for SQL at $\theta = 40^\circ\text{C}$.

(see Dowson and Higginson, 1966)

$$\frac{\rho(p)}{\rho(0)} = 1 + \frac{c_1 p}{1 + c_2 p}, \quad c_1, c_2 > 0,$$

where $\rho(0)$ is the density in the liquid at ambient pressure. Throughout the text, ambient pressure will be taken as zero; note that the atmospheric pressure is 0.1 MPa while the pressures involved will be of the order of 100 MPa. Three reference liquids are accurately characterized in (Bair, 2006), using the following two popular equations of state. The Tait equation (see the references in Dymond and Malhotra, 1988) writes

$$\frac{\rho_\theta(0)}{\rho_\theta(p)} = 1 - \frac{1}{1 + K'_0} \ln \left(1 + \frac{1 + K'_0}{K_{00} \exp(-\beta_K \theta)} p \right) =: \omega_\theta(p), \quad (1.9)$$

where θ denotes the temperature, and where K_{00} , K'_0 , and β_K are given material parameters (see Subsection 1.3.4). The Murnaghan equation (see Murnaghan, 1944) is written as

$$\frac{\rho_\theta(0)}{\rho_\theta(p)} = \left(1 + \frac{K'_0}{K_{00} \exp(-\beta_K \theta)} p \right)^{-1/K'_0}.$$

For illustration, we report the density (Tait equation, full line; Murnaghan equation, dotted) for squalane (SQL, see Subsection 1.3.4) in Figure 1.2. The models due to Bair (2006) are accurate with the experimental data up to $p = 400$ MPa.

What we would like to point out, is that while all liquids are essentially compressible, the density of the liquids (such as water or common lubricants) varies slightly, say up to around 10 per cent, even when subject to very high pressures, say up to 3 GPa. Since we will report that the viscosity can change at the same conditions by several orders of magnitude, it seems reasonable to model such fluids as incompressible fluids with the pressure dependent viscosity.

1.3.2 On the viscosity dependence on pressure

There has been an amount of experimental work concerning the viscosity at high pressures, and we are not going to review the particular observations and models. The vast majority of engineering literature in elastohydrodynamic lubrication, see e.g. (Szeri, 1998), relies on the exponential pressure–viscosity relation by Barus (1893)

$$\mu = \mu_0 \exp(\alpha p), \quad \mu_0, \alpha > 0.$$

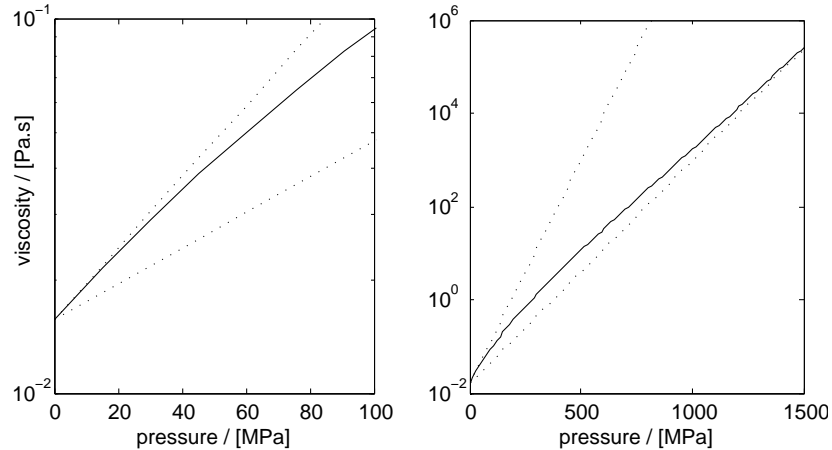


Figure 1.3: The low shear viscosity $\mu(p)$ for SQL at $\theta = 40$ °C.

Other formulae can be found in the literature, which better fit experimental results; they “invariably involve an exponential relationship of sorts” (see Málek and Rajagopal, 2007, for the references). Let us remark that at the pressures involved in elastohydrodynamic lubrication, say up to 3 GPa, the viscosity may be up to 10^8 of its value at ambient pressure; the fluid gets close to undergoing glass transition, and the viscosity increases more rapidly than exponentially (see Bair and Kottke, 2003).

In a recent paper by Bair (2006), three reference materials are accurately characterized for the purposes of quantitative elastohydrodynamic lubrication considerations. In Subsection 1.3.4 we will present these liquids, and we will use them as reference examples through the thesis (in particular, see Chapter 5). According to Bair, “the free volume viscosity model has been used almost exclusively” for the accurate description of pressure dependence at high pressures; the viscosity at small shear rates

$$\mu = \mu_0 a_\theta(p)$$

is described by the Doolittle equation (see Doolittle, 1951) which we write including the linear corrections due to temperature as follows:

$$a_\theta(p) = \exp \left[BR_0 \left(\frac{1}{\omega_\theta(p) \frac{1+a_V(\theta-\theta_R)}{1+\varepsilon_V(\theta-\theta_R)} - R_0} - \frac{1}{1-R_0} \right) \right], \quad (1.10)$$

where $\theta_R = 40$ °C is a reference temperature, B , R_0 , a_V , and ε_V given parameters, and $\omega_\theta(p)$ is defined by (1.9). Note that $\omega_\theta(p)$ has the physical meaning of the relative volume change due to the pressure, and that the above equation is in fact the density–viscosity relation for a compressible fluid. However, while we will assume (approximate) that the fluid is incompressible and its density is constant, we will consider the couple (1.9), (1.10) as a pressure–viscosity relation, cf. (1.8).

We again illustrate in Figure 1.3 the observed relation for squalane (SQL, see Subsection 1.3.4) at $\theta = 40$ °C. The two figures differ in the range of pressures, the displayed curves being the same. The dotted lines represent for comparison the exponential (Barus) relation, fitted to the reference model once at lower and once at higher pressures. The reference model describes measured viscosities up to $p = 1200$ MPa accurately (see Bair, 2006).

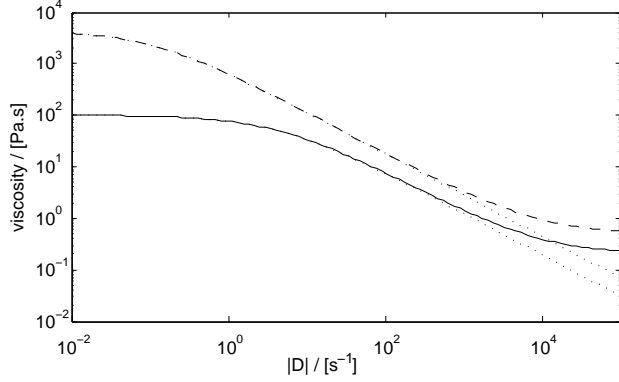


Figure 1.4: The viscosity $\eta(|\mathbf{D}|)$ for SRM 2490 at $\theta = 25$ °C.

1.3.3 On the viscosity dependence on shear rate

We do not attempt to list the many empirical models for the relation between the viscosity and the shear rate. The behavior of shear-thinning and shear-thickening liquids typically obeys the *power-law* relation (for large shear rates)

$$\frac{\partial \ln |\mu \mathbf{D}|}{\partial \ln |\mathbf{D}|} = n$$

where the power-law exponent $n > 0$ is a material parameter. Obviously, $n > 1$ for shear-thickening and $n < 1$ for shear-thinning fluids. The simple power-law model

$$\mu = m |\mathbf{D}|^{n-1}, \quad m > 0,$$

is frequently considered, one of its advantages being that it allowed to find analytical solutions to a variety of flow problems. However, it should be noted (see Bird et al., 1987) that it does not realistically describe the viscosity of liquids at very small shear rates.

In numerical simulations it is more standard to fit the experimental shear rate–viscosity curves to the *Carreau–Yasuda* model (Carreau, 1968, 1972; Yasuda, 1979)

$$\mu = \mu_\infty + (\mu_0 - \mu_\infty) (1 + (|\mathbf{D}|/G)^a)^{(n-1)/a}, \quad \mu_\infty \geq 0, \mu_0, G, a > 0 \quad (1.11)$$

or its variants. If $\mu_\infty > 0$ then it corresponds to the *second Newtonian plateau*, apparent with some important liquids such as some multigrade motor oils, see e.g. Bird et al. (1987). For illustration see Figure 1.4, where we depict the *Cross model* (i.e., the above equation with $a = 1 - n$) for the NIST non-Newtonian Standard Reference Material, SRM 2490 The viscosity dependence on shear rate and is drawn in a logarithmic scale. For $p = 0$ (full line) and $p = 200$ MPa (dash) the model fits to experimental data for shear rates up to 10^5 s⁻¹, where the second Newtonian plateau is displayed (see Bair and Gordon, 2006). The dotted curves show the models with $\mu_\infty = 0$, for comparison.

In order to obtain the correct shear dependence of viscosity at arbitrary temperature and pressure, a *shifting rule* for G is taken in the equation (see the *time-temperature-pressure superposition* or the *method of reduced variables*, e.g. in Bair et al., 2002; Bird et al., 1987). The power-law exponent n is in general independent of temperature and pressure. The reference

models by Bair presented in what follows are described by the *Carreau equation* (i.e. (1.11) with $a = 2$), perhaps the most frequently used shear-thinning model. Since the reference liquids do not display the second Newtonian plateau, $\mu_\infty = 0$. We denote the equation as follows,

$$\eta_\theta(p, |\mathbf{D}(\mathbf{v})|) = \mu_0 a_\theta(p) \left(1 + (b_\theta(p)|\mathbf{D}(\mathbf{v})|)^2\right)^{\frac{r-2}{2}}, \quad (1.12)$$

where $r = n + 1$, and $a_\theta(p)$ describes the viscosity variation due to pressure (and temperature) at small shear rates, while $b_\theta(p)$ represents a shifting rule for temperature and pressure. Here $\mu_0 = \eta_{\theta_R}(0, 0)$ is the Newtonian viscosity at reference temperature. We will usually omit the subscript θ for the viscosity, writing only $\eta(p, |\mathbf{D}(\mathbf{v})|)$.

Bair (2006) employs two formulae for the shifting rule $b_\theta(p)$ in the paper, written in our notation as

$$b_\theta(p) = \frac{\mu_0 a_\theta(p)}{G_R} \frac{\theta_R \rho_{\theta_R}(0)}{\theta \rho_\theta(p)} \sqrt{2} = \left(\frac{\mu_0}{G_R} \frac{\theta_R}{\theta} (1 + a_V(\theta - \theta_R)) \right) a_\theta(p) \omega_\theta(p) \sqrt{2} \quad (1.13)$$

$$b_\theta(p) = \frac{\mu_0}{G_R} a_\theta(p)^{1-m} \sqrt{2}, \quad (1.14)$$

the former labeled as a “standard (Ferry) shifting rule” (see also Bair et al., 2002; Ferry, 1980),

1.3.4 Three reference lubricants characterization

The presented thesis is motivated by the problem of hydrodynamic lubrication. The recent work by Bair (2006) gives accurate material characterizations and constitutive models for three reference liquid lubricants, selected to represent the viscosity dependence on temperature, pressure and shear rate that may be observed in elastohydrodynamic lubrication. The considered range of parameters, chosen to be relevant for elastohydrodynamic simulations, is more than sufficient for our purposes (note certain limitations presented in Chapter 5). The liquids considered are

SQL, squalane; a low-molecular-weight branched alkane, 2,6,10,15,19,23-hexamethyltetracosane; selected to represent the character of a low viscosity paraffinic mineral oil or polyalphaolefin, it “should be Newtonian throughout the EHL inlet zone...”—it does not exhibit shear-thinning up to shear rate of 10^9 s^{-1} for ambient pressure; see Figure 5.5;

PGLY, a high-molecular-weight polyglycol, poly(ethylene glycol-ran-propylene glycol); chosen to represent high-molecular-weight base oils such as polyglycols, viscous polyalphaolefins, perfluorinated polyalkylethers, and silicones; it manifests apparent shear-thinning; see Figure 5.6;

SQL+PIP, a solution of 15% by weight cis-polyisoprene in squalane; selected as a representative of the polymer blended multigrade gear oils and engine oils; see Figure 5.7.

All three reference models are pressure-thickening and shear-thinning and are described by the Carreau equation (1.12), and by the Doolittle-Tait equation (1.10) and (1.9). The shear-thinning does not display a second Newtonian plateau. The shifting rule (1.13) is used for SQL, while for PGLY and SQL+PIP (1.14) is applied. The resulting models were fitted to experimental data for $|\mathbf{D}(\mathbf{v})|$ up to 10^5 s^{-1} and pressures up to (at least) 300 MPa, see the data provided in Bair (2006); Bair et al. (2002). Note that the high shear measurements were

provided only for θ around 20 or at most 40 °C, while we will use $\theta = 40$ and 100 °C in what follows (because higher temperatures can occur in lubrication problems); but it appears from both papers that such extrapolation can be trusted.

The material parameters for the above models of SQL, PGLY and SQL+PIP provided by Bair (2006) are summarized in Table 1.1. The viscosities depending on shear rate are presented in Figures 5.5–5.7 (a,c) by black lines: full line for $p = 0$, dashed line for $p = 200$ MPa and dotted line for $p = 400$ MPa.

	SQL	PGLY	SQL+PIP
μ_0 / Pa s	0.0157	16.3	0.0711
K'_0	11.74	10.80	11.29
K_{00} / GPa	8.658	19.49	8.375
β_K / 10^{-3} K $^{-1}$	6.332	7.64	6.765
B	4.710	3.661	4.200
R_0	0.6568	0.6813	0.6580
a_V / 10^{-3} K $^{-1}$	0.836	0.775	0.752
ε_V / 10^{-3} K $^{-1}$	-0.7871	-1.157	-0.9599
G_R / MPa	6.94	0.256	0.010
m	–	0.10	0
r	1.463	1.33	1.80

Table 1.1: Material parameters for three reference liquids, (1.12)–(1.14), $\theta_R = 40$ °C.

We shall employ the above three accurately characterized reference liquids particularly in Chapter 5, where we will discuss (and specify quantitatively) the limitations of the current theoretical results and of the presented numerical method. The above models will be also used in the numerical experiments of Chapter 4.

Let us mention the series of papers by Davies, Gwynlyw, Li and Phillips (see the bibliography) concerned with numerical simulations in a realistic journal bearing, where the authors consistently use another set of models fitted to the experimentally measured viscosities of selected lubricants. Namely, the shear-thinning is described by the Cross model (eq. (1.12) with $a = 1 - n$) with a second Newtonian plateau ($\mu_\infty > 0$), and both $a(p)$ and $b(p)$ are exponentials of pressure. Note, however, that these models had been fitted to measurements in considerably smaller ranges of parameters (see Hutton et al., 1983) than the above models provided by Bair; the ranges sufficient for the purposes of journal bearing lubrication flow simulations, but unsuited for the purposes of Chapter 5.

1.4 Boundary conditions

1.4.1 The fluid–solid interface

On the interface of the viscous fluid with the impermeable solid surface one usually assumes that the fluid adheres to the surface, i.e., the velocity of the fluid at the boundary equals to

that of the solid; one prescribes the Dirichlet boundary conditions,

$$\mathbf{v} = \mathbf{v}_D \quad \text{on some } \Gamma \subset \partial\Omega, \quad (1.15)$$

where \mathbf{v}_D denotes the velocity of the solid surface. In our numerical simulations we will accept this condition, for simplicity. Since we will consider only problems in a fixed geometry, $\mathbf{v}_D \cdot \mathbf{n} = 0$ (where \mathbf{n} denotes the unit outward normal vector on $\partial\Omega$).

Alternatively, one can allow for the fluid to slip at the solid boundary, for example by prescribing the following Navier's slip boundary condition

$$\mathbf{v} \cdot \mathbf{n} = 0 \quad \text{and} \quad -(\mathbf{T}\mathbf{n})_\tau = \alpha(\mathbf{v} - \mathbf{v}_D), \quad \alpha \geq 0 \quad \text{on some } \Gamma \subset \partial\Omega \quad (1.16)$$

where $\mathbf{u}_\tau := \mathbf{u} - (\mathbf{u} \cdot \mathbf{n})\mathbf{n}$ is the projection of a vector \mathbf{u} to the tangent plane, and \mathbf{v}_D is again the velocity of the solid surface. The parameter α characterizes the fluid–solid interface; note that $\alpha = 0$ corresponds to the so-called *free slip* boundary condition, while the limit $\alpha \nearrow +\infty$ formally leads (multiplying (1.16) by $1/\alpha$ first) to the Dirichlet boundary condition. Various more sophisticated relations between the shear stress and the slip velocity

$$\mathbf{v} \cdot \mathbf{n} = 0 \quad \text{and} \quad -(\mathbf{T}\mathbf{n})_\tau = (\mathbf{b}(\mathbf{v} - \mathbf{v}_D))_\tau, \quad \text{on some } \Gamma \subset \partial\Omega, \quad (1.17)$$

can be found in literature, but we will not discuss them in detail. The assumption of slip or no-slip at solid boundary is a complex issue in the modeling of viscous fluids and the precise circumstances determining the validity of these assumptions are subject to an unceasing concern (e.g., see Granick et al., 2003; Neto et al., 2005).

1.4.2 The requirement to determine the level of pressure

As mentioned already in Subsection 1.1, there is a particular distinction of the piezoviscous fluid models that is related to the level of the pressure in the flow. If some of the conditions (1.15)–(1.17) is prescribed on the entire boundary (namely, if the normal part of the velocity, $\mathbf{v} \cdot \mathbf{n}$, is prescribed on the entire boundary) then the flow of an incompressible Newtonian fluid subject to such boundary conditions is not determined uniquely; the same apply for the non-Newtonian models of the class (1.7) considered in the thesis. As long as the viscosity does not vary with the pressure, it is well known that the ambiguity appears in the pressure field only, namely that the pressure is defined up to a constant. Indeed, since only the pressure gradient is present in the governing equations, the addition of an arbitrary constant to the pressure field has no other effect on the solution. This kind of non-uniqueness does not deserve any particular attention and is usually treated formally, by restricting the functional space where the pressure is sought by prescribing

$$\int_{\Omega} p \, d\mathbf{x} = 0. \quad (1.18)$$

For piezoviscous fluids this non-uniqueness has no such structure, both the pressure and the velocity fields are undetermined and the additional constraint on the pressure level becomes an important part of the model. Regrettably, the constraint (1.18) or, in general,

$$\int_{\Omega_0} p \, d\mathbf{x} = P_0, \quad \Omega_0 \subset \Omega, \quad P_0 \in \mathbb{R} \quad (1.19)$$

is not always practical from the point of view of applications; the modeller often has no hint on how to choose Ω_0 and P_0 . One example where this issue appears has been mentioned in Subsection 1.1.1: in the standard long-bearing approximation of the journal bearing lubrication flow the information about the level of pressure is not present in the model; see also Section 4.3.

The above difficulty of the pressure level being not determined seems to be a natural consequence of the incompressibility assumption, in conjunction with the fluid being mechanically isolated in a sense. A natural question arises, whether a unique solution is provided by the boundary conditions allowing for free inflow/outflow through the boundary; see the next subsection.

1.4.3 Permeable interfaces, artificial boundaries

There are basically two circumstances where a flow through the boundary occurs. Either the boundary describes an interface of the fluid with a permeable media (porous media, permeable membrane) or there is no physical interface involved and an artificial boundary is introduced in order to reduce the size of the considered (computational) domain. In both cases, the boundary condition allowing for inflow and outflow involves the influence of the (usually unknown) motion of the fluid beyond the boundary. As such, they are not concluded from the physical principles only, but they result from the model reduction considerations and can represent substantial simplification. The choice of the boundary condition at artificial boundaries is not a simple question even for a Newtonian fluid, see also the discussion in Heywood et al. (1996). Quite often the intention of the modeler is merely to ensure that “nothing (disturbing) happens” at the boundary, while it is not clear how to express this requirement mathematically.

For the sake of completeness, note that the Dirichlet boundary condition (1.15) is frequently used to prescribe the inflow in simple geometries; usually based on the expectation that the possible disturbances to the velocity field will occur only downstream, and the assumption that the velocity profile on the inlet is that of a simple unidirectional steady flow (e.g., the parabolic velocity profile in the Poiseuille flow of a Newtonian fluid) and is therefore explicitly known. However, the precise information on the velocity profile is often not at hand, the above assumption does not apply for outflow conditions, and in particular, such boundary conditions do not determine the level of pressure in the solution, as discussed in the previous subsection.

We will consider the boundary conditions that involve the traction on the boundary, namely,

$$-\mathbf{T}\mathbf{n} = \mathbf{b}(\mathbf{x}, \mathbf{v}) \quad \text{on some } \Gamma \subset \partial\Omega, \quad (1.20)$$

where \mathbf{b} is the prescribed traction, which may optionally depend on the velocity. The above condition with $\mathbf{b} \equiv \mathbf{0}$ is usually referred to as the *do nothing* condition. It will be shown in Chapter 2 that (1.20) allows for the existence of a weak solution and, importantly, it suffices to determine the solution uniquely.

It is worth emphasizing that the explicit knowledge of the traction on the artificial boundary may be as unavailable as the knowledge of the velocity profile (required in the case of Dirichlet boundary conditions). This is well illustrated by the example of Poiseuille flow discussed in Section 4.1: considering an artificial boundary established across the channel, perpendicular to

the flow, then while the normal part of the traction equals the pressure, and thus it is constant along the boundary, the tangential part of the traction is not constant and, in particular, it depends on the velocity profile. In such situation, it is more convenient to prescribe

$$\left. \begin{aligned} \mathbf{v}_\tau &= \mathbf{0} \\ -\mathbf{T}\mathbf{n} \cdot \mathbf{n} &= \mathbf{b}(\mathbf{x}, \mathbf{v}) \cdot \mathbf{n} \end{aligned} \right\} \quad \text{on } \Gamma \subset \partial\Omega. \quad (1.21)$$

The dependence of \mathbf{b} on the velocity may be important when the inertial forces are included (we will not discuss this case, see Lanzendörfer and Stebel 2011a,b) or in case of the interface with some permeable media. For example,

$$-\mathbf{T}\mathbf{n} \cdot \mathbf{n} = h + c_1 \mathbf{u} \cdot \mathbf{n}, \quad c_1 > 0$$

can be found in literature as the *filtration boundary condition*, with the parameters h and c_1 describing the ambient pressure and the resistance to the flow. Similarly, for the flow in the direction along the interface one may consider

$$-(\mathbf{T}\mathbf{n})_\tau = c_2 \mathbf{v}_\tau \quad c_2 > 0,$$

which corresponds to the Beavers–Joseph(–Saffman–Jones) condition for flows past porous media, based on experimental observations (see Beavers and Joseph, 1967; Jones, 1973; Nield, 2009; Saffman, 1971).

Chapter 2

Well-posedness of the mathematical problem

Contents

2.1	Definition of the problem	20
2.1.1	Structural assumptions (A1)–(A4)	21
2.1.2	Boundary conditions	22
2.1.3	Weak formulation	23
2.2	Central features and discrete approximation	25
2.2.1	A priori estimates	25
2.2.2	Inf-sup inequality; pressure and boundary conditions	26
2.2.3	Galerkin approximation and inf-sup conditions	29
2.3	Well-posedness results	31
2.3.1	Existence of discrete solutions	32
2.3.2	Uniqueness	33
2.3.3	Convergence of discrete solutions; existence of a weak solution	36
2.4	Auxiliary tools	38

2.1 Definition of the problem

We briefly recall the governing equations introduced in the previous chapter. We shall investigate the steady flow of an incompressible homogeneous viscous fluid in a bounded fixed domain $\Omega \subset \mathbb{R}^d$, $d = 2$ or 3 , governed by the following system of PDEs:

$$\left. \begin{aligned} \operatorname{div} \mathbf{v} &= 0 \\ -\operatorname{div} \mathbf{T} &= \mathbf{f} \end{aligned} \right\} \text{ in } \Omega, \quad (2.1)$$

where \mathbf{v} , \mathbf{f} , \mathbf{T} represent the velocity, the body force and the Cauchy stress tensor, respectively. We consider

$$\mathbf{T} = -p\mathbf{I} + \mathbf{S}, \quad \text{where} \quad \mathbf{S} \equiv \mathbf{S}(p, \mathbf{D}(\mathbf{v})) = 2\eta(p, |\mathbf{D}(\mathbf{v})|)\mathbf{D}(\mathbf{v}), \quad (2.2)$$

with p the pressure, $\eta(p, |\mathbf{D}(\mathbf{v})|)$ the generalized viscosity and $\mathbf{D}(\mathbf{v}) = \frac{1}{2}(\nabla \mathbf{v} + \nabla \mathbf{v}^T)$ the symmetric part of the velocity gradient. Note that $\mathbf{S} = \mathbf{S}^T$ and that (due to $\operatorname{div} \mathbf{v} = 0$) $\operatorname{tr} \mathbf{S} = 0$ such that $-\frac{1}{3} \operatorname{tr} \mathbf{T} = p$. The theory we are going to expose is based on the assumption that η is shear-thinning, while additional dependence of the viscosity on pressure is allowed at the same time, see below. Note that in (2.1)₂ the inertial forces are neglected, which allows us to focus on the structure of \mathbf{T} while avoiding the mathematical difficulties due to the convective term^a.

The domain boundary is fixed, it is Lipschitz and consists of three Lipschitz parts^b $\partial\Omega = \Gamma_D \cup \Gamma_N \cup \Gamma_P$ on which we prescribe

$$\mathbf{v} = \mathbf{v}_D \quad \text{on } \Gamma_D, \quad (2.3a)$$

$$\left. \begin{aligned} \mathbf{v} \cdot \mathbf{n} &= \mathbf{v}_D \cdot \mathbf{n} \\ -(\mathbf{T}\mathbf{n})_\tau &= (\mathbf{b}(\mathbf{v} - \mathbf{v}_D))_\tau \end{aligned} \right\} \text{ on } \Gamma_N, \quad (2.3b)$$

$$-\mathbf{T}\mathbf{n} = \mathbf{b}(\mathbf{v} - \mathbf{v}_D) \quad \text{on } \Gamma_P, \quad (2.3c)$$

where \mathbf{n} is the unit outward normal vector on $\partial\Omega$. For any vector $\boldsymbol{\omega}$, we denote $\boldsymbol{\omega}_\tau := \boldsymbol{\omega} - (\boldsymbol{\omega} \cdot \mathbf{n})\mathbf{n}$ its tangential part. Here, \mathbf{v}_D is the given velocity on the boundary (velocity of the wall; typically, $\mathbf{v}_D \equiv \mathbf{0}$ on $\Gamma_N \cup \Gamma_P$). The function $\mathbf{b} \equiv \mathbf{b}(\mathbf{x}, \mathbf{v} - \mathbf{v}_D)$ prescribes the force on the boundary. In principal, \mathbf{b} need not depend on the velocity, i.e. $\mathbf{b} \equiv \mathbf{b}(\mathbf{x})$ is allowed^c (see also Lemma 1). Whether to write $\tilde{\mathbf{b}}(\mathbf{v})$ instead of $\mathbf{b}(\mathbf{v} - \mathbf{v}_D)$ is a matter of personal preference only.

If $|\Gamma_P| = 0$ such that (2.3c) does not take effect, an additional constraint has to be posed in order to fix the level of pressure; this is achieved by setting (cf. Bulíček and Fišerová, 2009;

^a The reader is, however, encouraged to see e.g. Bulíček and Fišerová (2009); Lanzendörfer (2009); Lanzendörfer and Stebel (2011a,b).

^b The fourth combination

$$\left. \begin{aligned} -\mathbf{T}\mathbf{n} \cdot \mathbf{n} &= \mathbf{b}(\mathbf{v} - \mathbf{v}_D) \cdot \mathbf{n} \\ \mathbf{v}_\tau &= (\mathbf{v}_D)_\tau, \end{aligned} \right\}$$

is mentioned in Subsections 1.4.3 and 4.1. We shall omit this case for better readability; the mathematical analysis would not encounter additional difficulties, provided that the Korn inequality was ensured.

^c This is in contrast to the generalized Navier–Stokes case, where a suitable form of $\mathbf{b}(\mathbf{v})$ is needed for the existence of solution, in order to balance the kinetic energy due to the inflow, cf. Lanzendörfer and Stebel (2011a,b).

Bulíček et al., 2009b; Franta et al., 2005; Lanzendörfer, 2009)

$$\int_{\Omega_0} p \, d\mathbf{x} = P_0 \quad (2.4)$$

with $P_0 \in \mathbb{R}$ and Ω_0 being a subset of Ω (e.g., $\Omega_0 \equiv \Omega$). Without loss of generality, we set $P_0 = 0$. For technical reasons, we shall always assume $|\Omega_0| > 0$; however, the condition (2.4) is imposed if and only if $|\Gamma_P| = 0$. One our aim is to show that, instead of imposing (2.4), the pressure level is fixed by the boundary condition (2.3c) as soon as $|\Gamma_P| > 0$.

In the following, the structural assumptions on $\mathbf{S}(p, \mathbf{D}(\mathbf{v}))$ and the assumptions on $\mathbf{b}(\cdot)$ and \mathbf{v}_D are specified and the weak formulation of the problem is defined. The basic *a priori* estimates are derived in the next section, the important relation of the inf–sup inequality to the boundary condition (2.3c) or to the constraint (2.4) is discussed and the Galerkin discrete problem is formulated. After giving the references to the preceeding studies, the existence of solution to the discrete problem, its convergence to the solution of the original problem, and the uniqueness of both are established in Section 2.3.

2.1.1 Structural assumptions (A1)–(A4)

See the basic notation on page ii. We assume that the mapping \mathbf{S} belongs to $C^1(\mathbb{R} \times \mathbb{R}_{sym}^{d \times d}; \mathbb{R}_{sym}^{d \times d})$, is of the form (2.2), and has the following properties:

(A1) For a given $r \in (1, 2)$, there are positive constants C_1, C_2 and ε such that for all $\mathbf{B}, \mathbf{D} \in \mathbb{R}_{sym}^{d \times d}$ and all $p \in \mathbb{R}$:

$$C_1(\varepsilon^2 + |\mathbf{D}|^2)^{\frac{r-2}{2}} |\mathbf{B}|^2 \leq \frac{\partial \mathbf{S}(p, \mathbf{D})}{\partial \mathbf{D}} \cdot (\mathbf{B} \otimes \mathbf{B}) \leq C_2(\varepsilon^2 + |\mathbf{D}|^2)^{\frac{r-2}{2}} |\mathbf{B}|^2,$$

where $(\mathbf{B} \otimes \mathbf{B})_{ijkl} = \mathbf{B}_{ij} \mathbf{B}_{kl}$.

(A2) There is $\gamma_0 \geq 0$ such that for all $\mathbf{D} \in \mathbb{R}_{sym}^{d \times d}$ and for all $p \in \mathbb{R}$:

$$\left| \frac{\partial \mathbf{S}(p, \mathbf{D})}{\partial p} \right| \leq \gamma_0(\varepsilon^2 + |\mathbf{D}|^2)^{\frac{r-2}{4}} \leq \gamma_0 \varepsilon^{\frac{r-2}{2}}.$$

(A3) For a given $0 < \beta \leq 1$ there holds

$$\gamma_0 \varepsilon^{\frac{r-2}{2}} \left(1 + \frac{C_2}{C_1} \right) < \beta.$$

Note that various values of β will be specified.

We will later (in particular in Section 2.3.2 and in Chapter 5) discuss a weaker assumption

(A4) For a given $0 \leq \gamma'_0 < \beta \leq 1$ and for all $\mathbf{D} \in \mathbb{R}_{sym}^{d \times d}$ and $p \in \mathbb{R}$:

$$\left| \frac{\partial \mathbf{S}(p, \mathbf{D})}{\partial p} \right| \leq \gamma'_0.$$

For every $p \in \mathbb{R}$ and $\mathbf{D} \in \mathbb{R}_{\text{sym}}^{d \times d}$ (see Málek et al., 1996, Lemma 1.19 of Chapter 5) there hold (due to **(A1)**)

$$|\mathbf{S}(p, \mathbf{D})| \leq \frac{C_2}{r-1} |\mathbf{D}|^{r-1}, \quad (2.5a)$$

$$\mathbf{S}(p, \mathbf{D}) : \mathbf{D} \geq \frac{C_1}{2r} (|\mathbf{D}|^r - \varepsilon^r). \quad (2.5b)$$

Next, for all $\mathbf{D}^i \in \mathbb{R}_{\text{sym}}^{d \times d}$, or $\mathbf{v}^i \in \mathbf{W}^{1,r}(\Omega)$, $i = 1, 2$, we define the distances

$$\begin{aligned} \hat{d}(\mathbf{D}^1, \mathbf{D}^2)^2 &:= |\mathbf{D}^1 - \mathbf{D}^2|^2 \int_0^1 (\varepsilon^2 + |\mathbf{D}^1 + s(\mathbf{D}^2 - \mathbf{D}^1)|^2)^{\frac{r-2}{2}} ds, \\ d(\mathbf{v}^1, \mathbf{v}^2)^2 &:= \int_{\Omega} \hat{d}(\mathbf{D}(\mathbf{v}^1), \mathbf{D}(\mathbf{v}^2))^2 d\mathbf{x}. \end{aligned}$$

One can show that the following inequalities (see e.g. (Bulíček et al., 2007, Lemma 1.4))

$$\frac{C_1}{2} \hat{d}(\mathbf{D}^1, \mathbf{D}^2)^2 \leq (\mathbf{S}(p^1, \mathbf{D}^1) - \mathbf{S}(p^2, \mathbf{D}^2)) : (\mathbf{D}^1 - \mathbf{D}^2) + \frac{\gamma_0^2}{2C_1} |p^1 - p^2|^2, \quad (2.6a)$$

$$|\mathbf{S}(p^1, \mathbf{D}^1) - \mathbf{S}(p^2, \mathbf{D}^2)| \leq C_2 \hat{d}(\mathbf{D}^1, \mathbf{D}^2) + \gamma_0 |p^1 - p^2|, \quad (2.6b)$$

$$\|\varepsilon + |\mathbf{D}(\mathbf{v}^1)| + |\mathbf{D}(\mathbf{v}^2)|\|_r^{r-2} \|\mathbf{D}(\mathbf{v}^1) - \mathbf{D}(\mathbf{v}^2)\|_r^2 \leq d(\mathbf{v}^1, \mathbf{v}^2)^2 \quad (2.6c)$$

hold (due to **(A1)**, **(A2)**) for all $p^i \in \mathbb{R}$ and $\mathbf{D}^i \in \mathbb{R}_{\text{sym}}^{d \times d}$, or $\mathbf{v}^i \in \mathbf{W}^{1,r}(\Omega)$, $i = 1, 2$.

2.1.2 Boundary conditions

In order to simplify the notation, we define $\Gamma := \Gamma_N \cup \Gamma_P$ and denote

$$\langle \mathbf{b}(\mathbf{u}), \varphi \rangle_{\Gamma} := \int_{\Gamma} \mathbf{b}(\mathbf{u}) \cdot \varphi d\mathbf{x},$$

and treat the behaviour of \mathbf{b} on Γ_N and Γ_P in common. We assume the following properties of $\mathbf{b}(\cdot)$.

(B1) *There exists a constant $\gamma \geq r$ such that the mapping $\mathbf{b}(\cdot) : \mathbf{L}^{\gamma}(\Gamma) \rightarrow \mathbf{L}^{\gamma'}(\Gamma)$ is continuous and bounded.*

(B2) *With some $B_l, B_c \geq 0$,*

$$\langle \mathbf{b}(\mathbf{u}), \mathbf{u} \rangle_{\Gamma} \geq B_c \|\mathbf{u}\|_{\gamma; \Gamma}^{\gamma} - B_l \|\mathbf{u}\|_{\gamma; \Gamma} \quad \text{for all } \mathbf{u} \in \mathbf{L}^{\gamma}(\Gamma), \mathbf{u} \cdot \mathbf{n} = 0 \text{ on } \Gamma_N.$$

If $\gamma > r^{\#}$, then we require the coercivity: $B_c > 0$. Here, $r^{\#} = \frac{(d-1)r}{d-r}$ such that $\text{tr } \mathbf{W}^{1,r}(\Omega) \hookrightarrow \mathbf{L}^{r^{\#}}(\Gamma)$, where tr is the trace operator.

(B3) *For all $\varphi, \mathbf{u}, \{\mathbf{u}_n\}_{n=1}^{\infty}$ uniformly bounded in $\mathbf{L}^{\gamma}(\Gamma)$, such that $\mathbf{u}_n \rightarrow \mathbf{u}$ a.e. on Γ ,*

$$\begin{aligned} \langle \mathbf{b}(\mathbf{u}_n), \varphi \rangle_{\Gamma} &\xrightarrow{n \rightarrow \infty} \langle \mathbf{b}(\mathbf{u}), \varphi \rangle_{\Gamma}, \\ \liminf_{n \rightarrow \infty} \langle \mathbf{b}(\mathbf{u}_n), \mathbf{u}_n \rangle_{\Gamma} &\geq \langle \mathbf{b}(\mathbf{u}), \mathbf{u} \rangle_{\Gamma}, \end{aligned}$$

and, for all $\psi, \{\psi_n\}_{n=1}^{\infty}$ uniformly bounded in $\mathbf{L}^{\gamma^+}(\Gamma)$, $\gamma^+ > \gamma$, such that $\psi_n \rightarrow \psi$ a.e. on Γ ,

$$\langle \mathbf{b}(\mathbf{u}_n), \psi_n \rangle_{\Gamma} \xrightarrow{n \rightarrow \infty} \langle \mathbf{b}(\mathbf{u}), \psi \rangle_{\Gamma}.$$

Properties **(B1)**–**(B3)** can be ensured e.g. by the following pointwise assumptions: Let

$$\mathbf{b}(\cdot) \equiv \mathbf{b}(\mathbf{x}, \cdot) = \mathbf{b}_c(\mathbf{x}, \cdot) + \mathbf{b}_l(\mathbf{x}, \cdot),$$

where, with given $\gamma \geq r$, $\gamma > \gamma_l$, for all $\mathbf{x}, \mathbf{w} \in \mathbb{R}^d$,

$$\begin{aligned} |\mathbf{b}_c(\mathbf{x}, \mathbf{w})| &\leq b_c(\mathbf{x}) + \bar{b}_c |\mathbf{w}|^{\gamma-1}, & \text{with } b_c(\cdot) \in L^{\gamma'}(\Gamma), \bar{b}_c \geq 0, \\ |\mathbf{b}_l(\mathbf{x}, \mathbf{w})| &\leq b_l(\mathbf{x}) + \bar{b}_l |\mathbf{w}|^{\gamma_l-1}, & \text{with } b_l(\cdot) \in L^{\gamma'_l}(\Gamma), \bar{b}_l \geq 0, \\ \mathbf{b}_c(\mathbf{x}, \mathbf{w}) \cdot \mathbf{w} &\geq B_c |\mathbf{w}|^\gamma, & \text{with } B_c \geq 0, \\ \mathbf{b}_l(\mathbf{x}, \mathbf{w}) \cdot \mathbf{w} &\geq -\hat{b}_l(\mathbf{x}) |\mathbf{w}|, & \text{with } \hat{b}_l(\cdot) \in L^{\gamma'_l}(\Gamma). \end{aligned}$$

Indeed, it is easy to verify **(B1)** and **(B2)**. Also, for any $\{\mathbf{u}_n\}_{n=1}^\infty$, $\mathbf{u}, \boldsymbol{\varphi}$ uniformly bounded in $\mathbf{L}^\gamma(\Gamma)$ and $\{\boldsymbol{\psi}_n\}_{n=1}^\infty$, $\boldsymbol{\psi}$ uniformly bounded in $\mathbf{L}^{\gamma^+}(\Gamma)$, $\gamma^+ > \gamma$, such that $\mathbf{u}_n \rightarrow \mathbf{u}$ a.e. on Γ and $\boldsymbol{\psi}_n \rightarrow \boldsymbol{\psi}$ a.e. on Γ ,

$$\begin{aligned} \langle \mathbf{b}(\mathbf{u}_n), \boldsymbol{\varphi} \rangle_\Gamma &\xrightarrow{n \rightarrow \infty} \langle \mathbf{b}(\mathbf{u}), \boldsymbol{\varphi} \rangle_\Gamma, \\ \langle \mathbf{b}(\mathbf{u}_n), \boldsymbol{\psi}_n \rangle_\Gamma &\xrightarrow{n \rightarrow \infty} \langle \mathbf{b}(\mathbf{u}), \boldsymbol{\psi} \rangle_\Gamma, \\ \langle \mathbf{b}_l(\mathbf{u}_n), \mathbf{u}_n \rangle_\Gamma &\xrightarrow{n \rightarrow \infty} \langle \mathbf{b}_l(\mathbf{u}), \mathbf{u} \rangle_\Gamma, \end{aligned}$$

hold due to Vitali's lemma and due to $\gamma_l < \gamma$ and $\gamma^+ > \gamma$, while Fatou's lemma yields

$$\liminf_{n \rightarrow \infty} \langle \mathbf{b}_c(\mathbf{u}_n), \mathbf{u}_n \rangle_\Gamma \geq \langle \mathbf{b}_c(\mathbf{u}), \mathbf{u} \rangle_\Gamma.$$

Further, we assume that the Dirichlet boundary data can be extended on Ω as follows.

(BD) *The function \mathbf{v}_D in (2.3) is the trace of a function \mathbf{v}_0 with the following properties:*

$$\mathbf{v}_0 \in \mathbf{W}^{1,r}(\Omega), \quad \operatorname{div} \mathbf{v}_0 = 0 \quad \text{a.e. in } \Omega, \quad \mathbf{v}_0 = \mathbf{v}_D \quad \text{on } \partial\Omega.$$

2.1.3 Weak formulation

Following the boundary conditions (2.3) with the assumptions **(B1)**–**(BD)**, the constraint (2.4), and (2.5), we define the natural function spaces for the weak solution:

$$\begin{aligned} \mathcal{X}^{r,\gamma} &:= \left\{ \mathbf{w} \in \mathbf{W}^{1,r}(\Omega); \operatorname{tr} \mathbf{w} \big|_{\Gamma_D} = \mathbf{0}, \operatorname{tr} \mathbf{w} \cdot \mathbf{n} \big|_{\Gamma_N} = 0, \operatorname{tr} \mathbf{w} \big|_\Gamma \in \mathbf{L}^\gamma(\Gamma) \right\}, \\ \mathcal{Q}^r &:= \left\{ q \in L^{r'}(\Omega); \text{if } |\Gamma_P| = 0 \text{ then } \int_{\Omega_0} q \, d\mathbf{x} = 0 \right\}. \end{aligned}$$

Let us also denote

$$\|\cdot\|_{(r,\gamma)} := \max\{\|\cdot\|_{1,r}, \|\cdot\|_{\gamma;\Gamma}\}.$$

We use the following variant of the Korn inequality (see Lanzendörfer and Stebel (2011a)). In what follows, we will assume that the inequality (2.7) holds with I_K defined by

$$I_K := \begin{cases} 1, & \text{if } B_c > 0, \\ 0, & \text{if } B_c = 0. \end{cases}$$

Lemma 1 (Korn's inequality). *Let $I_K \in \{0, 1\}$ and $r > 1$. Let Ω , $\partial\Omega$ and Γ_N , Γ_D be as above. Assume that at least one of the following conditions apply:*

- i) $|\Gamma_D| > 0$,*
- ii) $|\Gamma_N| > 0$ and Γ_N is not a part of boundary of any rotational body in \mathbb{R}^d ,*
- iii) $|\Gamma| > 0$ and $I_K = 1$.*

Then the following inequality holds, with $c_K \equiv c_K(\Omega, \Gamma_D, \Gamma_N, \Gamma_P, r)$:

$$\|\mathbf{w}\|_{1,r} \leq c_K (\|\mathbf{D}(\mathbf{w})\|_r + I_K \|\mathbf{w}\|_{r;\Gamma}) \quad \text{for all } \mathbf{w} \in \mathcal{X}^{r,\gamma}. \quad (2.7)$$

Proof. The case *i)* with $\Gamma_D = \partial\Omega$, namely the inequality

$$c(\Omega, s) \|\mathbf{w}\|_{1,s} \leq \|\mathbf{D}(\mathbf{w})\|_s, \quad \text{for any } \mathbf{w} \in \mathbf{W}_0^{1,s}(\Omega), \quad s \in (1, +\infty),$$

can be found e.g. in Málek et al. (1996, Theorem 1.10 on p. 196). Its proof, in fact, covers even *i)* and *ii)* as formulated above; it is merely to notice that a vector field of the form $\mathbf{w} = \mathbf{a} + \mathbf{b} \times \mathbf{x}$ contradicts $\|\mathbf{w}\|_s = 1$ under either of the assumptions $\mathbf{w} = \mathbf{0}$ on Γ_D , or $\mathbf{w} \cdot \mathbf{n} = 0$ on Γ_N , with Γ_D , Γ_N as above.

The following inequality is then stated e.g. in Bulíček et al. (2007, Lemma 1.11),

$$c(\Omega, s) \|\mathbf{w}\|_{1,s} \leq \|\mathbf{D}(\mathbf{w})\|_s + \|\mathbf{w}\|_{2,\partial\Omega}, \quad \text{for any } \mathbf{w} \in \mathbf{W}^{1,s}(\Omega), \quad s \in (1, +\infty),$$

but its proof again covers^d also (2.7), under the assumption *iii)*. □

Let us summarize the general assumptions that will be used throughout this chapter.

Assumption 2. *We assume the following: Let $\Omega \subset \mathbb{R}^d$, $d = 2$ or 3 is a bounded domain, $\partial\Omega = \Gamma_D \cup \Gamma_N \cup \Gamma_P$ where $\partial\Omega$, Γ_D , Γ_N , $\Gamma_P \in C^{0,1}$; let $\Omega_0 \subset \Omega$, $|\Omega_0| > 0$. For given $r \in (1, 2)$ and $\gamma_0 > 0$, $C_1, C_2 > 0$, let **(A1)**–**(A2)** hold true, and the boundary data $(\mathbf{b}(\cdot); B_c, B_l, \gamma)$ meet **(B1)**–**(BD)**. Let $\mathbf{f} \in \mathbf{W}^{1,r}(\Omega)^*$ be given. Assume that the Korn inequality (2.7) is ensured, with $I_K = 1$ allowed only if $B_c > 0$.*

Then, we consider the following weak formulation of the problem (2.1)–(2.4).

Problem (P). *Find the pair (\mathbf{v}, p) such that $\mathbf{u} := (\mathbf{v} - \mathbf{v}_0) \in \mathcal{X}^{r,\gamma}$, $p \in \mathcal{Q}^r$ and*

$$(\xi, \operatorname{div} \mathbf{v})_\Omega = 0 \quad \text{for all } \xi \in \mathcal{Q}^r, \quad (2.8a)$$

$$(\mathbf{S}(p, \mathbf{D}(\mathbf{v})), \mathbf{D}(\boldsymbol{\varphi}))_\Omega - (p, \operatorname{div} \boldsymbol{\varphi})_\Omega = \langle \mathbf{f}, \boldsymbol{\varphi} \rangle - \langle \mathbf{b}(\mathbf{u}), \boldsymbol{\varphi} \rangle_\Gamma \quad \text{for all } \boldsymbol{\varphi} \in \mathcal{X}^{r,\gamma}. \quad (2.8b)$$

Note that $\langle \mathbf{b}(\mathbf{u}), \boldsymbol{\varphi} \rangle_\Gamma = \int_{\Gamma_N} \mathbf{b}(\mathbf{v} - \mathbf{v}_D)_\tau \cdot \boldsymbol{\varphi}_\tau \, d\mathbf{x} + \int_{\Gamma_P} \mathbf{b}(\mathbf{v} - \mathbf{v}_D) \cdot \boldsymbol{\varphi} \, d\mathbf{x}$ for all $\mathbf{u}, \boldsymbol{\varphi} \in \mathcal{X}^{r,\gamma}$, cf. (2.3). All integrals in (2.8) are finite, due to (2.5a) and **(BD)**, **(B1)**.

^dActually, for any $|\Gamma| > 0$, $\Gamma \subset \partial\Omega$ not lying on boundary of any rotational body, one can also see that $c(\Omega, \Gamma, s) \|\mathbf{w}\|_{1,s} \leq \|\mathbf{D}(\mathbf{w})\|_s + \|\mathbf{w} \cdot \mathbf{n}\|_{s;\Gamma}$.

2.2 Central features and discrete approximation

2.2.1 A priori estimates

In order to motivate what follows, let us briefly describe the basic structure of the problem by outlining the *a priori* estimates. Testing the weak formulation by solution, i.e. setting $\xi := p$ in (2.8a) and $\varphi := \mathbf{u}$ in (2.8b) and summing the equations, recalling that $\operatorname{div} \mathbf{v}_0 = 0$, we obtain

$$(\mathbf{S}(p, \mathbf{D}(\mathbf{v})), \mathbf{D}(\mathbf{u}))_{\Omega} + \langle \mathbf{b}(\mathbf{u}), \mathbf{u} \rangle_{\Gamma} = \langle \mathbf{f}, \mathbf{u} \rangle.$$

Applying (2.5) and the Hölder and Young inequalities we observe

$$\begin{aligned} (\mathbf{S}(p, \mathbf{D}(\mathbf{v})), \mathbf{D}(\mathbf{v}) - \mathbf{D}(\mathbf{v}_0))_{\Omega} &\geq \frac{C_1}{2r} (\|\mathbf{D}(\mathbf{v})\|_r^r - |\Omega| \varepsilon^r) - \frac{C_2}{r-1} \|\mathbf{D}(\mathbf{v}_0)\|_r \|\mathbf{D}(\mathbf{v})\|_r^{r-1} \\ &\geq \frac{C_1}{2r} \|\mathbf{D}(\mathbf{u})\|_r^r - C(1 + \|\mathbf{D}(\mathbf{u})\|_r^{r-1}) \geq C \|\mathbf{D}(\mathbf{u})\|_r^r - C. \end{aligned}$$

By C we always denote generic constants, positive and finite. Above, C depend on Ω , r , C_1 , C_2 , ε and $\|\mathbf{v}_0\|_{1,r}$.

Next, we apply **(B2)** and distinguish two cases: If $B_c = 0$ then we require $\gamma \leq r^\#$ and $I_K = 0$ in the Korn inequality (2.7) (the cases i) and ii) in Lemma 1). Using the embedding $\operatorname{tr} \mathbf{W}^{1,r}(\Omega) \hookrightarrow L^\gamma(\Gamma)$ and (2.7), we obtain

$$C \|\mathbf{D}(\mathbf{u})\|_r^r + \langle \mathbf{b}(\mathbf{u}), \mathbf{u} \rangle_{\Gamma} \geq C \|\mathbf{u}\|_{1,r}^r - B_l \|\mathbf{u}\|_{\gamma;\Gamma} \geq C \|\mathbf{u}\|_{1,r}^r - C.$$

If $B_c > 0$ then we do not need the embedding and we also allow for $I_K = 1$ in (2.7). Since $\gamma > r$, we obtain

$$C \|\mathbf{D}(\mathbf{u})\|_r^r + \langle \mathbf{b}(\mathbf{u}), \mathbf{u} \rangle_{\Gamma} \geq C \|\mathbf{D}(\mathbf{u})\|_r^r + \left(\frac{B_c}{2} \|\mathbf{u}\|_{\gamma;\Gamma}^\gamma + C \|\mathbf{u}\|_{r;\Gamma}^r - C\right) \geq C \|\mathbf{u}\|_{1,r}^r + \frac{B_c}{2} \|\mathbf{u}\|_{\gamma}^\gamma - C.$$

Here, C depend also on Γ_D , Γ_N , Γ_P , γ , and B_l , B_c .

By combining the inequalities above and using again (2.5a) to estimate $\|\mathbf{S}(p, \mathbf{D}(\mathbf{v}))\|_{r'}$, we arrive at the *a priori* estimate

$$\|\mathbf{v}\|_{1,r} + \|\mathbf{S}(p, \mathbf{D}(\mathbf{v}))\|_{r'} + \|\mathbf{u}\|_{\gamma;\Gamma} \leq K_{\mathbf{v}}, \quad (2.9)$$

with $K_{\mathbf{v}}$ depending on Ω , Γ_D , Γ_N , Γ_P , r , γ , C_1 , C_2 , ε , B_c , B_l , $\|\mathbf{v}_0\|_{1,r}$ and $\|\mathbf{f}\|_{\mathbf{W}^{1,r}(\Omega)^*}$.

Note that since the pressure p is involved in the nonlinear term $\mathbf{S}(p, \mathbf{D}(\mathbf{v}))$, we need also some *a priori* bound of the pressure. Using the last estimate and applying (2.5a), **(B1)** and the Hölder inequality to the equation (2.8b), we observe

$$\begin{aligned} (p, \operatorname{div} \varphi)_{\Omega} &\leq \|\mathbf{S}(p, \mathbf{D}(\mathbf{v}))\|_{r'} \|\mathbf{D}(\varphi)\|_r + \|\mathbf{f}\|_{\mathbf{W}^{1,r}(\Omega)^*} \|\varphi\|_{1,r} + \|\mathbf{b}(\mathbf{u})\|_{\gamma;\Gamma} \|\varphi\|_{\gamma;\Gamma} \\ &\leq C (\|\varphi\|_{1,r} + \|\varphi\|_{\gamma;\Gamma}) \end{aligned}$$

for all $\varphi \in \mathcal{X}^{r,\gamma}$. Suppose that we can find $\tilde{\varphi} \in \mathcal{X}^{r,\gamma}$ and $\beta > 0$ such that

$$\beta \|p\|_{r'} (\|\tilde{\varphi}\|_{1,r} + \|\tilde{\varphi}\|_{\gamma;\Gamma}) \leq (p, \operatorname{div} \tilde{\varphi})_{\Omega}. \quad (2.10)$$

This finally gives us the desired *a priori* bound

$$\beta \|p\|_{r'} \leq K_p, \quad (2.11)$$

with K_p depending on $K_{\mathbf{v}}$, $\|\mathbf{f}\|_{\mathbf{W}^{1,r}(\Omega)^*}$ and on $\sup_{\|\mathbf{u}\|_{\gamma;\Gamma} \leq K_{\mathbf{v}}} \|\mathbf{b}(\mathbf{u})\|_{\gamma';\Gamma}$, which is bounded due to **(B1)**.

Note that (2.9) and (2.11) are consistent with the choice of the spaces $\mathcal{X}^{r,\gamma}$ and \mathcal{Q}^r . We also remark that while deriving the estimates, Assumption **(A2)** has not been used; the viscosity–pressure dependence has been controlled by **(A1)**.

Most importantly, mind that (2.11) relies on the inequality (2.10). It may seem that we did not encounter the requirements concerning how the pressure level is fixed (i.e. the restrictions (2.3c) or (2.4)); this issue is also connected with the inequality (2.10).

2.2.2 Inf–sup inequality; pressure and boundary conditions

The inequality (2.10) is the result of Corollary 6 proven below, which is crucial to the analysis of **(P)**. Note that the corollary not only allows for the *a priori* estimate (2.11), but it is used several more times in the sequel analysis. Its proof reveals the relation between the boundary conditions and the pressure.

First, let us define the “inner flow” spaces

$$\begin{aligned} \overline{\mathcal{X}}^{r,\gamma} &:= \{\mathbf{w} \in \mathcal{X}^{r,\gamma}; \operatorname{tr} \mathbf{w} \cdot \mathbf{n}|_{\Gamma} = 0\}, \\ \overline{\mathcal{Q}}_{\Omega_*}^r &:= L_{0;\Omega_*}^{r'}(\Omega) = \{q \in L^{r'}(\Omega); \int_{\Omega_*} q \, d\mathbf{x} = 0\}, \end{aligned}$$

where $\Omega_* \subset \Omega$, $|\Omega_*| > 0$. Note that if $|\Gamma_P| = 0$ then $(\overline{\mathcal{X}}^{r,\gamma}, \overline{\mathcal{Q}}_{\Omega_0}^r) = (\mathcal{X}^{r,\gamma}, \mathcal{Q}^r)$. Note that for any $\mathbf{w} \in \overline{\mathcal{X}}^{r,\gamma}$ there holds $\int_{\Omega} \operatorname{div} \mathbf{w} \, d\mathbf{x} = \int_{\partial\Omega} \mathbf{w} \cdot \mathbf{n} \, d\mathbf{x} = 0$.

The basic tool related to the inequality (2.10) is the following

Lemma 3. *Let Ω , Γ_D , Γ be as in Assumption 2, let $s \in (1, \infty)$ and $\nu \in \langle 1, \infty \rangle$. Then there exists a continuous linear operator $\overline{\mathcal{B}} : L_0^s(\Omega) \rightarrow \overline{\mathcal{X}}^{s,\nu}$ and a constant $\overline{C}_{\operatorname{div}}(s, \nu)$ (depending also on Ω and Γ) such that for all $f \in L_0^s(\Omega)$:*

$$\operatorname{div}(\overline{\mathcal{B}}f) = f \quad \text{a.e. in } \Omega, \quad \|\overline{\mathcal{B}}f\|_{(s,\nu)} \leq \overline{C}_{\operatorname{div}}(s, \nu) \|f\|_s. \quad (2.12)$$

Proof. The following result is well-known: there exists a continuous linear operator $\mathcal{B} : L_0^s(\Omega) \rightarrow \mathbf{W}_0^{1,s}(\Omega)$ such that for all $f \in L_0^s(\Omega)$:

$$\operatorname{div}(\mathcal{B}f) = f \quad \text{a.e. in } \Omega, \quad \|\mathcal{B}f\|_{1,s} \leq C_{\operatorname{div}}(s) \|f\|_s,$$

where $C_{\operatorname{div}}(s)$ depends on s and Ω . See Novotný and Straškraba (2004, Lemma 3.17) or Amrouche and Girault (1994); Bogovskii (1980). Since $\mathbf{W}_0^{1,s}(\Omega) \subset \overline{\mathcal{X}}^{s,\nu}$, this implies that (2.12) holds, e.g., with $\overline{C}_{\operatorname{div}}(s, \nu) := C_{\operatorname{div}}(s)$. \square

While the above proof is based on the properties of the divergence operator on $\mathbf{W}_0^{1,s}(\Omega)$, it is worth noting that an alternative approach has been used in the case of Navier’s slip boundary conditions, i.e., with $|\Gamma_D| = 0$, using the solution to the Neumann problem with the Laplace

operator, cf. (1.30)–(1.33) in Bulíček et al. (2007) or (2.24)–(2.27) in Bulíček et al. (2009b). One can consider a linear operator $\mathcal{N}_\Omega^{-1} : L_0^s(\Omega) \rightarrow \{u \in W^{2,s}(\Omega), \nabla u \cdot \mathbf{n} = 0 \text{ on } \partial\Omega\}$ and a constant $C_{\text{reg}}(s)$ (depending also on Ω) such that for all $f \in L_0^s(\Omega)$,

$$\operatorname{div}(\nabla \mathcal{N}_\Omega^{-1}(f)) = f \quad \text{a.e. in } \Omega, \quad \|\nabla \mathcal{N}_\Omega^{-1}(f)\|_{1,s} \leq C_{\text{reg}}(s) \|f\|_s.$$

It could be interesting to specify the operator $\bar{\mathcal{B}}$ more precisely in our setting (which combines the *no-slip* and *slip* boundary parts), and to estimate the optimal value of $\bar{C}_{\text{div}}(s, \nu)$, but we do not address that question here. One easily observes

$$C_{\text{reg}}(s) \leq \bar{C}_{\text{div}}(s, \nu) \leq C_{\text{div}}(s), \quad \text{for all } s \in (1, \infty), \nu \in (1, \infty). \quad (2.13)$$

We use the above lemma to show the inequality more fitting to our needs (especially to the discrete spaces discussed later) in the following

Corollary 4. *Let Ω, Γ_D, Γ be as in Assumption 2 and $\Omega_* \subset \Omega, |\Omega_*| > 0$. For any $s \in (1, \infty)$ and $\nu \in (1, \infty)$ there exists a constant $\beta_{\Omega_*}(s, \nu)$ (depending also on Ω, Ω_* and Γ) such that*

$$0 < \beta_{\Omega_*}(s, \nu) \leq \inf_{q \in \bar{\mathcal{Q}}_{\Omega_*}^s} \sup_{\mathbf{w} \in \bar{\mathcal{X}}^{s,\nu}} \frac{(q, \operatorname{div} \mathbf{w})_\Omega}{\|q\|_{s'} \|\mathbf{w}\|_{(s,\nu)}}. \quad (2.14)$$

Proof. For any $q \in \bar{\mathcal{Q}}_{\Omega_*}^s$, set $q = q_0 + (\int_\Omega q \, d\mathbf{x})$, so that $q_0 \in L_0^{s'}(\Omega)$. (Note that if $\Omega_* = \Omega$ then $q = q_0$.) Recall Lemma 3 and set $\mathbf{w} := \bar{\mathcal{B}}(|q_0|^{s'-2} q_0 - \int_\Omega |q_0|^{s'-2} q_0 \, d\mathbf{x})$, implying that $\mathbf{w} \in \bar{\mathcal{X}}^{s,\nu}$ and $(q, \operatorname{div} \mathbf{w})_\Omega = \|q_0\|_{s'}^{s'}$. Similarly as in Bulíček et al. (2009b) we observe by contradiction and since $\int_{\Omega_*} q \, d\mathbf{x} = 0$ and $\int_\Omega q_0 \, d\mathbf{x} = 0$ that $\|q\|_{s'} \sim \|q_0\|_{s'}$, with the constants depending on Ω, Ω_* and s . Hence, $\|q_0\|_{s'}^{s'} \geq C \|q\|_{s'}^{s'}$ and $\| |q_0|^{s'-2} q_0 - \int_\Omega |q_0|^{s'-2} q_0 \, d\mathbf{x} \|_s \leq C \|q\|_{s'}^{s'-1}$, concluding that (2.14) holds with $\beta_{\Omega_*}(s, \nu)$ depending on $\Omega, \Omega_*, \Gamma, s$ and ν . \square

Remark 5. *For $s = 2$, we observe that*

$$\beta_{\Omega_0}(2, \nu) \geq \frac{|\Omega_0|}{|\Omega|} \beta_\Omega(2, \nu) \geq \frac{|\Omega_0|}{|\Omega|} \frac{1}{\bar{C}_{\text{div}}(2, \nu)} \geq \frac{|\Omega_0|}{|\Omega|} \frac{1}{C_{\text{div}}(2)}. \quad (2.15)$$

Proof. We repeat the procedure above. Same as in Bulíček et al. (2009b), since $\int_{\Omega_0} q \, d\mathbf{x} = 0$, we note that

$$\|q_0\|_2^2 = \|q\|_2^2 - \frac{1}{|\Omega|} \left(\int_\Omega q \, d\mathbf{x} \right)^2 = \|q\|_2^2 - \frac{1}{|\Omega|} \left(\int_{\Omega \setminus \Omega_0} q \, d\mathbf{x} \right)^2 \geq \frac{|\Omega_0|}{|\Omega|} \|q\|_2^2$$

and that $\|q\|_2 \geq \|q_0\|_2$. Since $\mathbf{w} = \bar{\mathcal{B}}(q_0)$, and due to (2.13), the assertion follows. \square

In the case $|\Gamma_P| = 0$, i.e. if no free flow through the boundary is allowed, Corollary 4 with $\Omega_* = \Omega_0$ ensures the important inequality (2.10). We can also see why the constraint (2.4) is required: obviously,

$$\inf_{q \in L^{s'}(\Omega)} \sup_{\mathbf{w} \in \bar{\mathcal{X}}^{s,\nu}} \frac{(q, \operatorname{div} \mathbf{w})_\Omega}{\|q\|_{s'} \|\mathbf{w}\|_{(s,\nu)}} = 0.$$

However, if $|\Gamma_P| > 0$ then the constraint (2.4) is redundant^e, as shows the following generalization of Corollary 4:

^e And, as follows later from Theorem 12, it is inappropriate then.

Corollary 6. *Let $\Omega, \Gamma_D, \Gamma_N$ and Γ_P be as in Assumption 2. For any $s \in (1, \infty)$ and $\nu \in \langle 1, \infty \rangle$ there exists a constant $\beta(s, \nu)$ (depending also on $\Omega, \Omega_0, \Gamma_N$ and Γ_P) such that*

$$0 < \beta(s, \nu) \leq \inf_{q \in \mathcal{Q}^s} \sup_{\mathbf{w} \in \mathcal{X}^{s, \nu}} \frac{(q, \operatorname{div} \mathbf{w})_\Omega}{\|q\|_{s'} \|\mathbf{w}\|_{(s, \nu)}}. \quad (2.16)$$

Proof. Since if $|\Gamma_P| = 0$ then $(\overline{\mathcal{X}}^{s, \nu}, \overline{\mathcal{Q}}_{\Omega_0}^s) = (\mathcal{X}^{s, \nu}, \mathcal{Q}^s)$, the assertion follows from Corollary 4 by setting $\beta(s, \nu) := \beta_{\Omega_0}(s, \nu)$. It remains to show (2.16) for $|\Gamma_P| > 0$, see e.g. Haslinger and Stebel (2011); Hirn et al. (2010).

For any $q \in \mathcal{Q}^s = L^{s'}(\Omega)$, we write $q = q_0 + (\int_\Omega q \, d\mathbf{x})$. Since $q_0 \in L_0^{s'}(\Omega) = \overline{\mathcal{Q}}_\Omega^s$ and due to (2.14), there exists $\mathbf{w}_0 \in \overline{\mathcal{X}}^{s, \nu}$, $\|\mathbf{w}_0\|_{(s, \nu)} = 1$, such that $\beta_\Omega(s, \nu) \|q_0\|_{s'} \leq (q_0, \operatorname{div} \mathbf{w}_0)_\Omega = (q, \operatorname{div} \mathbf{w}_0)_\Omega$. Since $\Gamma_P \in C^{0,1}$, $|\Gamma_P| > 0$, there exists some $\boldsymbol{\xi} \in \mathcal{X}^{s, \nu}$ such that $\int_\Omega \operatorname{div} \boldsymbol{\xi} \, d\mathbf{x} = \int_{\Gamma_P} \boldsymbol{\xi} \cdot \mathbf{n} \, d\mathbf{x} = 1$. Taking

$$\mathbf{w} := \mathbf{w}_0 + \delta \operatorname{sign}(\int_\Omega q \, d\mathbf{x}) \boldsymbol{\xi}, \quad \text{with } \delta := \frac{\beta_\Omega(s, \nu) |\Omega|^{1/s'}}{1 + |\Omega|^{1/s'} \|\operatorname{div} \boldsymbol{\xi}\|_s},$$

we observe $\mathbf{w} \in \mathcal{X}^{s, \nu}$, and by using $\|q\|_{s'} \leq \|q_0\|_{s'} + |\Omega|^{1/s'} |\int_\Omega q \, d\mathbf{x}|$ we obtain:

$$\begin{aligned} (q, \operatorname{div} \mathbf{w})_\Omega &= (q, \operatorname{div} \mathbf{w}_0)_\Omega + \delta \operatorname{sign}(\int_\Omega q \, d\mathbf{x}) (q_0, \operatorname{div} \boldsymbol{\xi})_\Omega + \delta |\int_\Omega q \, d\mathbf{x}| (1, \operatorname{div} \boldsymbol{\xi})_\Omega \\ &\geq \beta_\Omega(s, \nu) \|q_0\|_{s'} - \delta \|q_0\|_{s'} \|\operatorname{div} \boldsymbol{\xi}\|_s + \delta |\int_\Omega q \, d\mathbf{x}| \\ &\geq \frac{\beta_\Omega(s, \nu)}{1 + |\Omega|^{1/s'} \|\operatorname{div} \boldsymbol{\xi}\|_s} \|q\|_{s'}. \end{aligned}$$

Finally, since $\|\mathbf{w}\|_{(s, \nu)} \leq 1 + \delta \|\boldsymbol{\xi}\|_{(s, \nu)}$ we conclude that (2.16) hold e.g. with

$$\beta(s, \nu) := \frac{\beta_\Omega(s, \nu)}{1 + |\Omega|^{1/s'} \|\operatorname{div} \boldsymbol{\xi}\|_s + \beta_\Omega(s, \nu) |\Omega|^{1/s'} \|\boldsymbol{\xi}\|_{(s, \nu)}}. \quad (2.17)$$

□

Remark 7. *In some previous studies (see Lanzendörfer and Stebel, 2011a,b), the inf-sup inequality has not been formulated, but (for $|\Gamma_P| > 0$) a modified operator $\tilde{\mathcal{B}}$ is applied instead: Starting e.g. with $\overline{\mathcal{B}}$ from Lemma 3, one considers $\tilde{\mathcal{B}}f := \overline{\mathcal{B}}(f - (\int_\Omega f \, d\mathbf{x}) \operatorname{div} \boldsymbol{\xi}) + (\int_\Omega f \, d\mathbf{x}) \boldsymbol{\xi}$ with the estimate $\|\tilde{\mathcal{B}}f\|_{1, s} + \|\tilde{\mathcal{B}}f\|_{\nu; \Gamma} \leq \tilde{C}_{\operatorname{div}}(s, \nu) \|f\|_s$ (cf. Lemma 2.4 in Lanzendörfer and Stebel (2011b) for the case $|\Gamma_N| = 0$). We remark that this approach is equivalent: similarly as in Remark 5, with $\beta(s, \nu)$ defined by (2.17) one observes*

$$\beta(s, \nu) = \frac{1}{\tilde{C}_{\operatorname{div}}(s, \nu)}.$$

Indeed: Obviously, $\tilde{\mathcal{B}}: \mathcal{Q}^s \rightarrow \mathcal{X}^{s, \nu}$ and, for any $f \in \mathcal{Q}^s = L^{s'}(\Omega)$,

$$\|\tilde{\mathcal{B}}f\|_{(s, \nu)} \leq \overline{C}_{\operatorname{div}}(s, \nu) \|f - (\int_\Omega f \, d\mathbf{x}) \operatorname{div} \boldsymbol{\xi}\|_s + |\int_\Omega f \, d\mathbf{x}| \|\boldsymbol{\xi}\|_{(s, \nu)} \leq \tilde{C}_{\operatorname{div}}(s, \nu) \|f\|_s,$$

where

$$\tilde{C}_{\operatorname{div}}(s, \nu) := \overline{C}_{\operatorname{div}}(s, \nu) (1 + |\Omega|^{1/s'} \|\boldsymbol{\xi}\|_s) + |\Omega|^{1/s'} \|\boldsymbol{\xi}\|_{(s, \nu)}.$$

Setting $\mathbf{w} := \tilde{\mathcal{B}}(|q|^{s'-2} q)$ we easily observe

$$\frac{(q, \operatorname{div} \mathbf{w})_\Omega}{\|q\|_{s'} \|\mathbf{w}\|_{(s, \nu)}} \geq \frac{1}{\tilde{C}_{\operatorname{div}}(s, \nu)}.$$

□

Corollary 6 provides (2.10), implying the *a priori* estimates (2.9), (2.11) with $\beta := \beta(r, \gamma)$ for Problem **(P)**.

2.2.3 Galerkin approximation and inf–sup conditions

For given $h > 0$, let \mathbf{X}_h, Y_h be finite-dimensional spaces and let

$$\mathcal{X}_h^{r,\gamma} := \mathbf{X}_h \cap \mathcal{X}^{r,\gamma}, \quad \mathcal{Q}_h^r := Y_h \cap \mathcal{Q}^r.$$

At the moment, we do not specify the choice of \mathbf{X}_h, Y_h and do not impose any particular meaning on the parameter h (although the inspiration by finite elements is obvious). We only require that the families $\{\mathcal{X}_h^{r,\gamma}\}_{h>0}, \{\mathcal{Q}_h^r\}_{h>0}$ are dense in $\mathcal{X}^{r,\gamma}, \mathcal{Q}^r$, respectively, i.e.

$$\lim_{h \searrow 0} \inf_{\mathbf{w}_h \in \mathcal{X}_h^{r,\gamma}} \|\mathbf{w} - \mathbf{w}_h\|_{1,r} = \lim_{h \searrow 0} \inf_{q_h \in \mathcal{Q}_h^r} \|q - q_h\|_{r'} = 0 \quad \text{for all } \mathbf{w} \in \mathcal{X}^{r,\gamma} \text{ and } q \in \mathcal{Q}^r. \quad (2.18)$$

The Galerkin approximation of **(P)** consists in replacing $\mathcal{X}^{r,\gamma}, \mathcal{Q}^r$ by their finite dimensional subspaces $\mathcal{X}_h^{r,\gamma}, \mathcal{Q}_h^r$:

Problem (\mathbf{P}_h) . Find (\mathbf{v}_h, p_h) such that $\mathbf{u}_h := (\mathbf{v}_h - \mathbf{v}_{h,0}) \in \mathcal{X}_h^{r,\gamma}, p_h \in \mathcal{Q}_h^r$ and

$$(\xi_h, \operatorname{div} \mathbf{v}_h)_\Omega = 0 \quad \text{for all } \xi_h \in \mathcal{Q}_h^r, \quad (2.19a)$$

$$(\mathbf{S}(p_h, \mathbf{D}(\mathbf{v}_h)), \mathbf{D}(\boldsymbol{\varphi}_h))_\Omega - (p_h, \operatorname{div} \boldsymbol{\varphi}_h)_\Omega = \langle \mathbf{f}, \boldsymbol{\varphi}_h \rangle - \langle \mathbf{b}(\mathbf{u}_h), \boldsymbol{\varphi}_h \rangle_\Gamma \quad \text{for all } \boldsymbol{\varphi}_h \in \mathcal{X}_h^{r,\gamma}. \quad (2.19b)$$

Here, $\mathbf{v}_{h,0}$ is an approximation of the Dirichlet data which satisfies

$$(\xi_h, \operatorname{div} \mathbf{v}_{h,0})_\Omega = 0 \quad \text{for all } \xi_h \in \mathcal{Q}_h^r \quad \text{and} \quad \lim_{h \searrow 0} \|\mathbf{v}_0 - \mathbf{v}_{h,0}\|_{1,r} = 0. \quad (2.20)$$

For example, $\mathbf{v}_{h,0} \in \mathbf{X}_h$ is typical in the finite elements setting; but one can also simply consider $\mathbf{v}_{h,0} = \mathbf{v}_0$.

Let us consider the *a priori* estimates for the discrete problem **(P_h)**. Obviously, since we can test the equations (2.19) by the discrete solution, we obtain exactly (2.9) also for the discrete solution. However, in order to obtain the pressure estimate we need to ensure (2.10) on the discrete level, i.e. with $\tilde{\boldsymbol{\varphi}} \in \mathcal{X}_h^{r,\gamma}$. In contrast to the continuous level, where (2.10) is ensured by Corollary 6, here the inequality involves an additional constraint for the choice of discrete spaces \mathbf{X}_h and Y_h .

In the following, we require for given $s \in (1, \infty)$ and $\nu \in \langle 1, \infty \rangle$ that the families of spaces $\{\mathcal{X}_h^{s,\nu}\}_{h>0}, \{\mathcal{Q}_h^s\}_{h>0}$ satisfy the discrete inf–sup condition, cf. (2.16):

(IS^{s,ν}) There exists a constant $\tilde{\beta}(s, \nu)$ independent of h such that

$$0 < \tilde{\beta}(s, \nu) \leq \inf_{q \in \mathcal{Q}_h^s} \sup_{\mathbf{w} \in \mathcal{X}_h^{s,\nu}} \frac{(q, \operatorname{div} \mathbf{w})_\Omega}{\|q\|_{s'} \|\mathbf{w}\|_{(s,\nu)}}.$$

The value of $\tilde{\beta}(s, \nu)$ (and existence of such positive number) depends on the particular choice of the discrete spaces \mathbf{X}_h, Y_h . In the finite element discretization, this is an important issue.

For the purpose of our existence analysis, namely in the proof of Corollary 15, we utilize favourable Galerkin spaces for which the value of the discrete $\tilde{\beta}$ (almost) equals to β of the continuous level, see Lemma 9 below. Let us emphasize that the value of β represents an important constraint on the model, see the assumptions of Theorems 12, 14 and of Corollary 15. In view of this, it is worth noting (from (2.17) in the case $|\Gamma_P| > 0$ and from (2.15) in the case $|\Gamma_P| = 0$) that $\beta(s, \nu)$ can possibly be much less than $\beta_\Omega(s, \nu)$ (although (2.17) and (2.15) prove only the lower bound for $\beta(s, \nu)$).

Therefore, in a hope that $\beta_\Omega(s, \nu) \geq \beta(s, \nu)$, we formulate also the following variant of the discrete inf-sup condition, cf. (2.14):

($\mathbf{IS}_\Omega^{s, \nu}$) *There exists a constant $\tilde{\beta}_\Omega(s, \nu)$ independent of h such that*

$$0 < \tilde{\beta}_\Omega(s, \nu) \leq \inf_{q \in Y_h \cap \overline{\mathcal{Q}}_\Omega^s} \sup_{\mathbf{w} \in \mathbf{X}_h \cap \overline{\mathcal{X}}^{s, \nu}} \frac{(q, \operatorname{div} \mathbf{w})_\Omega}{\|q\|_{s'} \|\mathbf{w}\|_{(s, \nu)}}.$$

Remind that $\overline{\mathcal{Q}}_\Omega^s = L_0^s(\Omega)$ and note that if $|\Gamma_P| = 0$ and $\Omega_0 = \Omega$ then **($\mathbf{IS}_\Omega^{s, \nu}$)** is exactly **($\mathbf{IS}^{s, \nu}$)**. In general, **($\mathbf{IS}_\Omega^{s, \nu}$)** need not be implied by **($\mathbf{IS}^{s, \nu}$)** and vice versa.

In Theorem 14 we will apply **($\mathbf{IS}_\Omega^{s, \nu}$)** by means of the following

Remark 8. *Let $r \in (1, 2)$, $\nu \in \langle 1, \infty \rangle$ and let **($\mathbf{IS}_\Omega^{2, \nu}$)** hold. Then, for all $q \in \mathcal{Q}_h^r$,*

$$\tilde{\beta}_\Omega(2, \nu) \left(\|q\|_2 - |\Omega|^{1/2} |f_\Omega q \, d\mathbf{x}| \right) \leq \sup_{\mathbf{w} \in \mathbf{X}_h \cap \overline{\mathcal{X}}^{2, \nu}} \frac{(q, \operatorname{div} \mathbf{w})_\Omega}{\|\mathbf{w}\|_{(2, \nu)}}. \quad (2.21)$$

Indeed: For arbitrary $q \in \mathcal{Q}_h^r \subset L^2(\Omega)$, we can write $q = q_0 + (f_\Omega q \, d\mathbf{x})$, where^f $q_0 \in Y_h \cap L_0^2(\Omega) = Y_h \cap \overline{\mathcal{Q}}_\Omega^2$. Since $\|q\|_2 \leq \|q_0\|_2 + |\Omega|^{1/2} |f_\Omega q \, d\mathbf{x}|$, and $\overline{\mathcal{X}}^{2, \nu} \subset \mathcal{X}^{2, \nu}$, we obtain (2.21) from **($\mathbf{IS}_\Omega^{2, \nu}$)**. \square

Lemma 9. *Let Ω , Γ_D , Γ_N , Γ_P , Ω_0 and r, γ be as in Assumption 2. Then, for any $\delta > 0$ (small), there exists a family of finite-dimensional spaces $\{\mathbf{X}_{h_n}\}_{h_n > 0}$, $\{Y_{h_n}\}_{h_n > 0}$, $h_n \searrow 0$, satisfying (2.18) and **($\mathbf{IS}_\Omega^{r, \gamma}$)**, **($\mathbf{IS}_\Omega^{2, \gamma}$)** with*

$$\tilde{\beta}(r, \gamma) \geq \beta(r, \gamma) - \delta \quad \text{and} \quad \tilde{\beta}_\Omega(2, \gamma) \geq \beta_\Omega(2, \gamma) - \delta. \quad (2.22)$$

Proof. Consider arbitrary $h_n \searrow 0$, $n = 1, \dots$. Since $\overline{\mathcal{X}}^{2, \gamma}$, $\mathcal{X}^{r, \gamma}$, \mathcal{Q}^r are separable Banach spaces with the bases $\{\bar{\mathbf{w}}_n\}_{n=1}^\infty$, $\{\mathbf{w}_n\}_{n=1}^\infty$, $\{q_n\}_{n=1}^\infty$, respectively, and since $\overline{\mathcal{X}}^{2, \gamma} \subset \mathcal{X}^{r, \gamma}$, we can define Galerkin spaces by $\mathbf{X}^m := \operatorname{span}\{\bar{\mathbf{w}}_i, \mathbf{w}_i\}_{i=1}^m$ and $Y^n := \operatorname{span}\{q_i\}_{i=1}^n$, $m, n = 1, \dots$, obviously allowing for the density (2.18). In order to ensure the discrete inf-sup conditions with (2.22), we only need to choose suitable pairs of the spaces, i.e. to any discrete pressure space to assign a rich enough discrete velocity space. We show this only for **($\mathbf{IS}_\Omega^{2, \gamma}$)** and $(2.22)_2$, the inclusion of **($\mathbf{IS}^{r, \gamma}$)** is obvious.

Due to the density and Corollary 4, for any $q \in \overline{\mathcal{Q}}_\Omega^2$ there exists $k(q)$ such that

$$\beta_\Omega(2, \gamma) - \delta \leq \sup_{\mathbf{w} \in \mathbf{X}^{k(q)} \cap \overline{\mathcal{X}}^{2, \gamma}} \frac{(q, \operatorname{div} \mathbf{w})_\Omega}{\|q\|_2 \|\mathbf{w}\|_{(2, \gamma)}}$$

^f Here we silently assume that constants belong to Y_h .

(we choose minimal such $k(q)$). For n fixed, define $m(n) := \sup_{\{q \in Y^n \cap \overline{\mathcal{Q}}_\Omega^2\}} k(q)$. It is easy to see that $Y_{h_n} := Y^n$ and $\mathbf{X}_{h_n} := \mathbf{X}^{m(n)}$ satisfy $(\mathbf{IS}_\Omega^{2,\gamma})$ and $(2.22)_2$. It remains to prove that $m(n)$ is finite, which we show by contradiction: Let $m(n)$ be infinite, then we find a sequence $q_j \in Y^n \cap \overline{\mathcal{Q}}_\Omega^2$, $\|q_j\|_2 = 1$, $j = 1, \dots$, such that $k(q_j) > j$ and

$$\sup_{\mathbf{w} \in \mathbf{X}^j \cap \overline{\mathcal{X}}^{2,\gamma}} \frac{(q_j, \operatorname{div} \mathbf{w})_\Omega}{\|\mathbf{w}\|_{(2,\gamma)}} < \beta_\Omega(2, \gamma) - \delta.$$

Since Y^n is of finite dimension, we find some $\tilde{q} \in Y^n \cap \overline{\mathcal{Q}}_\Omega^2$, $\|\tilde{q}\|_2 = 1$, and a subsequence $j_i > i$ such that $\|q_{j_i} - \tilde{q}\|_2 < \delta/2$ for $i = 1, \dots$. But then,

$$\sup_{\mathbf{w} \in \mathbf{X}^{j_i} \cap \overline{\mathcal{X}}^{2,\gamma}} \frac{(\tilde{q}, \operatorname{div} \mathbf{w})_\Omega}{\|\mathbf{w}\|_{(2,\gamma)}} < \beta_\Omega(2, \gamma) - \delta/2$$

holds for any $i = 1, \dots$, which combined with the density and Corollary 4 gives the contradiction. \square

2.3 Well-posedness results

Despite of the wide range of important applications, the rigorous mathematical analysis of the incompressible fluid flow models with the viscosity depending on the pressure has not attracted much research activity until the turn of century. The earlier results (by Gazzola, 1997; Gazzola and Secchi, 1998; Renardy, 1986), concerned with the viscosity depending solely on the pressure, established the existence for a short time interval and due to small data only. For the stationary problem, Renardy (1986) notes that the equations lose the ellipticity unless the derivative of the viscosity with respect to pressure is bounded by reciprocal of eigenvalues of $\mathbf{D}(\mathbf{v})$. For fluids whose viscosity depends solely on pressure or grows superlinearly with pressure, as far as no severe restrictions on the data size or time interval are imposed, the well-posedness of the mathematical problem is not known.

An opening result appeared in Málek et al. (2002) and Hron et al. (2003), where the viscosities depending both on the pressure and shear rate—their structure given by Assumptions **(A1)** and **(A2)**—were considered, allowing for the global and large data existence results. These results, established for periodic boundary conditions, were then extended to unsteady flows in bounded domains subject to Navier’s slip boundary conditions in Bulíček et al. (2007), see also Málek and Rajagopal (2007) for more references. The well-posedness of the steady problem (Problem **(P)** with the convective term included) was first studied by Franta et al. (2005) for the homogeneous Dirichlet boundary conditions. This result was generalized to cover the non-homogeneous Dirichlet data in Lanzendörfer (2009). The problem with the boundary condition (2.3c) allowing for free flow through the boundary present, i.e. the case $|\Gamma_P| > 0$, was studied in Lanzendörfer and Stebel (2011a,b).

We merely mention that the presented theoretical framework allowed to show also the *a priori* estimates of the discretization error, see Hirn et al. (2010) for more details.

In this section, we show the existence of discrete solutions to **(P_h)** (in Theorem 11), we discuss the conditions guaranteeing the uniqueness of solutions both to **(P)** and **(P_h)** (in Theorems 12 and 13), and we finally establish the existence of a weak solution to **(P)** as the limit of the discrete solutions (in Corollary 15).

Compared to the previous works Lanzendörfer (2009); Lanzendörfer and Stebel (2011a,b), we slightly relax the restriction on γ_0 when showing the existence. In fact, we bring its range back to that allowed in Franta et al. (2005) for the case $|\Gamma_P| = 0$ and $\Omega_0 = \Omega$, cf. Corollary 15 and (2.15), (2.17). The same was, however, not acquired for the uniqueness result, see Theorem 12. Our procedure also allows for $r \in (1, 2)$; but this is merely because the convective term is not present in our model.

The basic structure of the proof of existence of a weak solution to the steady problem in the above mentioned papers followed the procedure by Franta et al. (2005): First, a quasi-compressible approximation to (\mathbf{P}) was established (by the Galerkin method), and later its convergence (on the continuous level) to the “incompressible” solution to (\mathbf{P}) was shown. Note that here, since our concern lies with the discretization, the procedure is slightly different: the weak solution is established directly as a limit of discrete solutions and these discrete solutions already satisfy the incompressibility constraint.

2.3.1 Existence of discrete solutions

Remark 10. *Let Assumption 2 hold. Let $(\mathcal{X}_h^{r,\gamma}, \mathcal{Q}_h^r)$ fulfill $(\mathbf{IS}^{r,\gamma})$ with $\tilde{\beta}(r, \gamma) > 0$ arbitrary. Then, all (\mathbf{v}_h, p_h) the solutions to (\mathbf{P}_h) satisfy the a priori estimates*

$$\|\mathbf{v}_h\|_{1,r} + \|\mathbf{S}(p_h, \mathbf{D}(\mathbf{v}_h))\|_{r'} + \|\mathbf{u}_h\|_{\gamma;\Gamma} \leq K_{\mathbf{v}} \quad \text{and} \quad \tilde{\beta}(r, \gamma) \|p_h\|_{r'} \leq K_p, \quad (2.23)$$

with the constants $K_{\mathbf{v}}$ and K_p from (2.9) and (2.11).

Indeed: The estimates derives in exactly the same way as (2.9), (2.11) in Section 2.2.1. \square

Theorem 11 (Existence of discrete solutions). *Let Assumption 2 hold, let $\mathcal{X}_h^{r,\gamma}$ and \mathcal{Q}_h^r fulfill $(\mathbf{IS}^{r,\gamma})$ with $\tilde{\beta}(r, \gamma) > 0$ arbitrary. Then there exists a discrete solution to (\mathbf{P}_h) .*

Proof. For any $\delta > 0$ (small), we consider the following quasi-compressible approximate problem: Find $(\mathbf{v}_h^\delta, p_h^\delta)$ such that $\mathbf{u}_h^\delta := (\mathbf{v}_h^\delta - \mathbf{v}_{h,0}) \in \mathcal{X}_h^{r,\gamma}$, $p_h^\delta \in \mathcal{Q}_h^r$ and

$$\begin{aligned} \delta (p_h^\delta, \xi_h)_\Omega + (\xi_h, \operatorname{div} \mathbf{v}_h^\delta)_\Omega &= 0 & \text{for all } \xi_h \in \mathcal{Q}_h^r \\ (\mathbf{S}(p_h^\delta, \mathbf{D}(\mathbf{v}_h^\delta)), \mathbf{D}(\boldsymbol{\varphi}_h))_\Omega - (p_h^\delta, \operatorname{div} \boldsymbol{\varphi}_h)_\Omega &= \langle \mathbf{f}, \boldsymbol{\varphi}_h \rangle - \langle \mathbf{b}(\mathbf{u}_h^\delta), \boldsymbol{\varphi}_h \rangle_\Gamma & \text{for all } \boldsymbol{\varphi}_h \in \mathcal{X}_h^{r,\gamma}. \end{aligned}$$

The inserted term $\delta (p_h^\delta, \xi_h)_\Omega$ ensures the coercivity of the equations with respect to the pressure and allows to use the Brouwer fixed-point theorem to establish the solution to (\mathbf{P}_h) . Indeed, setting $(\boldsymbol{\varphi}_h, \xi_h) := (\mathbf{u}_h^\delta, p_h^\delta)$ and following the same steps as when deriving the *a priori* estimates (2.9), we verify the assumptions of Corollary 17 and obtain the solution $(\mathbf{v}_h^\delta, p_h^\delta)$ to the approximate problem and the *a priori* bound

$$\delta \|p_h^\delta\|_2^2 + \|\mathbf{v}_h^\delta\|_{1,r}^r + \|\mathbf{S}(p_h^\delta, \mathbf{D}(\mathbf{v}_h^\delta))\|_{r'}^r \leq K_{\mathbf{v}} \quad \text{and} \quad \tilde{\beta}(r, \gamma) \|p_h^\delta\|_{r'} \leq K_p,$$

where we have also used $(\mathbf{IS}^{r,\gamma})$, cf. (2.11).

The uniform bounds and the fact that $\mathcal{X}_h^{r,\gamma}$ and \mathcal{Q}_h^r are of finite dimension imply that there is $\mathbf{v}_h = \mathbf{v}_{h,0} + \mathbf{u}_h$, $\mathbf{u}_h \in \mathcal{X}_h^{r,\gamma}$ and $p_h \in \mathcal{Q}_h^r$ such that (for some sequence $\delta_n \searrow 0$)

$$\begin{aligned} \mathbf{v}_h^{\delta_n} &\rightarrow \mathbf{v}_h && \text{strongly in } \mathbf{W}^{1,r}(\Omega), \\ \mathbf{u}_h^{\delta_n} &\rightarrow \mathbf{u}_h && \text{strongly in } \mathbf{L}^\gamma(\Gamma), \\ p_h^{\delta_n} &\rightarrow p_h && \text{strongly in } L^{r'}(\Omega), \\ \mathbf{S}(p_h^{\delta_n}, \mathbf{D}(\mathbf{v}_h^{\delta_n})) &\rightarrow \mathbf{S}(p_h, \mathbf{D}(\mathbf{v}_h)) && \text{strongly in } L^{r'}(\Omega)^{d \times d}, \\ \mathbf{b}(\mathbf{u}_h^{\delta_n}) &\rightarrow \mathbf{b}(\mathbf{u}_h) && \text{strongly in } \mathbf{L}^\gamma(\Gamma). \end{aligned}$$

Consequently (\mathbf{v}_h, π_h) is a solution to (\mathbf{P}_h) . \square

2.3.2 Uniqueness

In the uniqueness considerations, Problems (\mathbf{P}) and (\mathbf{P}_h) can be treated identically, as will become obvious in a moment. One might have noticed that Assumption $(\mathbf{A2})$ was not utilized to show the *a priori* estimates nor to prove the existence of discrete solutions in the previous section. Its function appears right below.

First, we may ask whether the pressure is determined uniquely by the velocity field; i.e., given (\mathbf{v}, p^1) , (\mathbf{v}, p^2) two solutions to (\mathbf{P}) with identical velocity field, we want to show $\|p^1 - p^2\|_{s'} = 0$ for some $s \in (1, \infty)$. From the equation (2.8b), we estimate using (2.16),

$$\begin{aligned} \beta(s, \gamma) \|p^1 - p^2\|_{s'} &\leq \sup_{\mathbf{w} \in \mathcal{X}^{r,\gamma}} \frac{(p^1 - p^2, \operatorname{div} \mathbf{w})_\Omega}{\|\mathbf{w}\|_{1,s}} \\ &\leq \|\mathbf{S}(p^1, \mathbf{D}(\mathbf{v})) - \mathbf{S}(p^2, \mathbf{D}(\mathbf{v}))\|_{s'} = \left\| \int_{p^1}^{p^2} \frac{\partial \mathbf{S}(p, \mathbf{D}(\mathbf{v}))}{\partial p} dp \right\|_{s'}, \end{aligned}$$

which implies $\|p^1 - p^2\|_{s'} = 0$ provided that Assumption $(\mathbf{A4})$ is satisfied with $\beta := \beta(s, \gamma)$:

$$\sup_{p \in \mathbb{R}, \mathbf{D} \in \mathbb{R}_{sym}^{d \times d}} \left| \frac{\partial \mathbf{S}(p, \mathbf{D})}{\partial p} \right| < \beta(s, \gamma).$$

We pinpoint this basic estimate in order to emphasize that the assumption of the growth of the viscosity with pressure being sublinear is crucial. Without the alliance of Assumption $(\mathbf{A4})$ with the inf-sup inequality, the uniqueness is not guaranteed and we also have no idea how to establish the existence of solution to (\mathbf{P}) , see the next section. Note that Assumption $(\mathbf{A4})$ will be recalled in Chapter 3, where it will be observed to determine the stability of the numerical method.

Let $(\mathbf{v}^1, p^1) = (\mathbf{v}^2, p^2)$ be two possible solutions to (\mathbf{P}) . For simplicity, assume first that \mathbf{b} is independent of the velocity, i.e. $\mathbf{b} \equiv \mathbf{b}(\mathbf{x})$. Then,

$$(\mathbf{S}(p^1, \mathbf{D}(\mathbf{v}^1)) - \mathbf{S}(p^2, \mathbf{D}(\mathbf{v}^2)), \mathbf{D}(\boldsymbol{\varphi}))_\Omega = (p^1 - p^2, \operatorname{div} \boldsymbol{\varphi})_\Omega \quad \text{for all } \boldsymbol{\varphi} \in \mathcal{X}^{r,\gamma}.$$

In particular, choosing $\boldsymbol{\varphi} := \mathbf{v}^1 - \mathbf{v}^2$ we observe, due to $\operatorname{div} \mathbf{v}^1 = \operatorname{div} \mathbf{v}^2 = 0$,

$$(\mathbf{S}(p^1, \mathbf{D}(\mathbf{v}^1)) - \mathbf{S}(p^2, \mathbf{D}(\mathbf{v}^2)), \mathbf{D}(\mathbf{v}^1) - \mathbf{D}(\mathbf{v}^2))_\Omega = 0$$

and we thus obtain from (2.6a) that

$$d(\mathbf{v}^1, \mathbf{v}^2) \leq \frac{\gamma_0}{C_1} \|p^1 - p^2\|_2. \quad (2.25)$$

Hence, (2.16) and (2.6b) yields

$$\begin{aligned} \beta(2, \gamma) \|p^1 - p^2\|_2 &\leq \sup_{\boldsymbol{\varphi} \in \boldsymbol{\mathcal{X}}^{2, \gamma}} \frac{(p^1 - p^2, \operatorname{div} \boldsymbol{\varphi})_\Omega}{\|\boldsymbol{\varphi}\|_{1,2}} \\ &\leq \|\mathbf{S}(p^1, \mathbf{D}(\mathbf{v}^1)) - \mathbf{S}(p^2, \mathbf{D}(\mathbf{v}^2))\|_2 \\ &\leq C_2 d(\mathbf{v}^1, \mathbf{v}^2) + \gamma_0 \|p^1 - p^2\|_2, \end{aligned} \quad (2.26)$$

which together with (2.25) leads to $\|p^1 - p^2\|_2 = d(\mathbf{v}^1, \mathbf{v}^2) = 0$ as soon as $\beta(2, \gamma) - \gamma_0 \left(1 + \frac{C_2}{C_1}\right) > 0$. Due to the *a priori* bound (2.9), we conclude from (2.6c) that $\|\mathbf{D}(\mathbf{v}^1) - \mathbf{D}(\mathbf{v}^2)\|_r = 0$. This finally gives $\|\mathbf{v}^1 - \mathbf{v}^2\|_{1,r} = 0$, provided we have the appropriate Korn inequality available.

The theorem below allows for dependence of \mathbf{b} on the velocity, restricted by the Lipschitz continuity condition

(B λ) *With $\lambda > 0$ given*

$$\|\mathbf{b}(\mathbf{w}) - \mathbf{b}(\mathbf{z})\|_{\gamma'; \Gamma} \leq \lambda \|\mathbf{w} - \mathbf{z}\|_{\gamma; \Gamma} \quad \text{for all } \mathbf{w}, \mathbf{z} \in \mathbf{L}^\gamma(\Gamma).$$

Note that if $\gamma > 2$ then **(B λ)** is incompatible with the assumption $B_c > 0$. Indeed, taking $\mathbf{z} := \mathbf{0}$ and $\mathbf{w} := \mathbf{u}$ in **(B λ)**, we observe from **(B2)** that

$$B_c \|\mathbf{u}\|_{\gamma; \Gamma}^\gamma - B_l \|\mathbf{u}\|_{\gamma; \Gamma} \leq \langle \mathbf{b}(\mathbf{u}), \mathbf{u} \rangle_\Gamma \leq \|\mathbf{b}(\mathbf{u})\|_{\gamma'; \Gamma} \|\mathbf{u}\|_{\gamma; \Gamma} \leq \lambda \|\mathbf{u}\|_{\gamma; \Gamma}^2 + \|\mathbf{b}(\mathbf{0})\|_{\gamma'; \Gamma} \|\mathbf{u}\|_{\gamma; \Gamma}.$$

For $\gamma > 2$, this can not be satisfied for all $\mathbf{u} \in \mathbf{L}^\gamma(\Gamma)$, since it implies $\|\mathbf{u}\|_{\gamma; \Gamma} \leq c(\gamma, B_l, \frac{B_c}{\lambda}, \mathbf{b}(\mathbf{0}))$. It is true that we apply **(B λ)** only on functions bounded by $\|\mathbf{w}\|_{\gamma; \Gamma}, \|\mathbf{z}\|_{\gamma; \Gamma} \leq K_{\mathbf{v}}$, with $K_{\mathbf{v}}$ from (2.9), and one can thus imagine some generalizations taking this into account, but we will not proceed in this direction.

Theorem 12 (Uniqueness of solutions to **(P)**). *Let Assumption 2 hold. In addition, let Assumption **(A3)** hold with $\beta := \beta(2, \gamma)$. Assume that at least one of the following apply:*

- i) $\gamma \leq r^\#$, the Korn inequality (2.7) holds with $I_K = 0$ (see assumptions i) or ii) of Lemma 1):

$$\|\mathbf{w}\|_{1,r} \leq c_K \|\mathbf{D}(\mathbf{w})\|_r \quad \text{for all } \mathbf{w} \in \boldsymbol{\mathcal{X}}^{r, \gamma},$$

and **(B λ)** holds with $\lambda > 0$ small enough, depending on $\Omega, \Gamma_D, \Gamma_N, \Gamma_P, r, C_1, C_2, \gamma_0, \mathbf{f}, \mathbf{v}_D, B_l$ and $\beta(2, \gamma)$.

- ii) $\gamma = 2$, **(B λ)** holds with $\lambda > 0$ arbitrary, and \mathbf{b} is strongly monotone:

$$\langle \mathbf{b}(\mathbf{w}) - \mathbf{b}(\mathbf{z}), \mathbf{w} - \mathbf{z} \rangle_\Gamma \geq \frac{\lambda^2}{m^2} \|\mathbf{w} - \mathbf{z}\|_{2; \Gamma}^2 \quad \text{for all } \mathbf{w}, \mathbf{z} \in \mathbf{L}^2(\Gamma), \quad (2.27)$$

with $m > 0$ small enough, depending on C_1, C_2, γ_0 and $\beta(2, \gamma)$.

Then there is at most one solution to **(P)**.

Theorem 13 (Uniqueness of solutions to **(P $_h$)**). *Let the discrete spaces $\boldsymbol{\mathcal{X}}_h^{r, \gamma}, \mathcal{Q}_h^r$ satisfy **(IS $^{2, \gamma}$)** and let the assumptions of Theorem 12 hold with $\beta := \tilde{\beta}(2, \gamma)$. Then there is at most one solution to **(P $_h$)**.*

Proof. We formulate the proof for Theorem 12, Theorem 13 then follows analogically.

Take two possible solutions $(\mathbf{v}^i, p^i) = (\mathbf{v}_0 + \mathbf{u}^i, p^i)$, $i = 1, 2$. Subtracting (2.8b), we observe for all $\boldsymbol{\varphi} \in \mathcal{X}^{r,\gamma}$,

$$(p^1 - p^2, \operatorname{div} \boldsymbol{\varphi})_\Omega = (\mathbf{S}(p^1, \mathbf{D}(\mathbf{v}^1)) - \mathbf{S}(p^2, \mathbf{D}(\mathbf{v}^2)), \mathbf{D}(\boldsymbol{\varphi}))_\Omega + \langle \mathbf{b}(\mathbf{u}^1) - \mathbf{b}(\mathbf{u}^2), \boldsymbol{\varphi} \rangle_\Gamma.$$

Setting $\boldsymbol{\varphi} := \mathbf{v}^1 - \mathbf{v}^2$ we obtain from (2.6a), using $\operatorname{div} \mathbf{v}^i = 0$, $i = 1, 2$, that

$$\frac{C_1}{2} d(\mathbf{v}^1, \mathbf{v}^2)^2 + \langle \mathbf{b}(\mathbf{u}^1) - \mathbf{b}(\mathbf{u}^2), \mathbf{u}^1 - \mathbf{u}^2 \rangle_\Gamma \leq \frac{\gamma_0^2}{2C_1} \|p^1 - p^2\|_2^2, \quad (2.28)$$

while using (2.6b) we observe for all $\boldsymbol{\varphi} \in \mathcal{X}^{r,\gamma}$

$$(p^1 - p^2, \operatorname{div} \boldsymbol{\varphi})_\Omega \leq (C_2 d(\mathbf{v}^1, \mathbf{v}^2) + \gamma_0 \|p^1 - p^2\|_2) \|\boldsymbol{\varphi}\|_{1,2} + \|\mathbf{b}(\mathbf{u}^1) - \mathbf{b}(\mathbf{u}^2)\|_{\gamma';\Gamma} \|\boldsymbol{\varphi}\|_{\gamma;\Gamma},$$

which combined with the inf-sup inequality (2.16) and **(B λ)** implies

$$\beta(2, \gamma) \|p^1 - p^2\|_2 \leq C_2 d(\mathbf{v}^1, \mathbf{v}^2) + \gamma_0 \|p^1 - p^2\|_2 + \lambda \|\mathbf{v}^1 - \mathbf{v}^2\|_{\gamma;\Gamma}. \quad (2.29)$$

Case i): From (2.28) and **(B λ)** we obtain

$$d(\mathbf{v}^1, \mathbf{v}^2) \leq \frac{\gamma_0}{C_1} \|p^1 - p^2\|_2 + \sqrt{\frac{2\lambda}{C_1}} \|\mathbf{v}^1 - \mathbf{v}^2\|_{\gamma;\Gamma}$$

and we can conclude from (2.29) that

$$\left(\beta(2, \gamma) - \gamma_0 \left(1 + \frac{C_2}{C_1} \right) \right) \|p^1 - p^2\|_2 \leq \left(\lambda + C_2 \sqrt{\frac{2\lambda}{C_1}} \right) \|\mathbf{v}^1 - \mathbf{v}^2\|_{\gamma;\Gamma}. \quad (2.30)$$

The quantity in the left parentheses is positive by Assumption **(A3)**. The latter two estimates yields

$$d(\mathbf{v}^1, \mathbf{v}^2) \leq c(C_1, C_2, \beta(2, \gamma), \gamma_0) (\lambda + \sqrt{\lambda}) \|\mathbf{v}^1 - \mathbf{v}^2\|_{\gamma;\Gamma}. \quad (2.31)$$

The *a priori* estimate (2.9) ensures that $\|\mathbf{v}^i\|_{1,r} \leq K_{\mathbf{v}}$, $i = 1, 2$. Note that due to the assumptions stated in *i*), $K_{\mathbf{v}}$ does not depend on B_c . This implies, using (2.6c), that

$$c(K_{\mathbf{v}}, \Omega, r) \|\mathbf{D}(\mathbf{v}^1) - \mathbf{D}(\mathbf{v}^2)\|_r \leq d(\mathbf{v}^1, \mathbf{v}^2). \quad (2.32)$$

Thus, using the Korn inequality (2.7) and the embedding $\mathbf{W}^{1,r}(\Omega) \hookrightarrow \mathbf{L}^\gamma(\Gamma)$ it follows from (2.31) that

$$\|\mathbf{v}^1 - \mathbf{v}^2\|_{1,r} \leq C (\lambda + \sqrt{\lambda}) \|\mathbf{v}^1 - \mathbf{v}^2\|_{1,r},$$

with C depending only on Ω , r , C_1 , C_2 , Γ , γ , $\beta(2, \gamma)$, γ_0 , $K_{\mathbf{v}}$ and c_K . For λ small enough, this implies $\mathbf{v}^1 = \mathbf{v}^2$ a.e. in Ω and (2.30) immediately yields $p^1 = p^2$ a.e. in Ω .

Case ii): The strong monotonicity (2.27) of \mathbf{b} and (2.28) leads to

$$d(\mathbf{v}^1, \mathbf{v}^2) \leq \frac{\gamma_0}{C_1} \|p^1 - p^2\|_2 \quad \text{and} \quad \lambda^2 \|\mathbf{v}^1 - \mathbf{v}^2\|_{2;\Gamma}^2 \leq m^2 \frac{\gamma_0^2}{2C_1} \|p^1 - p^2\|_2^2.$$

Thus, (2.29) implies that

$$\left(\beta(2, \gamma) - \gamma_0 \left(1 + \frac{C_2}{C_1} \right) \right) \|p^1 - p^2\|_2 \leq \lambda \|\mathbf{v}^1 - \mathbf{v}^2\|_{2;\Gamma} \leq m \frac{\gamma_0}{\sqrt{2C_1}} \|p^1 - p^2\|_2.$$

Again, since the quantity in the left parentheses is positive, for m small enough (depending only on $C_1, C_2, \beta(2, \gamma)$ and γ_0) this implies $p^1 = p^2$ a.e. in Ω and $\mathbf{v}^1 = \mathbf{v}^2$ a.e. on Γ . Also, since $d(\mathbf{v}^1, \mathbf{v}^2) = 0$ and $\|\mathbf{v}^i\|_{1,r}$ is bounded^g, (2.6c) yields $\mathbf{D}(\mathbf{v}^1) = \mathbf{D}(\mathbf{v}^2)$ a.e. in Ω . We only use the Korn inequality for functions vanishing on the boundary:

$$\|\mathbf{v}^1 - \mathbf{v}^2\|_{1,r} \leq c(\Omega, r) \|\mathbf{D}(\mathbf{v}^1 - \mathbf{v}^2)\|_r, \quad \text{where } \mathbf{v}^1 - \mathbf{v}^2 \in \mathbf{W}_0^{1,r}(\Omega)$$

(i.e. without the restricting assumptions on $\Gamma_D, \Gamma_N, \Gamma_P$) to conclude that $\mathbf{v}^1 = \mathbf{v}^2$ a.e. in Ω . \square

2.3.3 Convergence of discrete solutions; existence of a weak solution

While in the uniqueness Theorem 13 above we used Assumption **(A3)** based on $(\mathbf{IS}^{2,\gamma})$ and $\tilde{\beta}(2, \gamma)$, in the following we take advantage of (2.21) and apply $(\mathbf{IS}_\Omega^{2,\gamma})$ and $\tilde{\beta}_\Omega(2, \gamma)$ instead. As explained already in Section 2.2.3, the motivation lies in (2.15) and (2.17) and in the assertion that $\tilde{\beta}_\Omega(2, \gamma) \geq \tilde{\beta}(2, \gamma)$. The existence of a weak solution to **(P)** is thus guaranteed for larger range of γ_0 compared to its uniqueness.

Theorem 14 (Convergence of discrete solutions). *Let Assumption 2 hold, let $\mathcal{X}_h^{r,\gamma}$ and \mathcal{Q}_h^r fulfil $(\mathbf{IS}^{r,\gamma})$ with $\tilde{\beta}(r, \gamma) > 0$ arbitrary. Moreover, let the discrete spaces $\{(\mathcal{X}_h^{r,\gamma}, \mathcal{Q}_h^r)\}_{h>0}$ satisfy (2.18) and $\{\mathbf{v}_{h,0}\}_{h>0}$ satisfy (2.20). In addition, let $(\mathbf{IS}_\Omega^{2,\gamma})$ hold and Assumption **(A3)** be satisfied with $\beta := \tilde{\beta}_\Omega(2, \gamma^+)$ for some $\gamma^+ > \gamma$. Then there exists a solution to **(P)**, and the discrete solutions to **(P_h)** converge as follows,*

$$(\mathbf{v}_{h_n}, p_{h_n}) \rightarrow (\mathbf{v}, p) \quad \text{strongly in } \mathbf{W}^{1,r}(\Omega) \times L^{r'}(\Omega), \quad \text{for some } h_n \searrow 0. \quad (2.33)$$

If the weak solution to **(P)** is unique, the whole sequence $\{(\mathbf{v}_h, p_h)\}_{h>0}$ converges to (\mathbf{v}, p) .

Proof. Theorem 11 provides $(\mathbf{v}_h, p_h) = (\mathbf{v}_{h,0} + \mathbf{u}_h, p_h)$, the discrete solution to **(P_h)**, satisfying the uniform estimate (2.23). Therefore (since we work in reflexive Banach spaces) there is a sequence $h_n \searrow 0$ such that

$$\mathbf{v}_{h_n} \rightharpoonup \mathbf{v} \quad \text{weakly in } \mathbf{W}^{1,r}(\Omega), \quad (2.34a)$$

$$\mathbf{u}_{h_n} \rightharpoonup \mathbf{u} \quad \text{weakly in } \mathbf{L}^\gamma(\Gamma), \quad (2.34b)$$

$$p_{h_n} \rightharpoonup p \quad \text{weakly in } L^{r'}(\Omega), \quad (2.34c)$$

$$\mathbf{S}(p_{h_n}, \mathbf{D}(\mathbf{v}_{h_n})) \rightharpoonup \bar{\mathbf{S}} \quad \text{weakly in } L^{r'}(\Omega)^{d \times d}, \quad (2.34d)$$

where $\mathbf{v} = \mathbf{v}_0 + \mathbf{u}$, $\mathbf{u} \in \mathcal{X}^{r,\gamma}$ and $p \in \mathcal{Q}^r$ obviously satisfy the equation (2.8a).

If $\gamma < r^\#$ then (2.34a), the compact embedding $\mathbf{W}^{1,r}(\Omega) \hookrightarrow \mathbf{L}^\gamma(\Gamma)$ and **(B1)** give (for a subsequence)

$$\mathbf{b}(\mathbf{u}_{h_n}) \rightarrow \mathbf{b}(\mathbf{u}) \quad \text{strongly in } \mathbf{L}^{\gamma'}(\Gamma), \quad h_n \searrow 0.$$

If $\gamma \geq r^\#$, the compact embedding still gives

$$\mathbf{u}_{h_n} \rightarrow \mathbf{u} \quad \text{strongly in } \mathbf{L}^1(\Gamma) \quad \text{and thus} \quad \mathbf{u}_{h_n} \rightarrow \mathbf{u} \quad \text{a.e. on } \Gamma, \quad h_n \searrow 0.$$

^g Note that in this case the *a priori* bound for $\|\mathbf{v}^i\|_{1,r}$ can depend on B_c , but this does not affect the restriction on m .

Hence, (2.34) and $(\mathbf{B3})_1$ allow us to pass to the limit in (2.19b), obtaining (due to the density (2.18))

$$(\bar{\mathbf{S}}, \mathbf{D}(\boldsymbol{\varphi}))_{\Omega} - (p, \operatorname{div} \boldsymbol{\varphi})_{\Omega} = \langle \mathbf{f}, \boldsymbol{\varphi} \rangle - \langle \mathbf{b}(\mathbf{u}), \boldsymbol{\varphi} \rangle_{\Gamma} \quad \text{for all } \boldsymbol{\varphi} \in \mathcal{X}^{r,\gamma}. \quad (2.35)$$

In order to identify $\bar{\mathbf{S}}$ using Vitali's lemma, we aim to show the convergence

$$\mathbf{D}(\mathbf{v}_{h_n}) \rightarrow \mathbf{D}(\mathbf{v}) \quad \text{a.e. in } \Omega \quad \text{and} \quad p_{h_n} \rightarrow p \quad \text{a.e. in } \Omega, \quad h_n \searrow 0. \quad (2.36)$$

Subtracting (2.35) and (2.19b), we observe that for all $\boldsymbol{\varphi}_{h_n} \in \mathcal{X}_{h_n}^{r,\gamma}$,

$$(\mathbf{S}(p_{h_n}, \mathbf{D}(\mathbf{v}_{h_n})) - \bar{\mathbf{S}}, \mathbf{D}(\boldsymbol{\varphi}_{h_n}))_{\Omega} = (p_{h_n} - p, \operatorname{div} \boldsymbol{\varphi}_{h_n})_{\Omega} - \langle \mathbf{b}(\mathbf{u}_{h_n}) - \mathbf{b}(\mathbf{u}), \boldsymbol{\varphi}_{h_n} \rangle_{\Gamma}. \quad (2.37)$$

By setting $\boldsymbol{\varphi}_{h_n} := \mathbf{u}_{h_n}$ and using (2.34), (2.20) and then (2.37), (2.8a), (2.19a) and $(\mathbf{B3})_2$, we obtain

$$\begin{aligned} (\mathbf{S}(p_{h_n}, \mathbf{D}(\mathbf{v}_{h_n})) - \mathbf{S}(p, \mathbf{D}(\mathbf{v})), \mathbf{D}(\mathbf{v}_{h_n}) - \mathbf{D}(\mathbf{v}))_{\Omega} &= (\mathbf{S}(p_{h_n}, \mathbf{D}(\mathbf{v}_{h_n})) - \bar{\mathbf{S}}, \mathbf{D}(\mathbf{u}_{h_n}))_{\Omega} + o(1) \\ &\leq o(1), \quad h_n \searrow 0, \end{aligned} \quad (2.38)$$

where by $o(1)$ we denote an arbitrary sequence vanishing to zero if $h_n \searrow 0$. Recalling (2.6a), (2.6c) and the *a priori* bounds (2.9), (2.23), we conclude (cf. (2.32))

$$c(K_{\mathbf{v}}, \Omega, r) \|\mathbf{D}(\mathbf{v}_{h_n}) - \mathbf{D}(\mathbf{v})\|_r \leq d(\mathbf{v}_{h_n}, \mathbf{v}) \leq \frac{\gamma_0}{C_1} \|p_{h_n} - p\|_2. \quad (2.39)$$

Suppose, for a while, that

$$\tilde{\beta}_{\Omega}(2, \gamma) \|p_{h_n} - p\|_2 \leq \|\mathbf{S}(p_{h_n}, \mathbf{D}(\mathbf{v}_{h_n})) - \mathbf{S}(p, \mathbf{D}(\mathbf{v}))\|_2 + o(1). \quad (2.40)$$

Then, we obtain from (2.6b) that (cf. (2.29))

$$\tilde{\beta}_{\Omega}(2, \gamma) \|p_{h_n} - p\|_2 \leq C_2 d(\mathbf{v}_{h_n}, \mathbf{v}) + \gamma_0 \|p_{h_n} - p\|_2 + o(1), \quad h_n \searrow 0.$$

Thus, using (2.39) and the assumption $(\mathbf{A3})$, we conclude that $\|p_{h_n} - p\|_2 \leq o(1)$. Consequently, (2.39) also yields $\|\mathbf{D}(\mathbf{v}_{h_n}) - \mathbf{D}(\mathbf{v})\|_r \leq o(1)$, implying finally (for a subsequence) the a.e. convergence (2.36). This allows us to use Vitali's lemma and to identify $\bar{\mathbf{S}}$:

$$(\mathbf{S}(p_{h_n}, \mathbf{D}(\mathbf{v}_{h_n})), \mathbf{D}(\boldsymbol{\varphi}))_{\Omega} \rightarrow (\mathbf{S}(p, \mathbf{D}(\mathbf{v})), \mathbf{D}(\boldsymbol{\varphi}))_{\Omega} = (\bar{\mathbf{S}}, \mathbf{D}(\boldsymbol{\varphi}))_{\Omega} \quad \text{for all } \boldsymbol{\varphi} \in \mathbf{W}^{1,r}(\Omega).$$

Thus, it only remains to show (2.40) and the proof is complete. For $\gamma^+ > \gamma$ from the assumptions define $\tilde{\mathbf{w}}_{h_n} \in \mathcal{X}_{h_n}^{2,\gamma^+}$, $\|\tilde{\mathbf{w}}_{h_n}\|_{(2,\gamma^+)} = 1$, such that

$$\sup_{\boldsymbol{\varphi}_{h_n} \in \mathcal{X}_{h_n}^{2,\gamma^+}} \frac{(p_{h_n} - p, \operatorname{div} \boldsymbol{\varphi}_{h_n})_{\Omega}}{\|\boldsymbol{\varphi}_{h_n}\|_{(2,\gamma^+)}} = (p_{h_n} - p, \operatorname{div} \tilde{\mathbf{w}}_{h_n})_{\Omega}.$$

Then there exists $\tilde{\mathbf{w}} \in \mathcal{X}^{2,\gamma^+}$ such that (for a not-relabelled subsequence) $\tilde{\mathbf{w}}_{h_n} - \tilde{\mathbf{w}} \rightharpoonup 0$ weakly in $\mathbf{W}^{1,2}(\Omega)$ and^h $\|\tilde{\mathbf{w}}_{h_n} - \tilde{\mathbf{w}}\|_{1,2} \leq 1$. Moreover, $\tilde{\mathbf{w}}_{h_n} \rightarrow \tilde{\mathbf{w}}$ a.e. on Γ and $\|\tilde{\mathbf{w}}_{h_n}\|_{\gamma^+; \Gamma} \leq 1$.

^h Indeed, $\|\mathbf{w}\|_{1,2}^2 \leq 2(\mathbf{w}_{h_n}, \mathbf{w})_{1,2; \Omega}$ for n large enough, which implies $\|\mathbf{w}_{h_n} - \mathbf{w}\|_{1,2}^2 \leq \|\mathbf{w}_{h_n}\|_{1,2}^2 (= 1)$.

Hence, using (2.34c), (2.34d), **(B3)**₃ and (2.37), we obtain:

$$\begin{aligned}
(p_{h_n} - p, \operatorname{div} \tilde{\mathbf{w}}_{h_n})_\Omega &= (\mathbf{S}(p_{h_n}, \mathbf{D}(\mathbf{v}_{h_n})) - \bar{\mathbf{S}}, \mathbf{D}(\tilde{\mathbf{w}}_{h_n}) - \mathbf{D}(\tilde{\mathbf{w}}))_\Omega + \langle \mathbf{b}(\mathbf{u}_{h_n}) - \mathbf{b}(\mathbf{u}), \tilde{\mathbf{w}}_{h_n} \rangle_\Gamma + o(1) \\
&= (\mathbf{S}(p_{h_n}, \mathbf{D}(\mathbf{v}_{h_n})) - \mathbf{S}(p, \mathbf{D}(\mathbf{v})), \mathbf{D}(\tilde{\mathbf{w}}_{h_n}) - \mathbf{D}(\tilde{\mathbf{w}}))_\Omega + o(1) \\
&\leq \|\mathbf{S}(p_{h_n}, \mathbf{D}(\mathbf{v}_{h_n})) - \mathbf{S}(p, \mathbf{D}(\mathbf{v}))\|_2 + o(1), \quad h_n \searrow 0.
\end{aligned}$$

Further, since $\int_\Omega p_{h_n} - p \, d\mathbf{x} \rightarrow 0$, we may apply (2.21) and observe for all $q_{h_n} \in \mathcal{Q}_{h_n}^r$ that

$$\begin{aligned}
&\tilde{\beta}_\Omega(2, \gamma^+) \|p_{h_n} - q_{h_n}\|_2 \\
&\leq \sup_{\boldsymbol{\varphi}_{h_n} \in \boldsymbol{\mathcal{X}}_{h_n}^{2, \gamma^+}} \frac{(p_{h_n} - q_{h_n}, \operatorname{div} \boldsymbol{\varphi}_{h_n})_\Omega}{\|\boldsymbol{\varphi}_{h_n}\|_{(2, \gamma^+)}} + \tilde{\beta}_\Omega(2, \gamma^+) |\Omega|^{1/2} \left| \int_\Omega p_{h_n} - q_{h_n} \, d\mathbf{x} \right| \\
&\leq \sup_{\boldsymbol{\varphi}_{h_n} \in \boldsymbol{\mathcal{X}}_{h_n}^{2, \gamma^+}} \frac{(p_{h_n} - p, \operatorname{div} \boldsymbol{\varphi}_{h_n})_\Omega}{\|\boldsymbol{\varphi}_{h_n}\|_{(2, \gamma^+)}} + \|p - q_{h_n}\|_2 + \tilde{\beta}_\Omega(2, \gamma^+) \|p - q_{h_n}\|_2 + o(1) \\
&\leq \|\mathbf{S}(p_{h_n}, \mathbf{D}(\mathbf{v}_{h_n})) - \mathbf{S}(p, \mathbf{D}(\mathbf{v}))\|_2 + (1 + \tilde{\beta}_\Omega(2, \gamma^+)) \|p - q_{h_n}\|_2 + o(1), \quad h_n \searrow 0.
\end{aligned}$$

Using the density (2.18)₂, we finally assert (2.40):

$$\begin{aligned}
\tilde{\beta}_\Omega(2, \gamma^+) \|p_{h_n} - p\|_2 &\leq \tilde{\beta}_\Omega(2, \gamma^+) \inf_{q_{h_n} \in \mathcal{Q}_{h_n}^r} \{ \|p_{h_n} - q_{h_n}\|_2 + \|q_{h_n} - p\|_2 \} \\
&\leq \|\mathbf{S}(p_{h_n}, \mathbf{D}(\mathbf{v}_{h_n})) - \mathbf{S}(p, \mathbf{D}(\mathbf{v}))\|_2 + o(1), \quad h_n \searrow 0,
\end{aligned}$$

which completes the proof. \square

Corollary 15 (Existence of solutions to **(P)**). *Let Assumption 2 hold and Assumption **(A3)** be satisfied with $\beta := \beta_\Omega(2, \gamma^+)$. Then there exists a weak solution to **(P)**.*

Proof. The assumptions of Theorem 14 are satisfied due to Lemma 9. \square

2.4 Auxiliary tools

Theorem 16 (Brouwer fixed-point theorem). *A continuous mapping on a compact convex set in \mathbb{R}^n has a fixed point.*

Corollary 17. *Denote $B := \{|\mathbf{x}| \leq 1\}$ a closed unit ball in \mathbb{R}^n . Let $\kappa : \partial B \rightarrow (0, \infty)$ and $\mathcal{P} : \mathbb{R}^n \rightarrow \mathbb{R}^n$ be continuous mappings such that $\mathcal{P}(\mathbf{x}) \cdot \mathbf{x} \geq 0$ for any $\mathbf{x} = \kappa(\mathbf{z})\mathbf{z}$, $\mathbf{z} \in \partial B$. Then there exists $\mathbf{x}_0 = \kappa(\mathbf{z}_0)\mathbf{z}_0$, $\mathbf{z}_0 \in B$ such that $\mathcal{P}(\mathbf{x}_0) = \mathbf{0}$.*

Proof. We proceed by contradiction. Let such \mathbf{z}_0 does not exist, i.e. $|\mathcal{P}(\kappa(\mathbf{z})\mathbf{z})| > 0$ for any $\mathbf{z} \in B$. Therefore, we can define a continuous mapping $\mathcal{M} : B \rightarrow \partial B \subset B$ as follows,

$$\mathcal{M}(\mathbf{z}) := \frac{-\mathcal{P}(\kappa(\mathbf{z})\mathbf{z})}{|\mathcal{P}(\kappa(\mathbf{z})\mathbf{z})|}.$$

The Brouwer fixed-point theorem gives us $\mathbf{z} \in \partial B$ such that $\mathcal{M}(\mathbf{z}) = \mathbf{z}$, which implies, using the assumptions,

$$0 \geq -\mathcal{P}(\kappa(\mathbf{z})\mathbf{z}) \cdot \mathbf{z} = |\mathcal{P}(\kappa(\mathbf{z})\mathbf{z}) \cdot \mathbf{z}| \mathcal{M}(\mathbf{z}) \cdot \mathbf{z} = |\mathcal{P}(\kappa(\mathbf{z})\mathbf{z}) \cdot \mathbf{z}| |\mathbf{z}|^2 > 0.$$

\square

Theorem 18 (Vitali's lemma). *Let Ω be a bounded domain in \mathbb{R}^d and $f^n : \Omega \rightarrow \mathbb{R}$ be integrable for every $n \in \mathbb{N}$. Assume that*

- *$\lim_{n \rightarrow \infty} f^n(y)$ exists and is finite for almost all $y \in \Omega$;*
- *for every $\varepsilon > 0$ there exists $\delta > 0$ such that*

$$\sup_{n \in \mathbb{N}} \int_H |f^n(y)| \, dy < \varepsilon \quad \text{for all } H \subset \Omega, |H| < \delta .$$

Then

$$\lim_{n \rightarrow \infty} \int_{\Omega} f^n(y) \, dy = \int_{\Omega} \lim_{n \rightarrow \infty} f^n(y) \, dy.$$

Chapter 3

Numerical method

Contents

3.1	Description of the numerical method	41
3.2	Observed behavior of the numerical method	42
3.3	Condition (A4) seems to determine the numerical stability . . .	43

3.1 Description of the numerical method

Finite elements. Numerical simulations presented in the thesis are restricted to two-dimensional flows. The considered Galerkin discretization (\mathbf{P}_h) of the problem (\mathbf{P}) is based on quadrilateral meshes and the following finite elements. The discrete velocity/pressure spaces are generated by the second order $\mathbf{Q}_2/\mathbf{P}_{-1}$ finite elements pair described in Gresho and Sani (2000); Sani et al. (1981), see also Hron (2001); Hron et al. (2003). The conforming space of biquadratic elements \mathbf{Q}_2 is defined on the reference quadrilateral $T_{\text{ref}} = (-1, 1)^2$ by

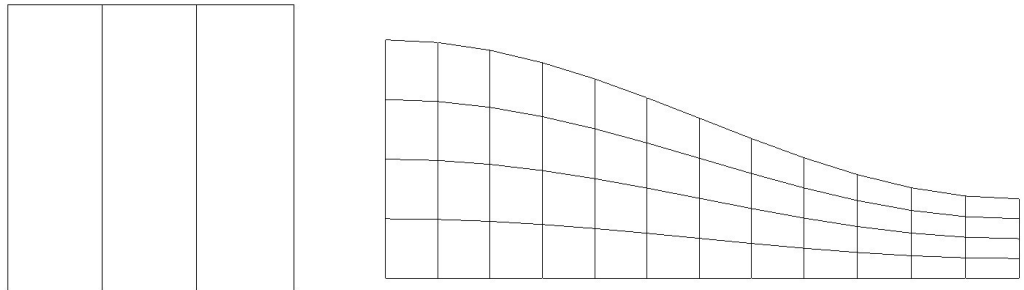
$$\mathbf{Q}_2(T_{\text{ref}}) = \text{span}\{1, x, y, xy, x^2, y^2, x^2y, xy^2, x^2y^2\},$$

with nine local degrees of freedom located at the vertices, the midpoints of edges and the center of quadrilateral. The space \mathbf{P}_{-1} is in general discontinuous and consists of functions linear on each quadrilateral,

$$\mathbf{P}_1(T_{\text{ref}}) = \text{span}\{1, x, y\},$$

with the value and two partial derivatives specified in the center of the quadrilateral.

Quadrilateral meshes. Meshes of quadrilaterals are generated by uniform refinement of a given coarse mesh. The given mesh is transformed within the code to the geometry of the problem and later to the geometry desired for visualization. For illustration, Fig. 3.1 shows a coarse input mesh of 3 elements and a refined computational mesh of 3×4^2 elements, for a problem of converging surfaces with given length and height parameters. The other obvious possibility—to keep the computational mesh undeformed and to transform the equations instead—is not considered in this thesis.



(a) Input coarse mesh of 3 quadrilaterals. (b) Computational refined mesh of 3×4^2 quadrilaterals.

Figure 3.1: Input and computational mesh for the converging surfaces ($L = 4$, $2H = 2$, $H = 1$).

To guarantee sufficient accuracy would require computable *a posteriori* error bounds, that are currently beyond our knowledge. Note that the *a priori* error estimates have been derived (under the assumptions of Chapter 2) only recently, although they are not presented in this text (see Hirn et al., 2010). In the absence of such theoretical results (which is not uncommon in the fluid mechanics) the standard approach how to check that the discrete solutions are reasonably close to the exact solution is to compare the solution computed on the current mesh (say, for the discretization parameter h) with the solution computed on a uniformly refined mesh (say, for $h/2$). The difference between the two solutions (if small) gives *certain idea* about the distance to the exact solution. The idea is based on (known or anticipated) *a priori* estimates on the rate of convergence of the error (e.g., see Repin, 2008). Minor differences

have been observed for the solutions presented in Chapter 4, which seems sufficient for the qualitative purposes of the thesis.

Algebraic solver. The resulting system of nonlinear algebraic equations is solved using the damped Newton method with line search, as described in Hron (2001). As soon as the approximation gets sufficiently close to the solution, the basic Newton method is known to give a q-quadratic convergence (provided that the algebraic system has a solution and has a nonsingular and Lipschitz continuous derivatives in the neighbourhood of the solution). The Jacobian matrix is approximated by computing the central finite differences, taking into account the sparsity of the matrix. The adaptive change of length of the correction vector, the line search, improves a chance for convergence when the initial guess is far from the solution. See Kelley (2003) for a nice brief review of Newton’s method. In the presented numerical experiments the (almost) q-quadratic convergence of the residua has been observed at the end of the iteration process, allowing us to require safe enough values of the stopping criteria for the non-linear loop.

The linear subproblems are unsymmetric and sparse, and are mostly solved by **UMFPACK** package solver (Davies, 2004), which implements the direct sparse **LU** factorization via the unsymmetric multifrontal method. Only problems too large to be factorized were solved by the restarted GMRES method preconditioned by incomplete **LU** factorization with s levels of fill (**ILU**(s)), implemented in **SPLIB** library (Bramley and Wang, 1995).

Software implementation. All numerical simulations presented in the thesis are performed by the software developed by Jaroslav Hron (see Hron, 2001; Hron et al., 2003) implemented in **ANSI C** using standard **BLAS** and **LAPACK** libraries and the packages **UMFPACK** and **SPLIB**. The contribution of the author of the thesis to the code was negligible, although some necessary or experimental modifications were performed.

The method described above belongs to those quite standard in computational fluid dynamics (e.g., see Gresho and Sani, 2000). The code has been successfully used for number of different nonlinear problems related to incompressible flows of different non-Newtonian fluids, to flow–structure interaction problems and others. It was one of the intended goals to confront this approach with the models with pressure dependent viscosities. We did *not* focus on seeking an optimal numerical approach to deal with the problems considered in Chapter 4. No comparisons with other methods are included and no reasoning is given to assert whether the chosen discretization is favourable for lubrication problems.

3.2 Observed behavior of the numerical method

After some experimentation with a few pressure–viscosity relations, one observes that for certain range of parameters (depending on the particular problem) the above numerical method does not deliver a solution. It is not clear, of course, if these failures are due to the numerical approach or whether the weak solution to the original problem does not exist. The present theory guarantees the existence of a weak solution only for viscosities satisfying Assumptions **(A1)**–**(A3)** (see page 21), while for a wide class of constitutive models the existence

is an open problem. The assumptions **(A2)**–**(A3)** are not needed to prove the existence of discrete solutions (see Theorem 11) but they are required to show its uniqueness.

It was an original intention of the author to verify whether the models satisfying **(A1)**–**(A3)** allow for a robust numerical treatment and whether they can be used to approximate lubricants in real-world applications. We illustrate in Chapter 5 that such models can approximate the real-world liquids only in a restricted range of parameters. However, the numerical experiments show that we obtain the discrete solutions for a set of problems *larger* than given by **(A1)**–**(A3)**. In fact, the author did observe *no obvious change of behavior* of the numerical method and no qualitative change of solutions, which could be linked to the violation of these assumptions. This indicates that **(A1)**–**(A3)** are related to the technique of the proofs, and that Problem **(P)** may be well-posed for a wider class of viscosity models.

In the following, we report on the numerical experiments suggesting that the condition determining the convergence of the considered numerical method to the discrete solution is **(A4)**. We show in Chapter 5 that this allows to model real liquids over significantly broader range of parameters, see Section 5.3.

3.3 Condition **(A4)** seems to determine the numerical stability

To illustrate the point, we examine the flow between converging plates, which is described in detail in Section 4.2. The viscosity (1.12) of the three reference liquids from Subsection 1.3.4 will be used. The flow is induced solely by the tangential motion of the lower surface, and a pressure peak is generated in the middle left part of the domain due to the converging geometry. The height of the domain will be fixed, $H = 10^{-5}$ m at the output and $2H$ at the input. We will play with two parameters: the length of the considered domain, L , and the velocity of the lower surface, V . Note that the velocity profile is approximately linear at the cross-section concurrent with the pressure peak location, and that the values of $|\mathbf{D}(\mathbf{v})|$ are then approximately of the order V/H . By increasing L , the resulting pressure values are increased, while by increasing V , both the values of $|\mathbf{D}(\mathbf{v})|$ and p are increased. Examples of the resulting flow are presented in detail in Section 4.2.

Here we proceed as follows: for different liquids, by taking different L and V we arrange for solutions with different values of $|\mathbf{D}(\mathbf{v})|$. Then, we increase V as long as the method converges to a discrete solution; the solution obtained for current V is always taken as the initial guess for the next problem. After certain limit is reached, the Newton method does not converge any more, not even if the next V is taken very close to the previous one (so that the initial residual is very small). What happens is either that the Jacobian matrix becomes singular, or the nonlinear iterations diverge until the represented variables become infinite in computer arithmetic.

Table 3.1 shows a set of experiments with different liquids. We report the values of L , levels of mesh refinement, and three values of V : For the third value of V , the method does not converge any more; the second value of V is the “critical” value, while the first value is only a “sub-critical” example. For illustration, Figure 3.2 depicts the solution of the last experiment of the table for $V = 31.84$ m.

Reference liquid:	SQL+PIP	SQL+PIP	PGLY	PGLY	SQL	SQL
No. of elements:	3×4^4	3×4^4	3×4^4	3×4^4	1×4^3	6×4^5
L / m	10^{-1}	10^{-3}	10^{-1}	5×10^{-3}	10^{-2}	10^{-2}
V / ms^{-1}	0.9	250	5×10^{-3}	2×10^6	30	30
$\max_{\mathbf{x} \in \Omega} \partial \mathbf{S} / \partial p $	0.006	0.14	0.002	0.8	0.03	0.04
$\min_{\mathbf{x} \in \Omega} \eta(p, \mathbf{D}) / \text{Pa s}$	0.06	0.02	16	1×10^{-4}	0.01	0.02
$\max_{\mathbf{x} \in \Omega} \eta(p, \mathbf{D}) / \text{Pa s}$	6.8	0.32	1×10^3	2×10^{-2}	0.8	1.4
$\max_{\mathbf{x} \in \Omega} p$ / MPa	371	190	532	322	191	321
$\min_{\mathbf{x} \in \Omega} \mathbf{D} $ / s^{-1}	2×10^3	3×10^5	14	1×10^9	3×10^5	2×10^4
$\max_{\mathbf{x} \in \Omega} \mathbf{D} $ / s^{-1}	4×10^5	1×10^8	2×10^3	9×10^{11}	1×10^7	1×10^7
$\max_{\mathbf{x} \in \Omega} \mathbf{S} $ / MPa	0.9	13	0.8	217	4.3	6.4
V / ms^{-1}	0.919041	278.3810	5.83693×10^{-3}	2.3063×10^6	32.470	31.840
$\max_{\mathbf{x} \in \Omega} \partial \mathbf{S} / \partial p $	0.9	0.8	0.9	0.8	0.9	0.7
$\min_{\mathbf{x} \in \Omega} \eta(p, \mathbf{D}) / \text{Pa s}$	0.06	0.02	16	1×10^{-4}	0.01	0.02
$\max_{\mathbf{x} \in \Omega} \eta(p, \mathbf{D}) / \text{Pa s}$	904	2.8	3×10^5	3×10^{-2}	56	46
$\max_{\mathbf{x} \in \Omega} p$ / MPa	688	377	1740	436	466	992
$\min_{\mathbf{x} \in \Omega} \mathbf{D} $ / s^{-1}	2×10^3	3×10^5	17	1×10^9	3×10^5	2×10^4
$\max_{\mathbf{x} \in \Omega} \mathbf{D} $ / s^{-1}	4×10^5	1×10^8	2×10^3	1×10^{12}	1×10^7	1×10^7
$\max_{\mathbf{x} \in \Omega} \mathbf{S} $ / MPa	124	115	255	332	270	221
failure: V / ms^{-1}	0.919042	278.3811	5.83694×10^{-3}	2.3064×10^6	32.471	31.841

Table 3.1: Correlation of the convergence of the numerical method with the condition **(A4)**.

For the first two values of V of each experiment, the table reports the ranges of several quantities. While the maximal viscosity, pressure and shear rates differ, we observe that the maximal reached value of $|\partial \mathbf{S} / \partial p|$ is always almost exactly 1. Note that for “sub-critical” values of V , this quantity is typically much less than 1.

Another set of experiments, concerned with the journal bearing lubrication, will be presented in Section 4.3. For each experiment a sequence of numerical simulations are performed, with the geometrical parameter ε gradually increased until the method fails. In Figure 3.1 we report for all the performed experiments the maxima of $|\partial \mathbf{S} / \partial p|$ depending on ε . The last value achieved in each experiment is marked by a circle.

We made the following observation. Once the condition **(A4)** is violated, i.e. once the pressures and shear rates of the discrete solution are so large that $\max_{\mathbf{x} \in \Omega} |\partial \mathbf{S} / \partial p| \geq 1$, the non-linear iteration process fails. As long as the condition is satisfied, however, the non-linear solver converges. It may happen that the discrete solution satisfies **(A4)** but it is violated during the iteration process. In that case the process may fail due to numerical overflow. Typically, this can be prevented by using a solution of similar problem as an initial guess.

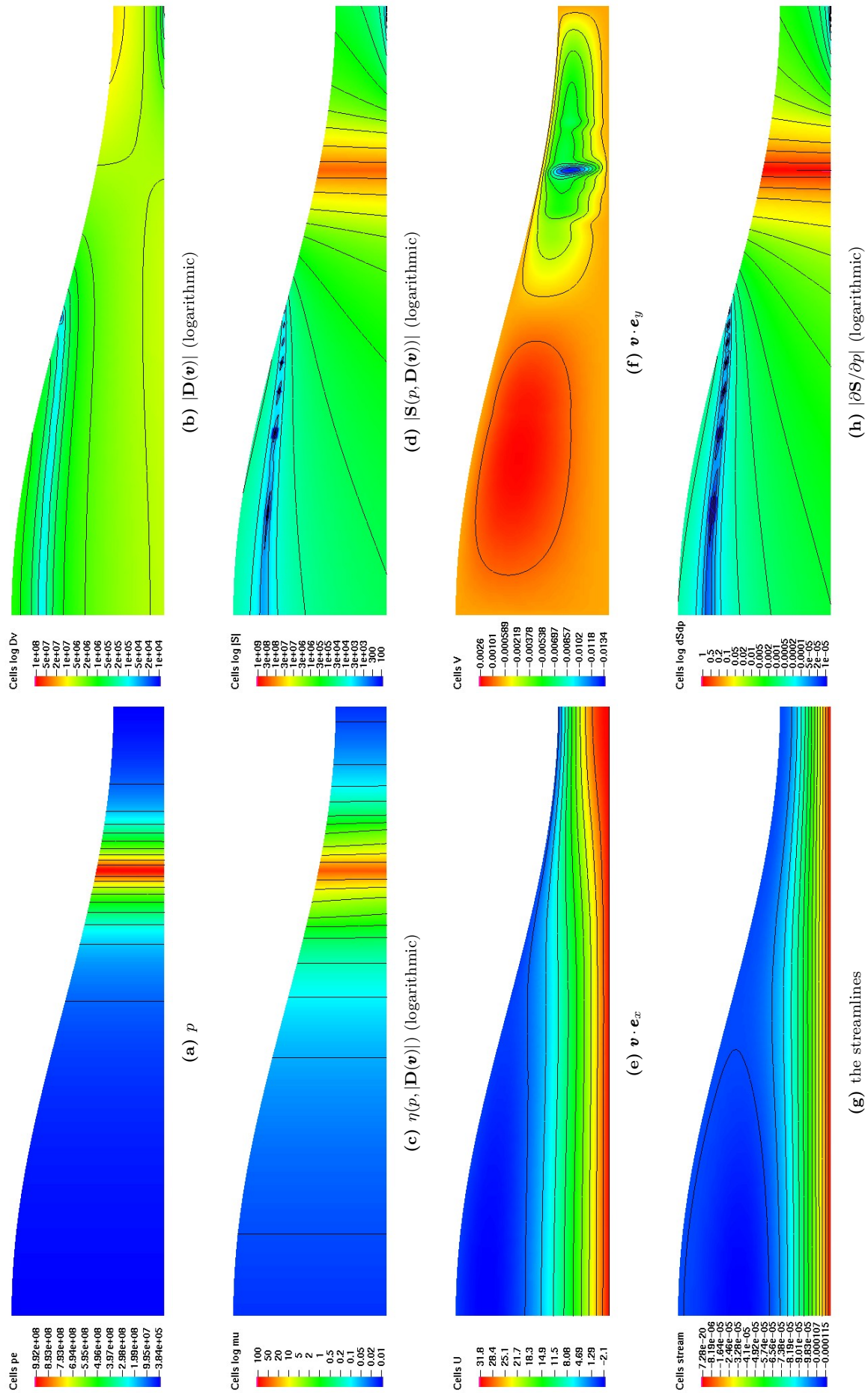


Figure 3.2: Example solution close to the limits of the numerical method.

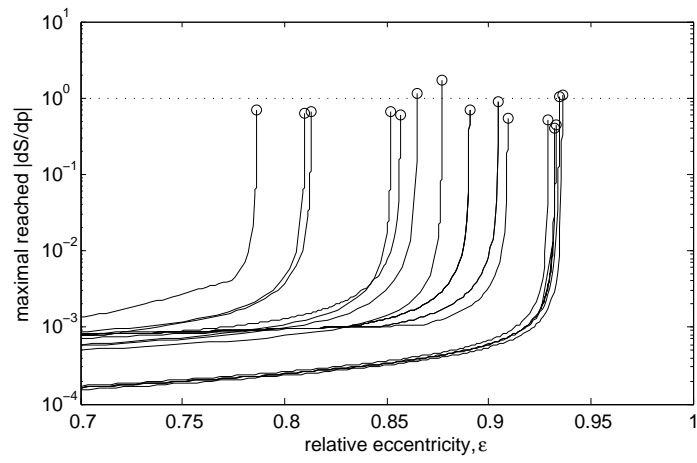


Figure 3.3: $\max_{\mathbf{x} \in \Omega} |\partial \mathbf{S} / \partial p|$ depending on ε for all experiments presented in Section 4.3.

Chapter 4

Numerical simulations

Contents

4.1	Planar Poiseuille flow	48
4.2	Sliding converging surfaces	49
4.2.1	Flow with pressure-thickening and shear-thinning lubricant	50
4.2.2	Sensitivity of the pressure field due to pressure-thickening	55
4.3	Planar steady flow in journal bearing	56
4.3.1	Basic features of the flow	58
4.3.2	Exact solution for the constant viscosity lubricant flow	58
4.3.3	The influence of shear-thinning and pressure-thickening	60
4.3.4	Importance of the level of pressure	67

4.1 Planar Poiseuille flow

Consider the classical example of the flow in between infinite parallel plates (say, $y = 0$ and $y = H > 0$), where everything is uniform with the z -coordinate and the flow is planar in the x, y -plane. Assume *no-slip* conditions at the plates which are held steady, i.e., set $\mathbf{v} = \mathbf{0}$ at the plates. For a Newtonian fluid, as well as for non-Newtonian fluids with the viscosity depending only on the shear rate, there exists a unidirectional Poiseuille flow driven by a constant pressure gradient

$$\eta = \eta(|\mathbf{D}|), \quad \mathbf{v} = (u(y), 0), \quad p = p(x) = G_p x, \quad (4.1)$$

where $G_p \in \mathbb{R}$ and the velocity profile are related by

$$G_p = u''(y) \left\{ \eta\left(\frac{|u'(y)|}{\sqrt{2}}\right) + \eta'\left(\frac{|u'(y)|}{\sqrt{2}}\right) \frac{|u'(y)|}{\sqrt{2}} \right\}.$$

The situation is more complex for the piezoviscous fluid, however. As was shown by Bair et al. (1998) and confirmed rigorously by Hron et al. (2011, 2001), e.g. for the Barus model $\eta = \eta_0 \exp(\alpha p)$ the unidirectional flow does not exist. A pressure gradient across the fluid film and a corresponding secondary flow has to be expected, which has however not been reached by analytical methods.

The following numerical simulation aims to show the behavior of the flow between stationary parallel plates. Naturally, we have to restrict ourselves to a finite domain, where the flow is induced by the pressure drop between inflow and outflow. Let us comment on the boundary conditions at the artificial boundaries $x = 0$ and $x = L > 0$. Note that the condition (1.20)

$$-\mathbf{T}\mathbf{n} = P(x)$$

is not a good choice as long as concerns this kind of flow (in straight channels). This can be illustrated by the example (4.1), where one observes (for $\mathbf{n} = \mathbf{e}_x$) that

$$-\mathbf{T}\mathbf{n} = \left(p(x), \eta\left(\frac{|u'(y)|}{\sqrt{2}}\right) u'(y) \right).$$

Note that the second component of the right hand side is not constant across the fluid film and, more importantly, it includes the complete information about the velocity profile. By setting (1.20) with $\mathbf{b} = (P(x), 0)$, the resulting flow would not be unidirectional (see Heywood et al., 1996).

Here, due to our concern with simple (unidirectional) flows, we set the condition (1.21)

$$\mathbf{v}_\tau = \mathbf{0} \quad \text{and} \quad -\mathbf{T}\mathbf{n} \cdot \mathbf{n} = P(x), \quad (4.2)$$

i.e., we enforce the flow parallel to the plates at the boundary ($\mathbf{v} \cdot \mathbf{e}_y = 0$), while we determine the pressure values by prescribing the normal part of the traction.

In the following example, we take the Barus viscosity model $\eta = \eta_0 \exp(\alpha p)$ with the parameters

$$\eta_0 = 16.3 \text{ Pa s}, \quad \alpha = 1.3 \times 10^{-8} \text{ Pa}^{-1},$$

(it approximates the PGLY reference liquid at $T = 40^\circ\text{C}$ if the shear-thinning is ignored, see Subsection 1.3.4). Moreover, merely in order to separate the interesting features of the flow from the (unknown) influence of the artificial boundary condition at the inflow, we cut off the viscosity above certain value; this results into a unidirectional flow near the inflow boundary. To summarize, we take the following setting:

$$\eta = \eta_0 \exp(\alpha \hat{p}), \quad \text{where} \quad \hat{p} = \min\{p, 150 \text{ MPa}\}$$

$$P(0) = 300 \text{ MPa}, \quad P(L) = 0, \quad L = 3 \times 10^{-5} \text{ m}, \quad H = 1 \times 10^{-5} \text{ m}.$$

The resulting flow is reported in Figure 4.1. In the left part near the inflow, where the pressure is above the cut-off and the viscosity is constant, we observe the unidirectional Poiseuille flow with the pressures constant across the film; in the middle and right part, the effect of the piezoviscous viscosity is visible: The pressure gradient is no more parallel to the plates and a secondary flow occurs. Note that we would observe analogous flows even without the cut-off; also note that the fluids with both pressure-thickening and shear-thinning viscosity would give analogous results in this example.

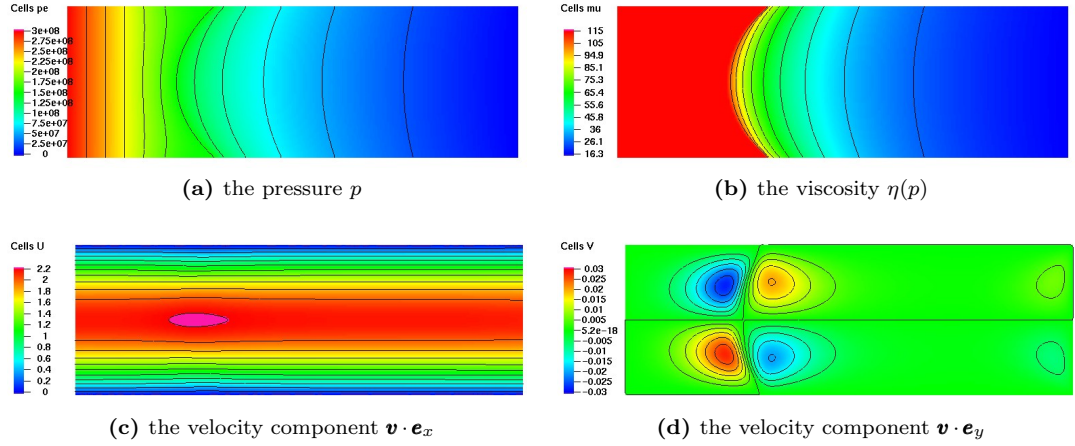


Figure 4.1: The flow of a piezoviscous fluid between parallel plates.

4.2 Sliding converging surfaces

The simple flows in straight channels or between parallel plates are lacking the most essential feature of hydrodynamic lubrication: the pressure peak generated by the flow, which allows to carry high loads. The simple problem which allows to study this feature is the flow between plates whose distance decreases in the direction of the flow.

We will study the following problem: everything is uniform in the z -coordinate and a planar flow is studied in the x, y -plane. The lower plate is defined by $y = 0$, the upper is described by $y = h(x) > 0$. We restrict our attention to the interval $x \in (0, L)$ and we set $h(x) = H(\frac{3}{2} + \frac{1}{2} \cos(x\pi/L))$; this is chosen so that $h(0) = 2H$, $h(L) = H$ and $h'(0) = h'(L) = 0$, see Figure 4.2. In this study, we always set $H = 10^{-5}$ m.

We concentrate on sliding conditions: the upper plate is considered steady, while the lower moves with the velocity V . These are more relevant to journal bearing lubrication than, for

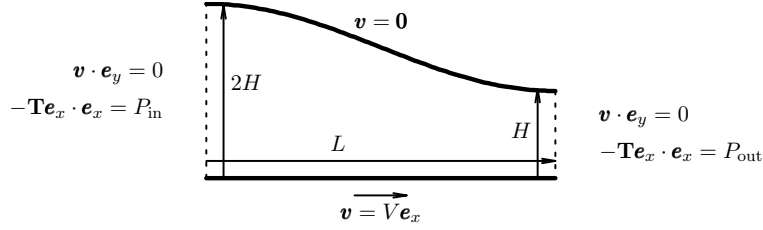


Figure 4.2: The geometry of converging surfaces problem.

example, rolling conditions where the upper plate would progress (tangentially) in the same direction as the lower plate, and the resulting flow would be of a different type. On the surfaces we will assume *no-slip* conditions, i.e. we set $\mathbf{v} = \mathbf{v}_\tau = V\mathbf{e}_x$ on the lower and $\mathbf{v} = \mathbf{0}$ on the upper boundary. On the artificial inflow and outflow boundaries we set the boundary condition (1.21), i.e., we prescribe that the flow through the boundaries is parallel to the lower plate and we determine the inflow and outflow pressures.

4.2.1 Flow with pressure-thickening and shear-thinning lubricant

We report numerical solutions to the following four examples with the reference liquids from Subsection 1.3.4.

- i) SQL, $L = 3 \times 10^{-3}$ m, $V = 10^2$ m/s, Figure 4.3;
- ii) PGLY, $L = 5 \times 10^{-3}$ m, $V = 10^1$ m/s, Figure 4.4;
- iii) SQL+PIP, $L = 10^{-2}$ m, $V = 10^1$ m/s, Figure 4.5;
- iv) SQL+PIP, $L = 10^{-3}$ m, $V = 10^2$ m/s, Figure 4.6.

In all the examples, $H = 10^{-5}$ m, and zero normal component of traction (4.2) is given at both the inflow and outflow boundaries, $P(0) = P(L) = 0$. The parameters chosen in the examples above do not follow any particular scheme, and analogous results could be achieved by using any one of the reference liquids.

In the SQL example, the viscosity field is clearly dominated by pressure-thickening and is, same as the pressure field, almost constant across the fluid film. In all the other examples both shear-thinning and pressure-thickening are significant, displaying two local maxima in the viscosity field: one due to the pressure peak, one due to the local minimum of shear rate which occurs at the point of bifurcation of the flow and extends upstream through the backward flow whirl. The resulting viscosity field then shows slightly different shapes in the three examples: the sharp and long ridge in Figure 4.6 following the narrow of the shear rate minimum; the round jutting more connected to the pressure peak area in Figure 4.5; or the well localized maximum adherent to the upper plate in the PGLY example in Figure 4.4.

The examples demonstrate that the viscosity cannot be considered constant across the fluid film once the shear-thinning takes place. Once the backward flow appears, a sharp minimum of the shear rates emerges which can affect the viscosity significantly.

The selected examples, however, show no surprising results. In particular, no secondary flow related solely to the pressure-thickening manifested within the range of parameters allowed

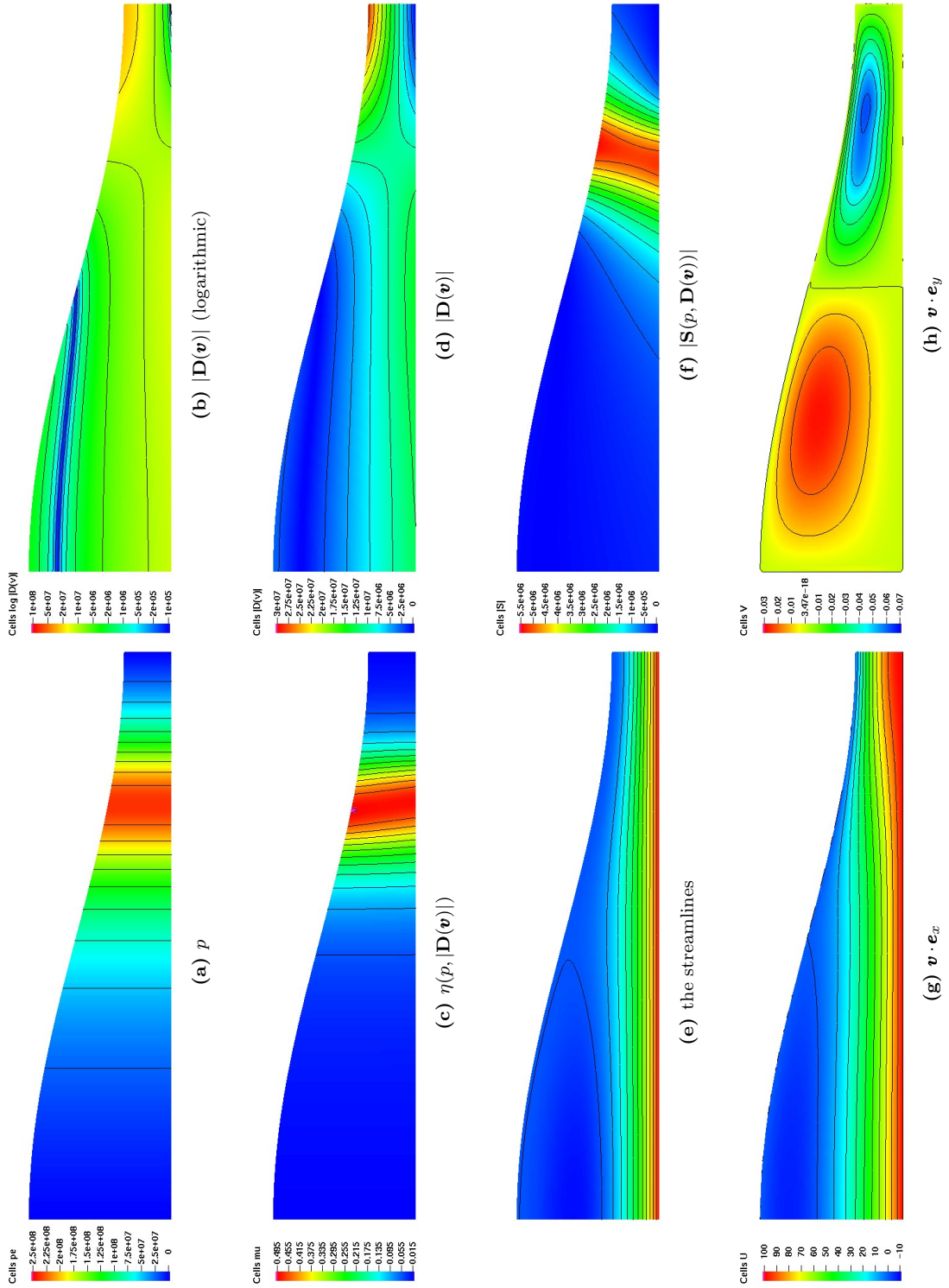


Figure 4.3: Example flow between converging plates, SQL , $L = 3 \times 10^{-3}$ m, $V = 10^2$ m/s.

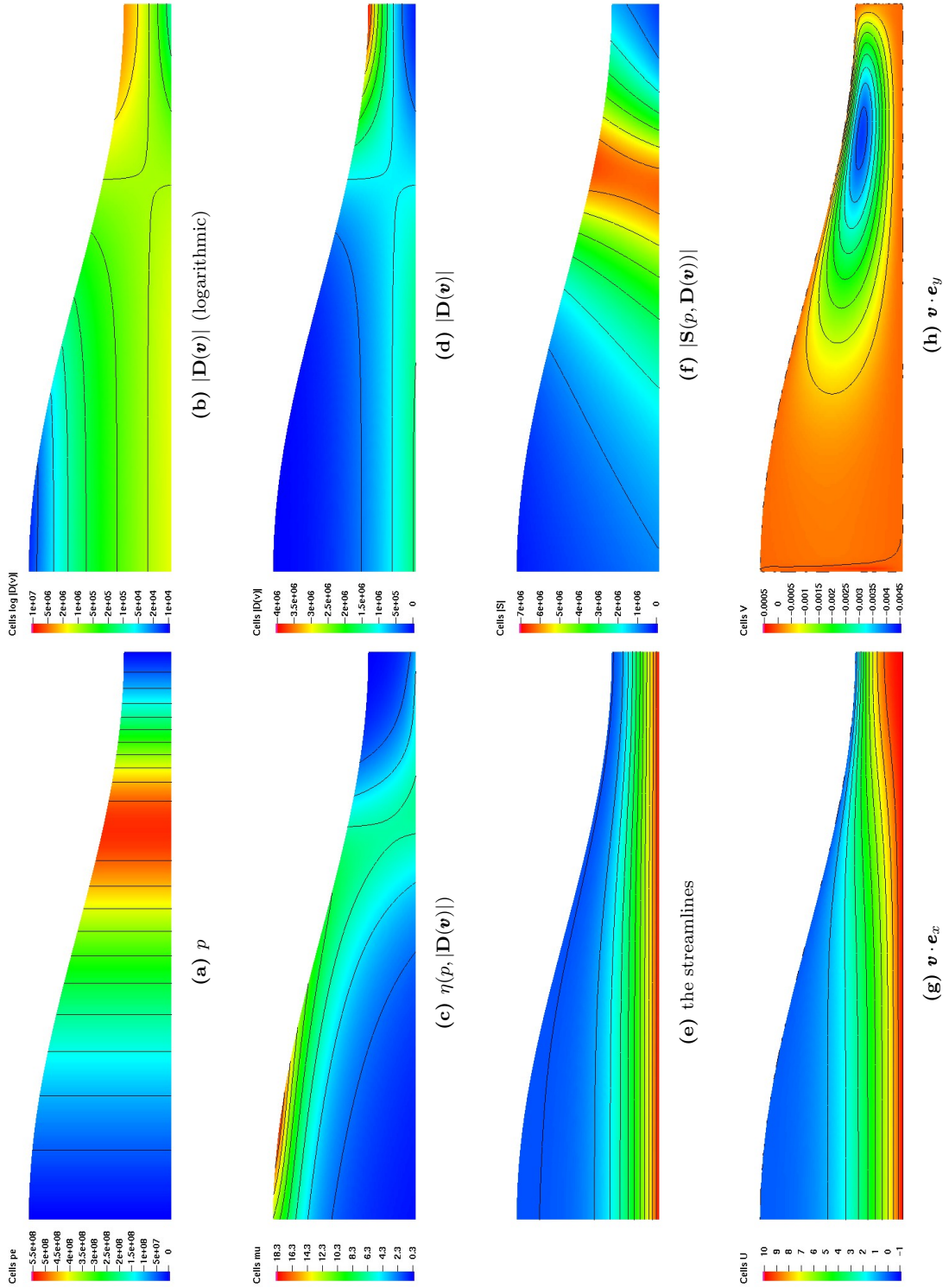


Figure 4.4: Example flow between converging plates, PGLY, $L = 5 \times 10^{-3}$ m, $V = 10^1$ m/s.

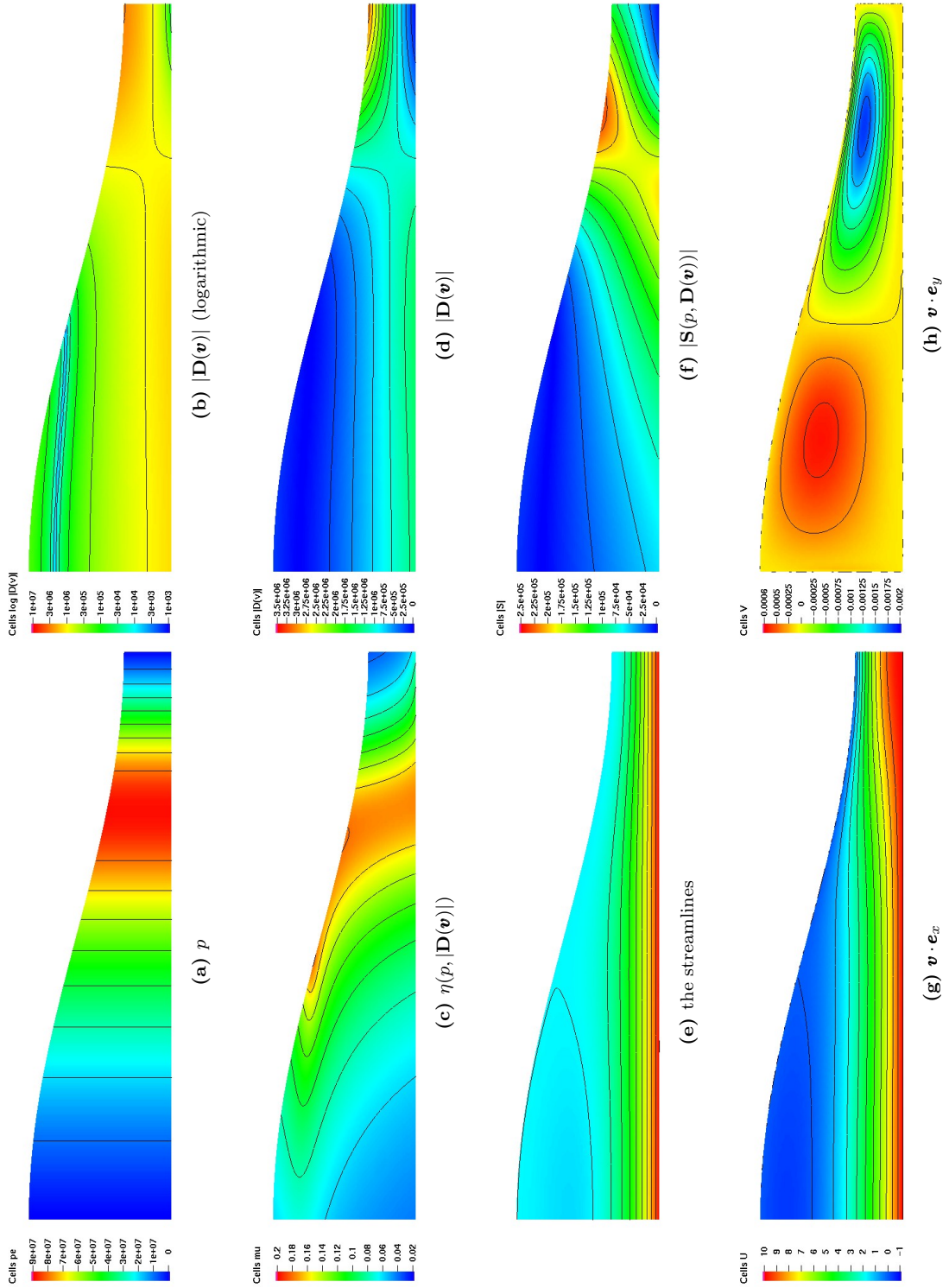


Figure 4.5: Example flow between converging plates, SQL+PIP, $L = 10^{-2}$ m, $V = 10^1$ m/s.

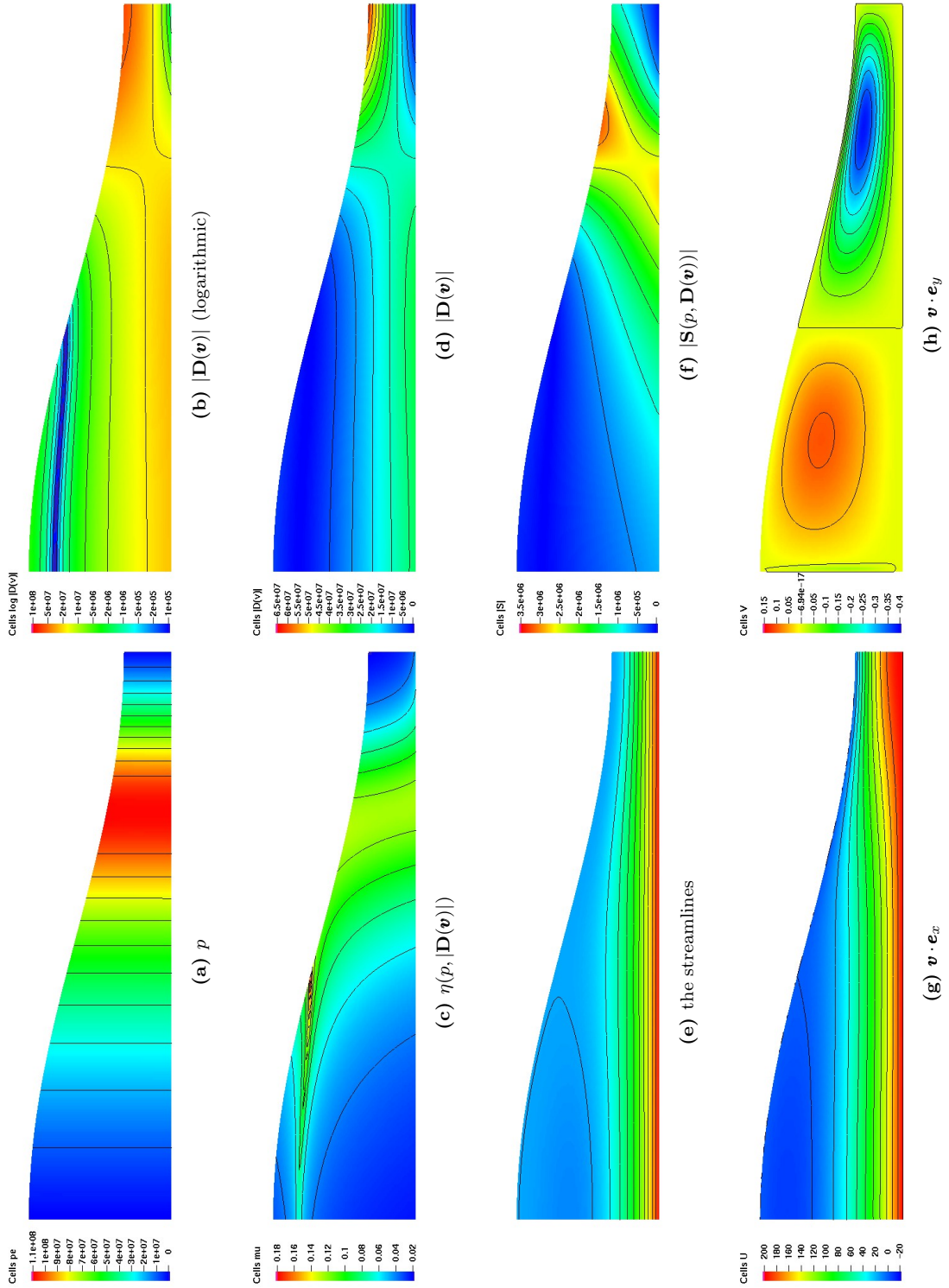


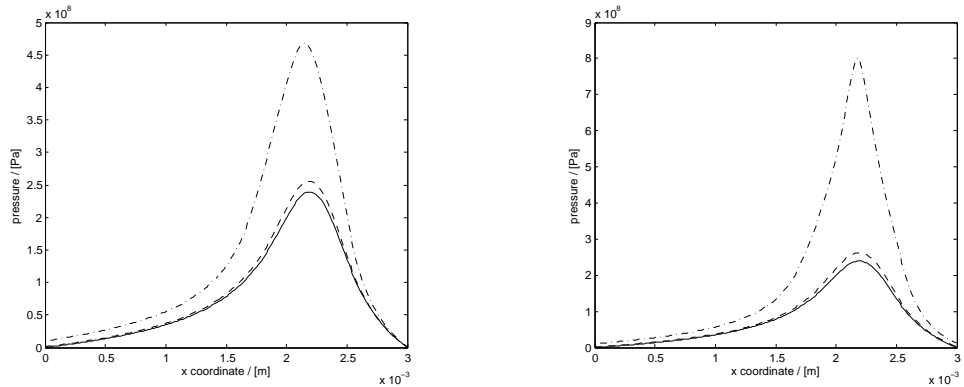
Figure 4.6: Example flow between converging plates, SQL+PIP, $L = 10^{-3}$ m, $V = 10^2$ m/s.

by the numerical method. The features observed in the examples ii)–iv) are related to the interplay between shear-thinning and pressure-thickening.

4.2.2 Sensitivity of the pressure field due to pressure-thickening

As shown by the preceding examples, the pressure field is virtually constant across the fluid film; thus, we can draw the pressure profiles of the resulting flow along the x -coordinate. In this subsection, we report on a feature specific to flows of pressure-thickening fluids. The pressure peak can display a significant sensitivity on the pressure values far from the area of interest.

This is a known fact, which however should be emphasized for its several consequences: The resulting flow can depend severely on the values prescribed at the inflow/outflow boundaries (or, in other words, on the resulting level of the pressure). Moreover, considering the error due to discretization and the numerical approximation, one should keep in mind that the error allowed at one place may possibly be magnified while carried to the other part of the domain. Further, one can expect that the properties of the numerical problems to be solved, such as the performance of the non-linear solver, the conditioning of the linear subproblems or, e.g., the requirements on their successful preconditioning, may be different compared to problems where the viscosity does not depend on pressure.



(a) Pressure profiles with $P(0) = 0$ (full line), 1 MPa (dash) and 10 MPa (dash dotted) and with $P(L) = 0$.

(b) Pressure profiles with $P(0) = P(L) = 0$ (full line), 1 MPa (dash) and 10 MPa (dash dotted).

Figure 4.7: Pressure profiles for SQL, $L = 3 \times 10^{-3}$ m, $V = 10^2$ m/s.

We illustrate the issue by the following simple observations based on the example i) of the previous subsection. In Figure 4.7a we increase the traction prescribed at the inflow from $P(0) = 0$ to $P(0) = 1$ MPa and 10 MPa; in Figure 4.7b both $P(0)$ and $P(L)$ are increased analogously. Note that since the viscosity depends on pressure approximately exponentially, the sensitivity of the pressure peak on the boundary values is the more intense the higher is the pressure peak, and can be much less or *much more* intense than in Figure 4.7.

4.3 Planar steady flow in journal bearing

In this section we will examine the basic features of the flow of lubricant in a simple model of journal bearing. Let us recall what was briefly introduced in Subsection 1.1.1 and specify the setting for our numerical experiments in more detail. The journal and the bearing are solid cylinders with parallel eccentric axes, the outer (bearing) is held steady while the inner (journal) rotates about its own axis. The lubricant is introduced between the solid surfaces and its flow is induced by the journal rotation. In hydrodynamic regime the solid surfaces are well separated by the fluid film.

It is not our ambition to approach the full complexity of the problem nor to give particular engineering predictions; our aim is merely to pinpoint some features related to the constitutive model. For clarity of exposition and in order to reduce the amount of model parameters, we take several simplifications: the solid cylinders are rigid; the space between them is filled by the fluid entirely (*full-film* conditions); the fluid is incompressible and is able to sustain arbitrary negative pressures; inertial forces are neglected; *no-slip* conditions are considered at the solid surfaces.

Planar flow. We take the *long bearing* approximation, considering only a planar flow, uniform in the direction of cylinders axes; in other words, we study a two-dimensional flow in an eccentric annulus. The geometry is depicted on Figure 4.8 and is described by three parameters, the radii $R_J < R_B$ and the relative eccentricity $\varepsilon \in (0, 1)$ defined by $\varepsilon(R_B - R_J) = e$, where e is the distance between the journal and bearing axes. Throughout this section, we take the geometrical parameters given by Table 4.1 that were used in a series of papers^a by Davies, Gwynllyw, Li and Phillips.

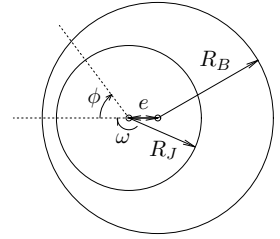


Figure 4.8

Steady flow. We confine ourselves to studying steady flows in fixed geometry, i.e., in the geometry with the relative eccentricity ε prescribed as an input parameter. With the steady solutions, we will be interested in the maxima and the distribution of several quantities within the flow field, and in the resulting force exerted on the journal by the fluid, defined by

$$\mathbf{F} = \int_{\Gamma_J} (-\mathbf{T}\mathbf{n}) \, d\mathbf{x},$$

where Γ_J denotes the journal surface and \mathbf{n} the unit outward normal vector. In real world, the rotating journal (when working in hydrodynamic regime) "floats" in the lubricant, being actuated by the resultant of applied load and of the forces due to the lubricant flow. Assuming that the motion of the journal axis is slow compared to the rotation speed, one can interpret the steady flow problem as a quasi-steady approximation to the unsteady flow at certain time and position of the journal axis. In particular, if the applied load is constant in time, the journal axis can eventually reach a steady state, where the applied load is in balance with the force \mathbf{F} exerted by the fluid. Note that such a stable equilibrium may or may not be reached; for example, it is well-documented in the literature (e.g., see Brindley et al. (1983); Li et al. (2000b)) that under the assumptions of full-film and constant viscosity lubricant, the journal

R_J	3.125×10^{-2} m
R_B	3.129×10^{-2} m

Table 4.1

^a See Gwynllyw et al. (1996a,b); Gwynllyw and Phillips (1996, 2005); Li et al. (2000a, 1999, 2000b)

exhibits a half-speed whirl: the trajectory of the journal spirals towards the bearing while the angular velocity of its path approaches $\omega/2$, where ω denotes the angular velocity of the journal rotation. On the other hand, the steady equilibria can be reached if cavitation and/or pressure-dependent viscosity is present in the model, see Gwynllyw et al. (1996b). We will not address the very interesting questions of dynamical behavior of the journal bearing system.

Problem setting. To summarize, we perform the following numerical experiments concerned with Problem (\mathbf{P}_h) . Gravity is neglected, $\mathbf{f} = \mathbf{0}$, and since the convective term is not considered either, the density of the lubricant does not appear in the governing equations. The domain is an eccentric annulus with the parameters given by Table 4.1 and with the relative eccentricity $\varepsilon \in (0, 1)$ given later. The viscosity models for the three reference lubricants described in Subsection 1.3.4 will be considered, always at the temperature $T = 100$ °C. At negative pressures, we simply extend these models by defining

$$\tilde{\eta}(p, |\mathbf{D}|) := \begin{cases} \text{if } p \geq 0, & \eta(p, |\mathbf{D}|), \\ \text{if } p < 0, & \eta_{\min}(|\mathbf{D}|) + (\eta(0, |\mathbf{D}|) - \eta_{\min}(|\mathbf{D}|)) \exp\left(\frac{\partial_p \eta(p, |\mathbf{D}|)|_{p=0}}{\eta(0, |\mathbf{D}|) - \eta_{\min}(|\mathbf{D}|)} p\right) \end{cases}$$

where $\eta_{\min}(|\mathbf{D}|) := \min\{10^{-3}\eta(0, 0), \frac{1}{2}\eta(0, |\mathbf{D}|)\}$. On the entire boundary, the Dirichlet boundary conditions are prescribed, namely $\mathbf{v} = \mathbf{0}$ on the outer circle and $\mathbf{v} = (\omega R_J)\boldsymbol{\tau}$ on the inner circle, where $\boldsymbol{\tau}$ is a clock-wise unit tangential vector and where ω is specified as follows: for SQL and SQL+PIP we set $\omega = 10^3$ rad/s, while for PGLY we choose $\omega = 10$ rad/s. The condition required to fix the level of pressure will be discussed.

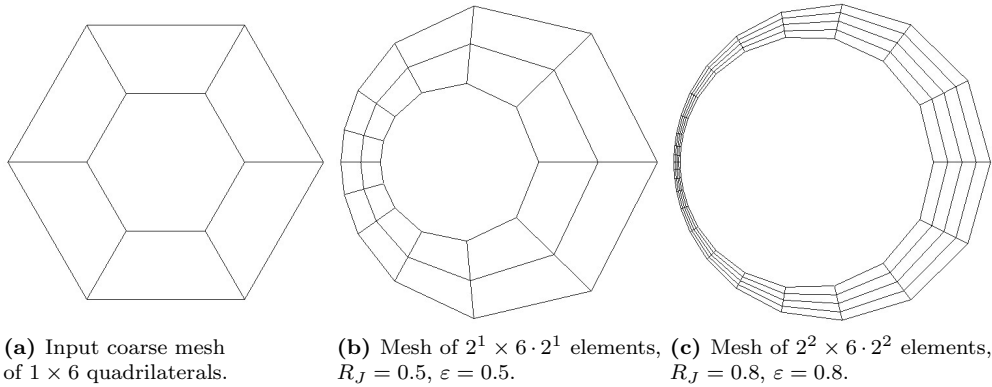


Figure 4.9: Input and transformed meshes for the journal bearing problem ($R_B = 1$).

Similarly as described in Subsection 3.1, the computational mesh of quadrilaterals is produced by geometrical transformation of the input coarse mesh, which has a simple concentric geometry. We will not specify this transformation in detail, see the example in Figure 4.9; note that while the geometrical deformation is linear in the radial direction, in the angular direction it is chosen such that the local ratio between the angular and radial lengths is preserved throughout the domain. The figures of the flow domain in this section use the same kind of transformation, usually with the radii 0.5 and 1 and the eccentricity $\varepsilon = 0.5$.

In all the numerical experiments presented, the computational mesh consists of $2^4 \times 128 \cdot 2^4$ quadrilaterals (2^n refers to n uniform refinements). This seems sufficient for our purposes (which are basically qualitative), the differences observed when compared to a solution at the coarser mesh have been minor.

4.3.1 Basic features of the flow

The basic character of the planar flow in the journal bearing is briefly illustrated in Figure 4.10; where streamlines, magnitude of the velocity vector, pressure and the norm of the symmetric velocity gradient are depicted. The figures show the solution of a Newtonian lubricant with $\eta = 10^{-2}$ Pa s, subject to the journal rotation at the angular velocity $\omega = 10^3$ rad/s. The displacement of the journal axis is in the direction $-\mathbf{e}_x$, with the relative eccentricity $\varepsilon = 0.75$. The pressure level is fixed by prescribing zero mean value over the domain, but this is unimportant since the viscosity does not depend on the pressure and the pressure field can be shifted by constant at ease, without affecting other quantities. Note that the annulus radii in the figures is different from those of the problem geometry, as explained earlier; the eccentricity, however, is unchanged here.

Since the viscosity is constant and only Stokes equations govern the flow, the pressure field is perfectly symmetric with respect to \mathbf{e}_x . The resulting force exerted on the journal by the fluid is then in the direction \mathbf{e}_y , i.e. perpendicular to the line connecting the journal and bearing centers. The depicted streamlines, typical for the journal bearing flow, show that only a part of the lubricant driven by the journal rotation is actually forced through the narrowest gap, the other part being transported by the reverse flow. The velocity profile (across the film) is approximately linear at the position of pressure minimum and maximum, while it is convex or concave otherwise, according to the width of the gap and in accordance with the direction of the pressure gradient. Due to the shape of the velocity profile, the velocity gradient varies significantly across the narrowest gap. Note from Figure 4.10c that the pressure is virtually constant along the radial direction; this allow us to draw the pressure profile along the angular direction in Figure 4.10e ($\phi = 0$ is the point of the narrowest gap while $\phi = \pm\pi$ the largest gap).

Note that in the above setting an analytical solution can be found in the literature, see the following subsection.

4.3.2 Exact solution for the constant viscosity lubricant flow

In Ballal and Rivlin (1976), a detailed analysis of the planar flow of a Newtonian (Navier–Stokes) fluid within an eccentric anulus can be found, including an exact solution to the problem without the inertial term, i.e. to the Stokes equations. We shortly recapitulate this exact solution here, since it can be (and has been) used to verify the FEM code in the journal bearing geometry. In contrast to the original paper, we restrict ourselves to the case that the journal is rotating and the bearing is held steady. See also Duffing (1924); Kamal (1966); Reissner (1935).

The following bipolar coordinate system is considered in Ballal and Rivlin (1976):

$$x = \frac{-b \sinh \xi}{\cosh \xi - \cos \zeta}, \quad y = \frac{b \sin \xi}{\cosh \xi - \cos \zeta},$$

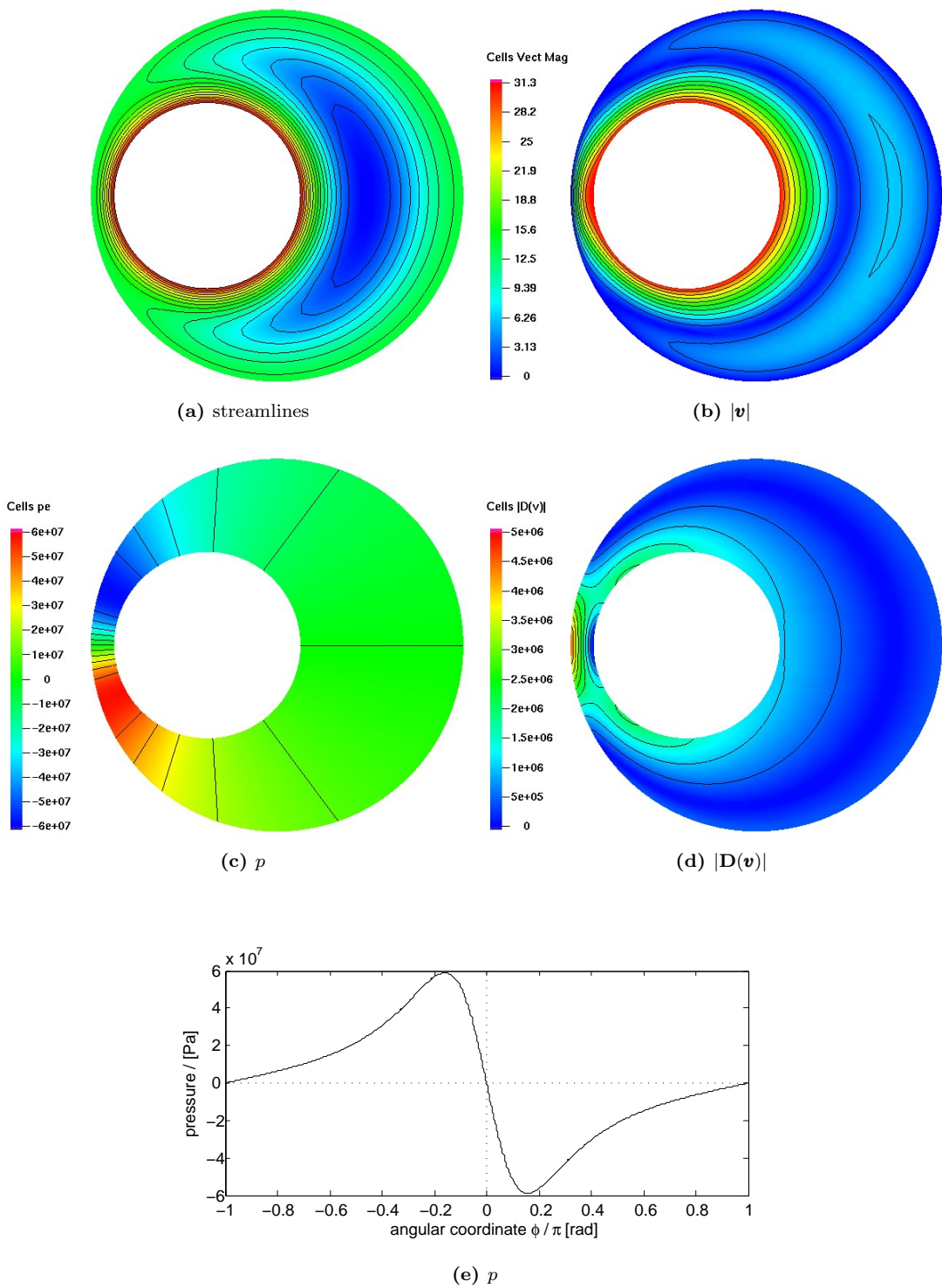


Figure 4.10: Basic features of the flow in journal bearing, $\varepsilon = 0.75$, $\omega = 10^3$ rad/s, $\eta = 10^{-2}$ Pa s.

where $\xi \in (\xi_J, \xi_B)$ and $\zeta \in (0, 2\pi)$ and where

$$\begin{aligned} b &= \frac{1}{2e} [(R_B^2 + R_J^2 - e^2)^2 - 4R_B^2 R_J^2]^{\frac{1}{2}}, \\ \sinh \xi_B &= -\frac{b}{R_B}, \\ \sinh \xi_J &= -\frac{b}{R_J}. \end{aligned}$$

The resulting pressure field is given by (P_0 being an arbitrary constant, μ denotes the constant viscosity)

$$p = P_0 + \frac{2\mu\omega R_J}{b} [q_1(\xi) \sin \zeta + q_2(\xi) \sin 2\zeta], \quad (4.3)$$

where

$$\begin{aligned} q_1(\xi) &= (f_8 - 2f_{10}) \sinh \xi - 2f_{12} \cosh \xi, \\ q_2(\xi) &= f_{10} \sinh 2\xi + f_{12} \cosh 2\xi, \\ f_8 &= -\sinh^2(\xi_B - \xi_J) \sinh \xi_B / \Delta^*, \\ f_{10} &= -h_2 \sinh(\xi_B + \xi_J) / (2\Delta^*), \\ f_{12} &= h_2 \cosh(\xi_B + \xi_J) / (2\Delta^*), \\ \Delta^* &= \sinh(\xi_B - \xi_J) [2 \sinh \xi_B \sinh \xi_J \sinh(\xi_B - \xi_J) \\ &\quad - (\xi_B - \xi_J)(\sinh^2 \xi_B + \sinh^2 \xi_J)] < 0, \\ h_2 &= -(\xi_B - \xi_J) \sinh \xi_J + \sinh \xi_B \sinh(\xi_B - \xi_J) > 0. \end{aligned}$$

For the velocity field, see Ballal and Rivlin (1976, (4.1) on p. 242). The reaction force $\mathbf{F} = (0, F_y)$ and the moment M of the forces acting on the unit length of the journal are given by

$$F_y = 2\mu\omega \frac{R_J^2}{R_B} \bar{F}, \quad (4.4)$$

$$M = 2\mu\omega (R_J^2 \bar{M} + R_B^2 \hat{M}), \quad (4.5)$$

where

$$\begin{aligned} \bar{F} &= -\frac{2\pi}{\Delta^*} \sinh \xi_J \sinh^2(\xi_B - \xi_J) < 0, \\ \bar{M} &= \frac{2\pi}{\Delta^*} \sinh^3(\xi_B - \xi_J) < 0, \\ \hat{M} &= \frac{2\pi \bar{\Delta}}{\Delta^*} \sinh^2(\xi_B) < 0, \\ \bar{\Delta} &= (\xi_B - \xi_J) \cosh(\xi_B - \xi_J) - \sinh(\xi_B - \xi_J) > 0. \end{aligned}$$

4.3.3 The influence of shear-thinning and pressure-thickening

We compute the steady flows for a sequence of relative eccentricities (we proceed by a natural parameter continuation: ε is gradually increased, taking the previous solution as an initial guess, while the next ε is chosen such that the algebraic residuum of the initial guess is below a given bound). Eventually, for some ε large enough, the resulting pressures and shear rates within the actual approximation are such that the condition **(A4)** is violated, and the

nonlinear algebraic solver fails as described in Section 3.2. Otherwise (i.e., for experiments where the viscosity does not depend on pressure, so that **(A4)** holds trivially), we stop the sequence at $\varepsilon = 0.99$. The pressure level is fixed by prescribing zero pressure at the point of the largest gap $\phi = \pi$ (see the next subsection for details).

We examine the following four variants of the three experiments:

- i) the original reference viscosity model, $\eta := \eta(p, |\mathbf{D}(\mathbf{v})|)$, full lines;
- ii) the shear-thinning model, $\eta := \eta(0, |\mathbf{D}(\mathbf{v})|)$, dash lines;
- iii) the pressure-thickening model, $\eta := \eta(p, \bar{D})$, dash dotted lines;
 here $\bar{D}\sqrt{2} = \omega R_J / (R_B - R_J)$, which yields $\bar{D} = 5.5 \times 10^5 \text{ s}^{-1}$ for SQL and SQL+PIP,
 and $\bar{D} = 5.5 \times 10^3 \text{ s}^{-1}$ for PGLY;
- iv) the constant viscosity model, $\eta := \eta(0, \bar{D})$, dotted lines.

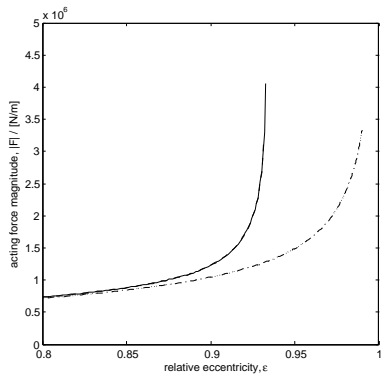
	liquid	SQL	PGLY	SQL+PIP
	angular velocity ω	10^3 rad/s	10 rad/s	10^3 rad/s
	applied load $ \mathbf{F} $	$2 \times 10^6 \text{ N/m}$	$1 \times 10^7 \text{ N/m}$	$4 \times 10^6 \text{ N/m}$
i)	reference model	0.925	0.80	0.80
ii)	shear-thinning	0.972	0.92	0.89
iii)	pressure-thickening	0.925	0.76	0.75
iv)	constant viscosity	0.972	0.91	0.84

Table 4.2: Relative eccentricities corresponding to given applied load, influence of non-Newtonian viscosity.

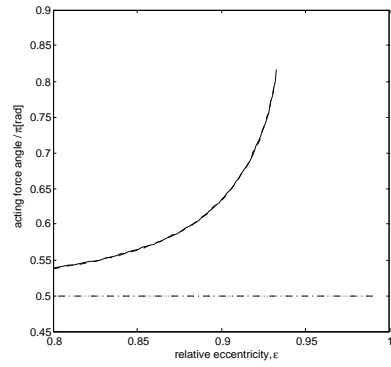
In Figures 4.11 and 4.12, we report the resulting dependence of $|\mathbf{F}|$ and of the angle $F_\phi := \angle(\mathbf{F}, -\mathbf{e}_x)$ on the relative eccentricity ε . In Table 4.2 we choose an example of applied load for each liquid, and we report the corresponding eccentricity at which the balanced position of the journal may be observed. Figures 4.13 and 4.14 depicts the maximum reached values of pressure, and the maximum and minimum values of viscosity.

The figures and the table are quite self-explanatory and the results are not surprising. The influence of the pressure-thickening is substantial in all examples. For SQL, no effects related to the shear-thinning are visible, since this liquid does not exhibit shear-thinning unless for higher shear rates. For the other liquids, however, its influence is significant, whether or not the pressure-thickening is also present in the model. Note from Figure 4.12 that when the viscosity does not vary with pressure, then $F_\phi = \pi/2$, i.e. the vector of exerted force is exactly perpendicular to the line connecting the cylinders axes; the dependence of the viscosity on pressure changes this behavior dramatically. (It should be mentioned that the presence of cavitation would have analogous effect.) Note that the maximal pressures we are able to approach with the numerical simulations are reaching 1 GPa for SQL and SQL+PIP, and even 3 GPa for PGLY lubricant examples; cf. Section 5.3 and Figure 5.10.

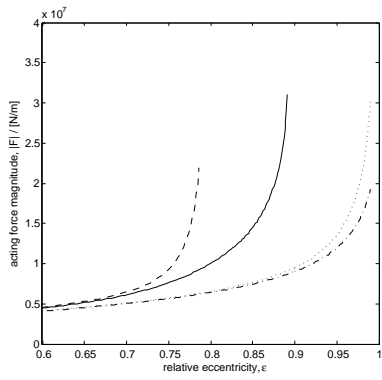
Figures 4.15–4.19 illustrate how the viscosity which depends both on pressure and shear rate varies. In the presented examples, the variation of the viscosity across the fluid film appears due to the dependence on the shear rate. For PGLY at both the relatively small eccentricity $\varepsilon = 0.5$ (Figure 4.15) and at the almost critical—from the point of view of the considered



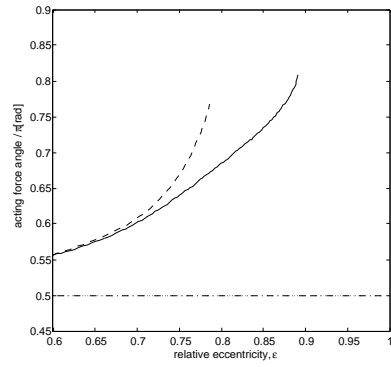
(a) SQL



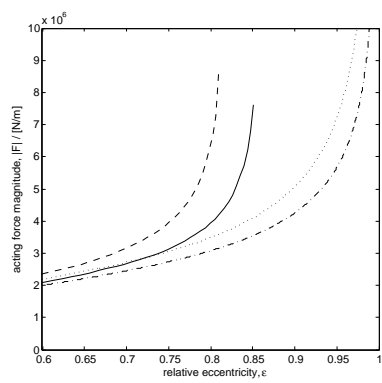
(a) SQL



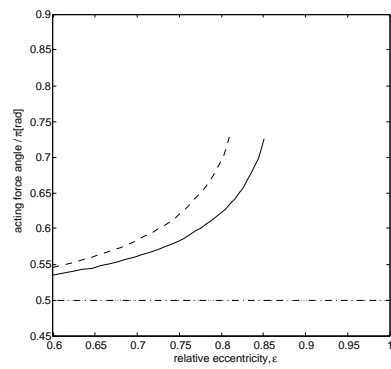
(b) PGLY



(b) PGLY



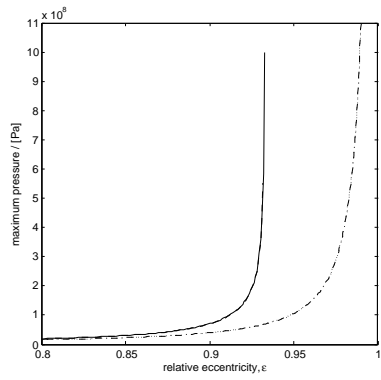
(c) SQL+PIP



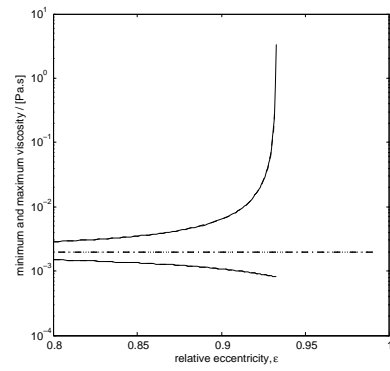
(c) SQL+PIP

Figure 4.11: $|F|$ depending on ε , influence of non-Newtonian viscosity.

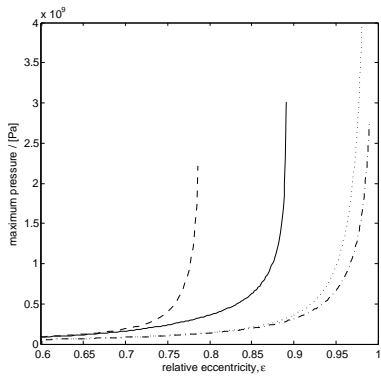
Figure 4.12: F_ϕ ($/\pi$ rad) depending on ε , influence of non-Newtonian viscosity.



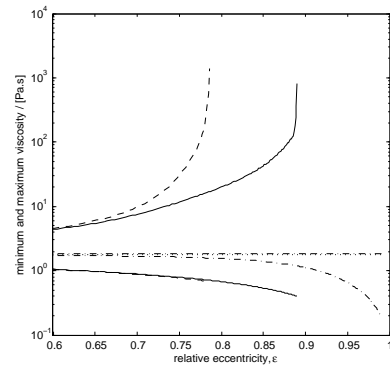
(a) SQL



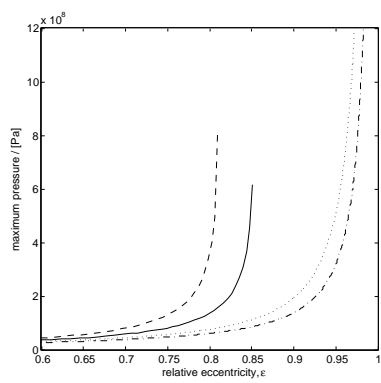
(a) SQL



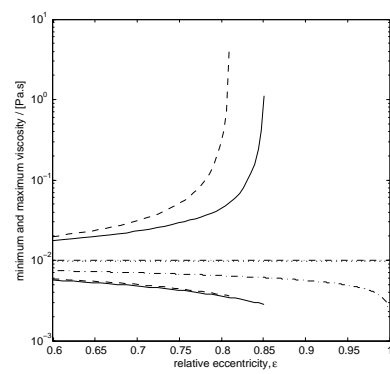
(b) PGLY



(b) PGLY



(c) SQL+PIP



(c) SQL+PIP

Figure 4.13: $\max_{\mathbf{x} \in \Omega} p$ depending on ε , influence of non-Newtonian viscosity.

Figure 4.14: $\min_{\mathbf{x} \in \Omega} \eta$ and $\max_{\mathbf{x} \in \Omega} \eta$, influence of non-Newtonian viscosity.

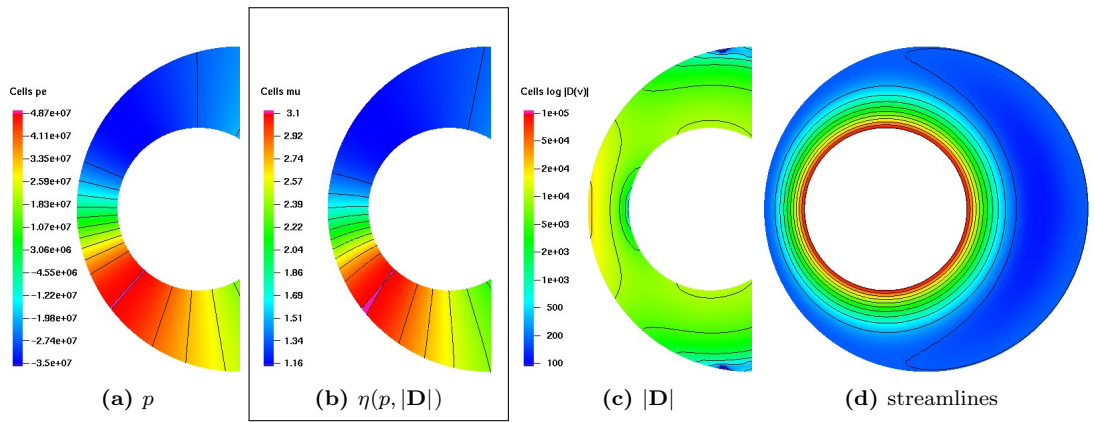


Figure 4.15: Basic features of the flow in journal bearing, PGLY, $\omega = 10$ rad/s, $\varepsilon = 0.5$.

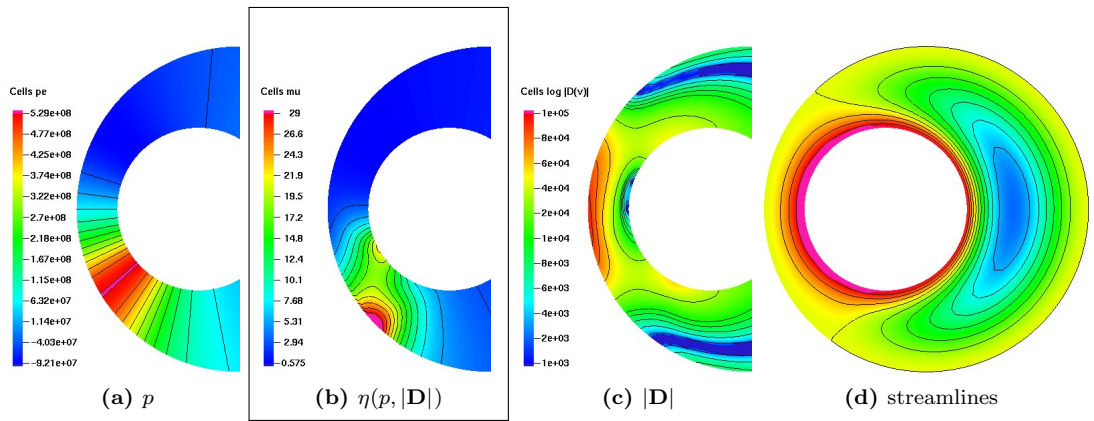


Figure 4.16: Basic features of the flow in journal bearing, PGLY, $\omega = 10$ rad/s, $\varepsilon = 0.837$.

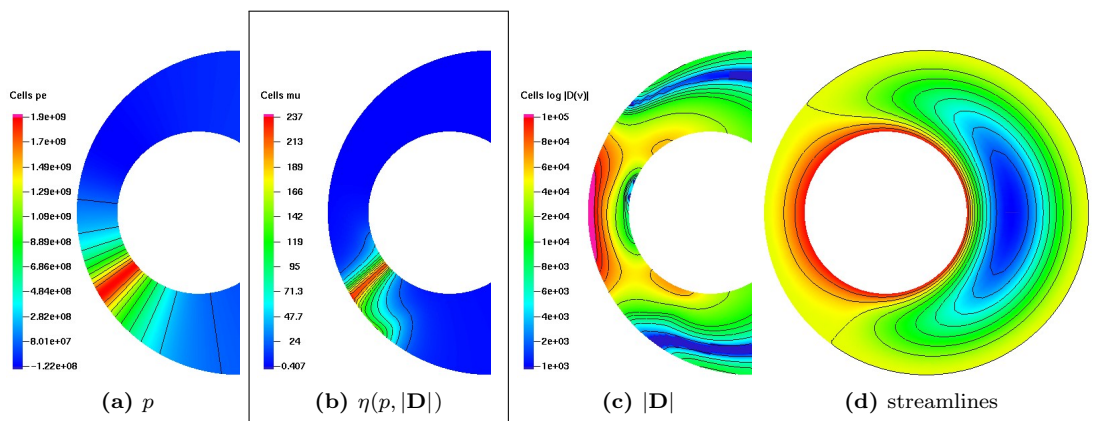


Figure 4.17: Basic features of the flow in journal bearing, PGLY, $\omega = 10$ rad/s, $\varepsilon = 0.888$.

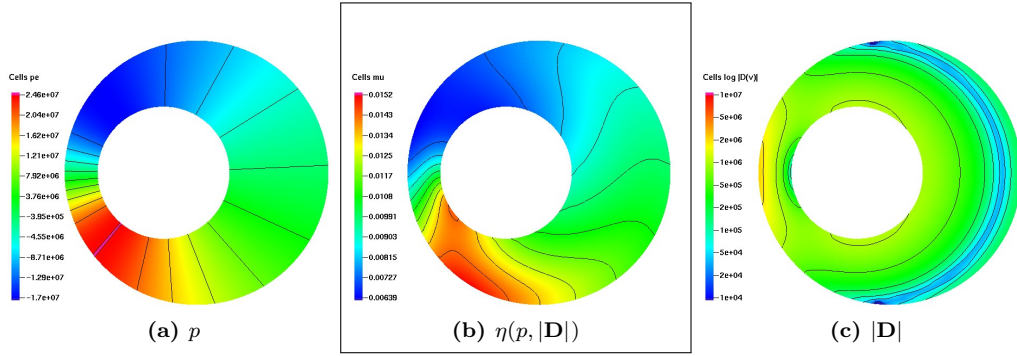


Figure 4.18: Basic features of the flow in journal bearing, SQL+PIP, $\omega = 10^3$ rad/s, $\varepsilon = 0.5$.

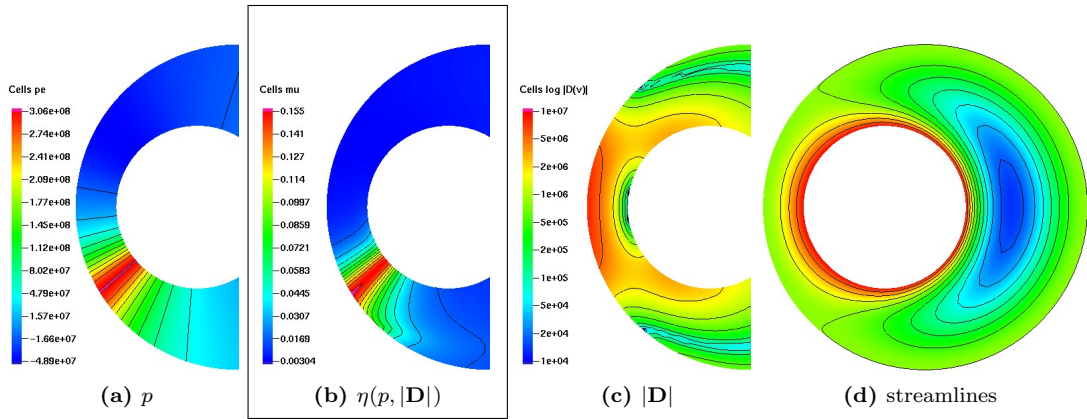


Figure 4.19: Basic features of the flow in journal bearing, SQL+PIP, $\omega = 10^3$ rad/s, $\varepsilon = 0.84$.

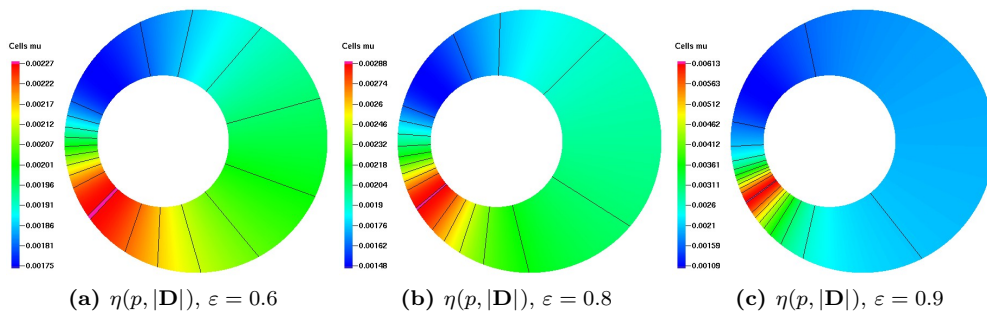
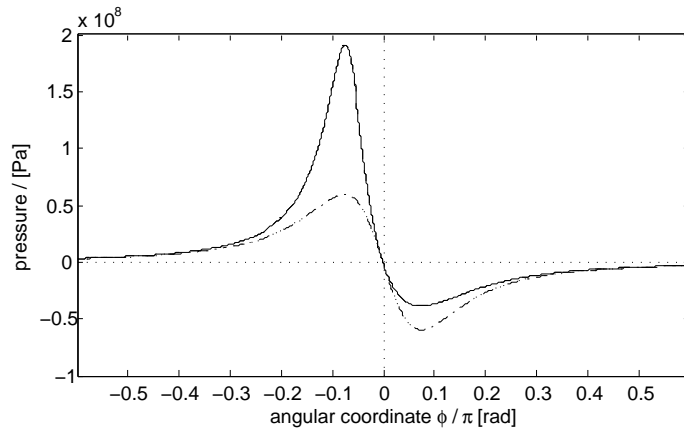
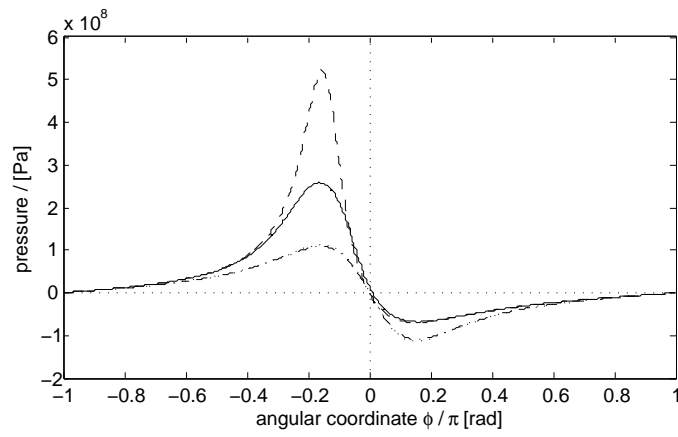


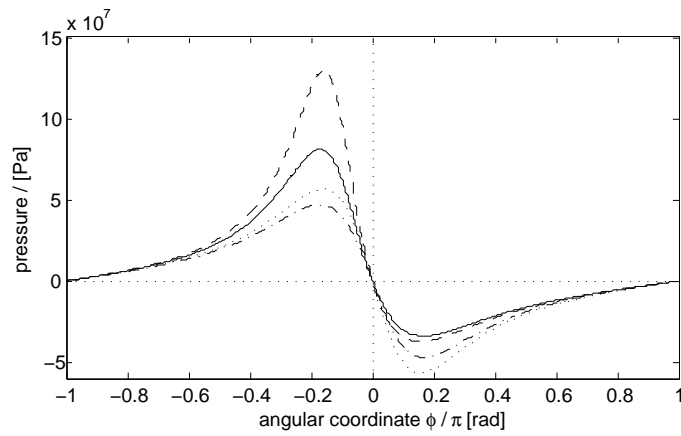
Figure 4.20: Viscosity in journal bearing, SQL, $\omega = 10^3$ rad/s.



(a) SQL, $\varepsilon = 0.925$ (the middle part only)



(b) PGLY, $\varepsilon = 0.76$



(c) SQL+PIP, $\varepsilon = 0.75$

Figure 4.21: Pressure profiles at given eccentricities, influence of non-Newtonian viscosity.

numerical method—eccentricity $\varepsilon = 0.888$ (Figure 4.17) the dependence on the pressure dominates the shape of the viscosity field and the viscosity peak matches the pressure peak. In between at $\varepsilon = 0.837$ we see that there are two distinct local maxima of the viscosity, neither of them matching the pressure peak: one tends to the local minimum of the shear rate at the narrowest gap, the other one tends towards the local minimum of the shear rate at the bifurcation point of the flow (see the streamlines). The similar is observed for SQL+PIP (Figures 4.18–4.19). Figure 4.20 then shows the viscosities resulting from the experiment with SQL, where the dependence on the pressure is dominant.

The pressure is in all the examples virtually constant across the film. This allow us to draw the pressure profiles along the angular direction for given ε , see Figure 4.21. Remind that $p = 0$ was prescribed at $\phi = \pm\pi$.

4.3.4 Importance of the level of pressure

The real-world journal bearing problem always offers the information on the level of pressure. For example, as we discussed in Subsection 1.1.1, if the finite bearing is considered, one prescribes suitable boundary conditions including the pressure at the terminals of the bearing, thus determining the pressure level in the domain. By taking the long bearing approximation, however, one loses this information. A natural question arises: how much can the pressure level influence the resulting quantities?

The issue has been recognized in the literature, of course; for example in Gwynllyw et al. (1996b) (concerned with the dynamics of the journal movement) the authors state that “. . . for a piezoviscous lubricant or a constant viscosity lubricant with cavitation incorporated into the model, the position at which the arbitrary level of pressure is specified influences the path of the journal. Therefore, it is important to specify this value in a consistent fashion. For the three-dimensional model this problem does not occur since pressure is specified at the ends of the geometry.” The authors continue by referring to Brindley et al. (1983) and other papers, where zero pressure level is prescribed at the point of the largest gap. (They further adjust this assumption using an approximation based on short bearing theory for constant viscosities, but the correction only concerns the dynamical problem and vanish once the journal position becomes steady.) The later papers by the authors on the topic (see the bibliography) then either follow this approach or, alternatively, prescribe the mean value of the pressure over the entire domain.

In general, there is no clear justification for the pressure value to be preserved right at the point of the largest gap, nor is any reason why the mean value over the domain should be preserved. We report on the following experiments with the three reference lubricant examples. We prescribe the zero pressure to be

- i) the value at the point of largest gap, i.e. at $\phi = \pi$, full lines;
- ii) the value at $\phi = \frac{1}{2}\pi$ (i.e. at the diverging part), dash lines;
- iii) the value at $\phi = \frac{3}{2}\pi$ (i.e. at the converging part), dash dotted lines;
- iv) the mean value over the domain, dotted lines.

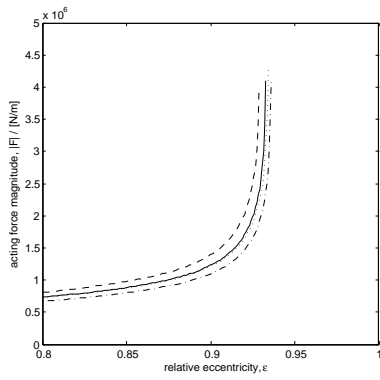
Techniqually, we prescribe the pressure “at given ϕ ” by prescribing $\int_{T_\phi} p \, d\mathbf{x} = 0$, where T_ϕ is the finite element adjacent to the outer (bearing) boundary and the nearest to given ϕ .

liquid	SQL	PGLY	SQL+PIP
angular velocity ω	10^3 rad/s	10 rad/s	10^3 rad/s
applied load $ \mathbf{F} $	2×10^6 N/m	1×10^7 N/m	4×10^6 N/m
i) $p = 0$ at $\phi = \pi$	0.925	0.80	0.80
ii) $p = 0$ at $\phi = \frac{1}{2}\pi$	0.919	0.67	0.69
iii) $p = 0$ at $\phi = \frac{3}{2}\pi$	0.930	0.86	0.86
iv) $\int_{\Omega} p \, d\mathbf{x} = 0$	0.926	0.83	0.82

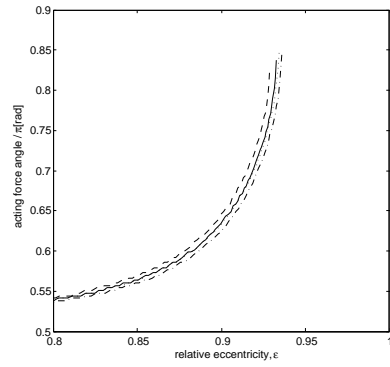
Table 4.3: Relative eccentricities corresponding to given applied load, influence of the condition on pressure.

In Figures 4.22 and 4.23, we report the resulting dependence of $|\mathbf{F}|$ and of the angle $F_{\phi} = \angle(\mathbf{F}, -\mathbf{e}_x)$ on the relative eccentricity ε . In Table 4.3 we follow the example of applied load for each liquid from the last subsection, and report the corresponding eccentricity of the balanced position of the journal. Figures 4.13 and 4.14 again depict the maximum reached values of pressure, and the maximum and minimum values of viscosity in the flow field. Figure 4.26 then draws the pressure profiles along the angular coordinate at given ε .

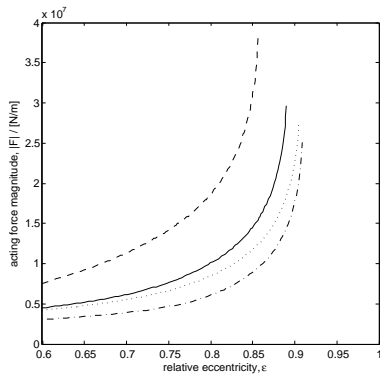
As expected, since the viscosity of the fluid increases with pressure, the less is the ϕ where the zero pressure is prescribed, the bigger is the reaction force $|\mathbf{F}|$. What can seem surprising is how substantive the difference can be. The examples clearly show that the condition on pressure has to be chosen with care, based on the particular engineering application.



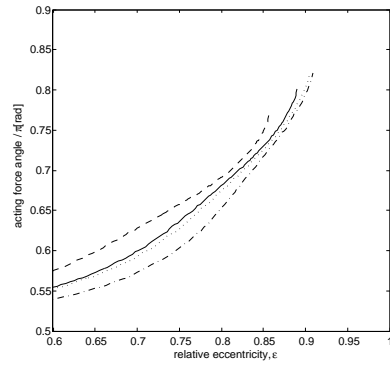
(a) SQL



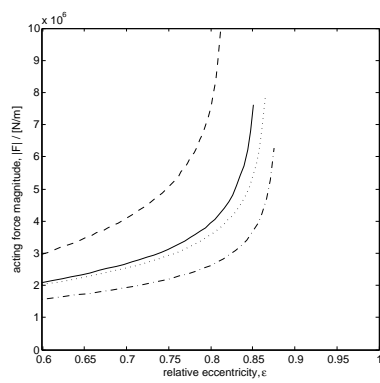
(a) SQL



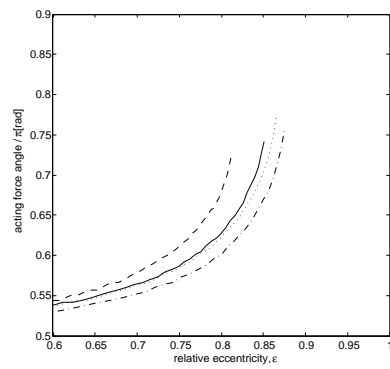
(b) PGLY



(b) PGLY



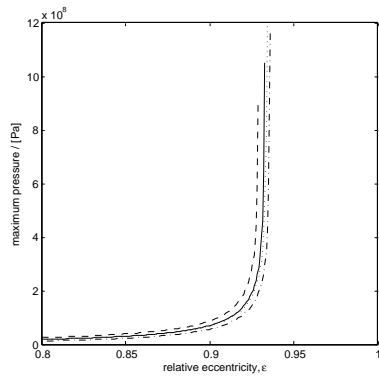
(c) SQL+PIP



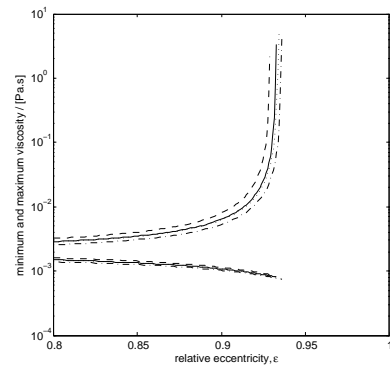
(c) SQL+PIP

Figure 4.22: $|F|$ depending on ε , influence of how the pressure level is fixed.

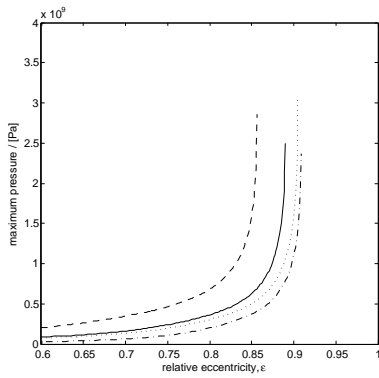
Figure 4.23: F_ϕ ($/\pi$ rad) depending on ε , influence of how the pressure level is fixed.



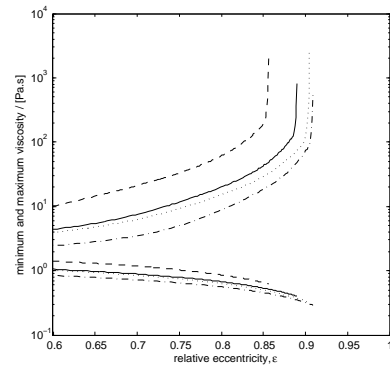
(a) SQL



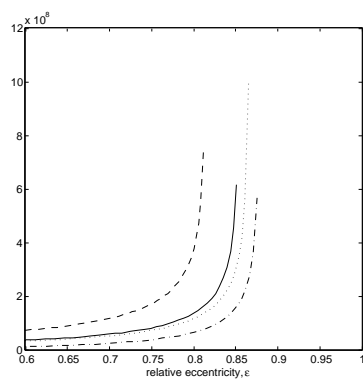
(a) SQL



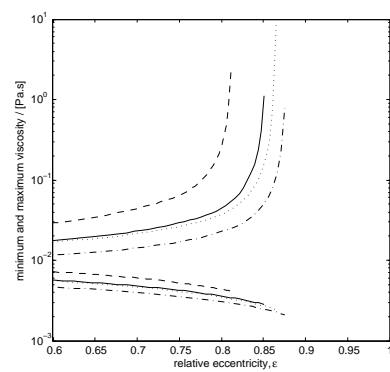
(b) PGLY



(b) PGLY



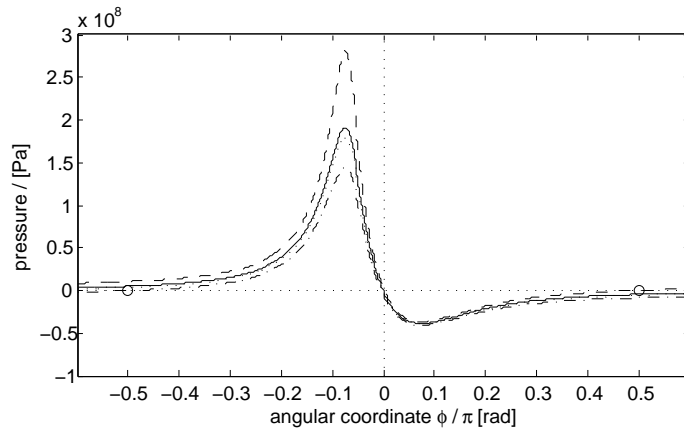
(c) SQL+PIP



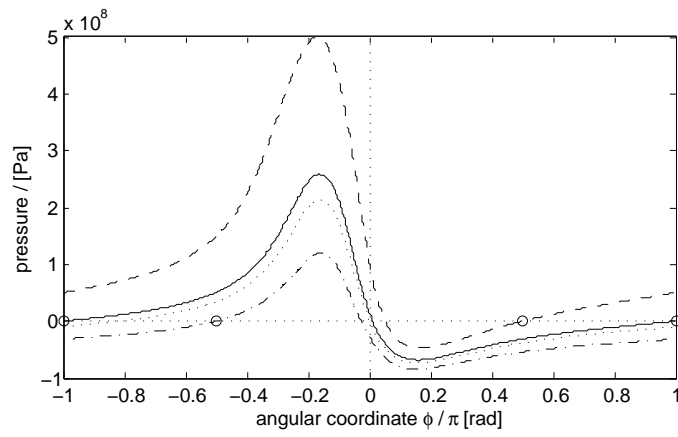
(c) SQL+PIP

Figure 4.24: $\max_{\mathbf{x} \in \Omega} p$ depending on ε , influence of how the pressure level is fixed.

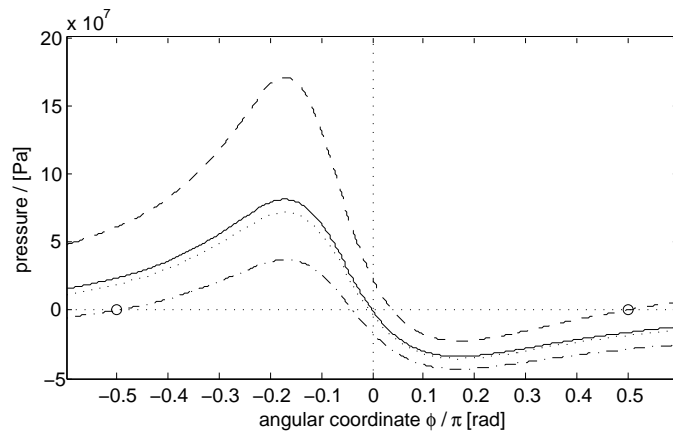
Figure 4.25: $\min_{\mathbf{x} \in \Omega} \eta$ and $\max_{\mathbf{x} \in \Omega} \eta$, influence of how the pressure level is fixed.



(a) SQL, $\varepsilon = 0.925$ (the middle part only)



(b) PGLY, $\varepsilon = 0.76$



(c) SQL+PIP, $\varepsilon = 0.75$

Figure 4.26: Pressure profiles at given eccentricities, influence of how the pressure level is fixed.

Chapter 5

Relation of the assumed and the real-world rheologies

Contents

5.1	Relevance of conditions (A1)–(A3) for the reference lubricants	74
5.2	“Well-posed” constitutive model approximation	75
5.3	Relevance of condition (A4) for the reference lubricants	80

There is a wide variety of constitutive models used to describe different fluids in different ranges of conditions. As we designated in Chapter 1, we confine our attention to isothermal flows, we take the approximation that the fluid is incompressible, and is described by (1.7), i.e.

$$\mathbf{T} = -p\mathbf{I} + \mathbf{S}, \quad \mathbf{S} = 2\eta(p, |\mathbf{D}|)\mathbf{D}, \quad \mathbf{D} = \frac{1}{2}(\nabla\mathbf{v} + \nabla\mathbf{v}^T).$$

We concentrate on fluids that exhibit shear-thinning and pressure-thickening.

The theoretical results presented in Chapter 2, following the framework built in the preceding results^a, are based on the further assumptions **(A1)**–**(A3)** (see page 21). The constant β involved in **(A3)** differs with different theoretical results (existence or uniqueness of weak solutions or of discrete solutions) and it can depend on the domain, the type of boundary conditions, and in case of discrete solutions also on the discretization; see Theorems 12, 14 and Corollary 15. Note that, always, $\beta \leq 1$. One can consider β to be “only” a constant related to particular technique used in the proofs; on the other hand, the structure of the estimates requiring **(A3)** is related to the ellipticity of the governing equations; in this sense, **(A3)** is a fundamental assumption of this approach. We will not discuss the value of β in this chapter, we merely state that if **(A1)**–**(A3)** are not fulfilled with $\beta = 1$ then the theory presented in Chapter 2 is not applicable.

The available experimental data for fluids occurring in real-world applications indicate that such fluids do not fulfill **(A1)** and **(A2)**. More precisely, none of the standard models fulfills these assumptions for *all* $p \in \mathbb{R}$ and *all* $\mathbf{D} \in \mathbb{R}_{sym}^{d \times d}$. On the other hand, the models are never *used*^{b,c} for infinite range of pressures and shear rates. Naturally, the question of how much is the presented theory applicable, can have different answers for different applications, depending on particular fluid *and* particular range of pressures and shear rates appearing in the resulting flow. At small pressures and shear rates, even the constant Newtonian viscosity describes the fluid very well. On the other hand, as we will show on selected examples of real lubricants, under the conditions occurring in elastohydrodynamic lubrication, say at pressures over 1 GPa and shear rates around 10^6 s^{-1} , the assumptions **(A1)**–**(A3)** *are not applicable*. Our aim is to observe the space in between these two extremes.

Numerical experiments presented in Chapter 3 indicate that **(A1)**–**(A3)** are not necessary in order to (discrete) solutions to exist. However, they suggest that the condition **(A4)** is required if the considered numerical approach is to succeed. Note that **(A4)** ensures (with certain β) that the pressure field of the solution is uniquely determined by the velocity field, see Subsection 2.3.2.

Similarly as above, the real-world viscosities violate **(A4)** once the pressures and shear rates are large enough. Obviously, though, **(A4)** is much less restrictive than **(A1)**–**(A3)**, and it seems that under the conditions occurring in the rigid-piezoviscous regime of hydrodynamic lubrication, such as in typical journal bearing problems, this assumption might be satisfied.

^a See the references in Chapter 2; **(A1)**–**(A3)** are required in all these works except one, that shows a possible generalization of this approach: see Bulíček et al. (2009a).

^b This is a simplification that we take liberty to make. Mathematically, this is not necessarily true, unless one proves $L^\infty(\Omega)$ –regularity for the pressure and $\mathbf{W}^{1,\infty}(\Omega)$ –regularity for the velocity.

^c In principal, the models may not even be valid for infinite range of parameters, since they are based on physical experiments performed in some finite range of conditions. This is, however, *not* the argument we address here, as will become more clear in the following text. For the real fluids we are going to examine in this chapter, the assumptions **(A1)**–**(A3)** are violated well inside the range of parameters where the viscosity models conform to the experimentally observed properties of the fluids.

In this chapter we consider the three models of reference lubricants presented in Section 1.3, proposed and accurately characterized by Bair (2006) on the basis of systematic experimental measurements in a wide range of shear rates and pressures (and at different temperatures), see Section 1.3 for details. We believe that for the purpose of this chapter the accuracy of these models can be trusted.

5.1 Relevance of conditions (A1)–(A3) for the reference lubricants

It is clear that for the above reference models neither (A1) nor (A2) can be fulfilled for all pressures, since both the viscosity and its derivative with respect to pressure are unbounded^d with increasing pressure. For bounded range of pressures (such that both $a_T(p)$ and $b_T(p)$ lie in a bounded positive interval) constants C_1 , C_2 and ε can be found such that (A1) holds for all \mathbf{D} . The same, however, does not apply to (A2); it is easy to see that if (A2) was to hold for (1.12) for all \mathbf{D} then $[a_T(p) b_T(p)^{r-2}]' = 0$ had to be satisfied for all p considered—the property which is not fulfilled by any of the three reference liquids (and which may not be expected, as will become clear below).

In summary, (A1) can be satisfied by (1.12) in any bounded range of pressures (as long as $a_T(p)$, $b_T(p)$ are bounded) for all shear rates, while (A2) can be satisfied in a bounded range of both pressures and shear rates. Since the publication of the first theoretical results in this framework, this qualitative observation has been giving hope that the assumptions are applicable to real pressure-thickening and shear-thinning fluids at least in some range of parameters. However, the constants involved are further restricted by (A3) and thus it remains to acquire some quantitative idea about the range of parameters in question. In the following paragraphs we confront the three reference liquids with the inequalities of (A1)–(A2). After that, we will discuss possible modifications (basically truncations) of the reference models such that (A1)–(A3) hold with given β for all pressures and shear rates.

Note that for all models described by (1.7), there is

$$\frac{\partial \mathbf{S}(p, \mathbf{D})}{\partial \mathbf{D}} \cdot \frac{(\mathbf{B} \otimes \mathbf{B})}{|\mathbf{B}|^2} = \eta(p, |\mathbf{D}|) + \frac{(\mathbf{B} \cdot \mathbf{D})}{|\mathbf{B}|^2 |\mathbf{D}|^2} \partial_{|\mathbf{D}|} \eta(p, |\mathbf{D}|) |\mathbf{D}|.$$

This occupies the interval $\langle \eta(p, |\mathbf{D}|) + \partial_{|\mathbf{D}|} \eta(p, |\mathbf{D}|), \eta(p, |\mathbf{D}|) \rangle$ (for shear-thinning fluids, where there is $\partial_{|\mathbf{D}|} \eta(p, |\mathbf{D}|) \leq 0$). The following quantities

$$I_{(\mathbf{A1})}(p, |\mathbf{D}|) := \frac{\sup_{q \leq p, |Q| \leq |\mathbf{D}|} \left\{ \eta(q, Q) / (\varepsilon^2 + Q^2)^{\frac{r-2}{2}} \right\}}{\inf_{q \leq p, |Q| \leq |\mathbf{D}|} \left\{ (\eta(q, Q) + \partial_Q \eta(q, Q) Q) / (\varepsilon^2 + Q^2)^{\frac{r-2}{2}} \right\}},$$

$$I_{(\mathbf{A2})}(p, |\mathbf{D}|) := \sup_{q \leq p, |Q| \leq |\mathbf{D}|} \left\{ |\partial_q \eta(q, Q)| Q / (\varepsilon^2 + Q^2)^{\frac{r-2}{4}} \right\} \varepsilon^{\frac{r-2}{2}}$$

^d In fact, $a_T(p)$ given by (1.9)–(1.10) goes to infinity at finite pressure, but this is not the point; this happens at pressure far off the range we are going to consider here.

are obviously related to **(A1)**–**(A2)**; note that (provided that C_1 , C_2 , and γ_0 exist, are finite and chosen in an optimal way) there hold

$$\sup_{q, Q \in \mathbb{R}} I_{(\mathbf{A1})}(q, Q) = \frac{C_2}{C_1}, \quad \sup_{q, Q \in \mathbb{R}} I_{(\mathbf{A2})}(q, Q) = \gamma_0 \varepsilon^{\frac{r-2}{2}}.$$

These quantities are plotted in Figures 5.5–5.7 (a,c) by green ($I_{(\mathbf{A1})}$) and red ($I_{(\mathbf{A2})}$) lines (full lines depict $p = 0$, dashed lines $p = 200$ MPa, dotted lines $p = 400$ MPa). Note that $I_{(\mathbf{A1})}$, $I_{(\mathbf{A2})}$ are non-dimensional quantities, although we use the same labelling of the y -axis as that for viscosity.

In this section we choose $\varepsilon^2 := b_T(0)^{-2}$ which seems to result in optimal estimates.

To illustrate better the relevance of **(A3)**, Figures 5.5–5.7 (b,d) depict the dependence of

$$I_{(\mathbf{A3})}(p, |\mathbf{D}|) := (1 + I_{(\mathbf{A1})}(p, |\mathbf{D}|)) I_{(\mathbf{A2})}(p, |\mathbf{D}|) \quad (5.1)$$

on shear rate and on pressure. In the upper-right part of the graph, where $I_{(\mathbf{A3})} \geq 1$, it is certain that the viscosity of the fluid violates the assumptions **(A1)**–**(A3)**. Otherwise, for $I_{(\mathbf{A3})} < 1$, the assumptions may be (locally) satisfied, depending on how small is the required value of β .

5.2 “Well-posed” constitutive model approximation

The phrase “well-posed” here refers to such constitutive model, or its approximation, which satisfies **(A1)**–**(A3)**, i.e. which fulfills the inequalities in **(A1)**–**(A2)** for all pressures and shear rates. We have seen in the previous section that for the three reference lubricants, these inequalities were violated as soon as the pressure or the shear rate exceeded certain bounds. Within these bounds, however, the inequalities in **(A1)**–**(A2)** were satisfied. If we were able to ensure—*a priori* for given application—that the pressures and shear rates to appear in the resulting flow will not exceed these bounds, then the theoretical results presented in Chapter 2 would apply. But that is not the usual situation.

It is, of course, more practical both for the theory and for the numerical simulations to work with a constitutive model which leads to a well-posed problem without additional priori requirement that the solution satisfies certain bounds. We thus seek to approximate the constitutive model of the given fluid at higher pressures and shear rates so that this approximation satisfies **(A1)**–**(A3)**. Naturally, this implies that at higher pressures and shear rates we obtain a well-posed problem but with fictive viscosity. The modeler has to verify that the resulted flow parameters does not exceed the range where the approximate model is complying the reality. The advantage compared to using the original model is that this verification can be made *a posteriori*, with a final solution in hand. Moreover, the numerical treatment of a well-posed problem should be more robust.

Definition. We start with (1.12) and rewrite it as follows,

$$\begin{aligned} \eta(p, |\mathbf{D}|) &= \eta_0 a(p) (1 + (b(p)|\mathbf{D}|)^2)^{\frac{r-2}{2}} \\ &= \eta_0 \left(a(p)^{-q} + (b(p)a(p)^{-q/2}|\mathbf{D}|)^2 \right)^{\frac{r-2}{2}}, \quad q = \frac{2}{2-r}. \end{aligned}$$

We have already mentioned in the previous section that **(A1)** requires $a(p)$ to be bounded and that **(A2)** requires $b(p)a(p)^{-q/2}$ not to vary with pressure. Hence, we replace $a(p)$ and $b(p)a(p)^{-q/2}$ by $A_M(p)$ and B defined as follows,

$$A_M(p)^q := \frac{M^q a(p)^q}{(M^q - 1) + a(0)^{-q} a(p)^q} = (M^{-q} a(0)^{-q} + (1 - M^{-q}) a(p)^{-q})^{-1}$$

$$B := b(p_b) a(p_b)^{-q/2},$$

where $M > 1$ and $p_b \geq 0$. We obtain a modified model

$$\eta_{M,B}(p, |\mathbf{D}|) := \eta_0 (A_M(p)^{-q} + (B |\mathbf{D}|)^2)^{\frac{r-2}{2}}$$

$$= \eta_0 (M^{-q} a(0)^{-q} + (1 - M^{-q}) a(p)^{-q} + B^2 |\mathbf{D}|^2)^{\frac{r-2}{2}}, \quad q = \frac{2}{2-r},$$

cf. Málek et al. (2002) and subsequent studies, where examples of this type were being mentioned.

Truncation parameter and well-posedness. Note that $A_M(0) = a(0)$, implying that if $p_b = 0$ then $\eta_{M,B}(0, |\mathbf{D}|) = \eta(0, |\mathbf{D}|)$ for all $|\mathbf{D}| \geq 0$. Moreover, $A'_M(0) = a'(0) (1 - M^{-q}) \sim a'(0)$ for $M \gg 1$, so that $\eta(p, |\mathbf{D}|)$ is well approximated for small pressures and shear rates. Meanwhile, $A_M(p) < M a(0)$; in this sense, M is a truncation parameter. Note that $A'_M(p)/A_M(p) = a'(p)/a(p) \cdot (M^q - 1)/(M^q - 1 + a(0)^{-q} a(p)^q) < a'(p)/a(p)$ for all $p \in \mathbb{R}$. There hold the following

Lemma 19. *Let $M > 1$, $B > 0$ and $\eta_0 > 0$, $1 < r < 2$. Let the viscosity be defined by*

$$\eta_{M,B}(p, |\mathbf{D}|) := \eta_0 (M^{-q} \tilde{a}(0)^{-q} + (1 - M^{-q}) \tilde{a}(p)^{-q} + B^2 |\mathbf{D}|^2)^{\frac{r-2}{2}}, \quad q = \frac{2}{2-r}, \quad (5.2)$$

where $\tilde{a}(p) \in \mathcal{C}^1(\mathbb{R})$ and $\tilde{a}(p) \geq \underline{a} > 0$ for all $p \in \mathbb{R}$. Let us set $\varepsilon^2 = B^{-2} \underline{a}^{-q}$. Then **(A1)** is satisfied with $C_1 = \eta_0 B^{r-2} (r-1)$ and $C_2 = \eta_0 B^{r-2} M \tilde{a}(0) / \underline{a}$. Provided that $|\tilde{a}'(p)| / \tilde{a}(p) \leq \alpha$ for all $p \in \mathbb{R}$, **(A2)** holds with $\gamma_0 = \eta_0 \alpha B^{(r-4)/2} 2^{-1} \underline{a}^{2r/(r-2)}$. Thus, if

$$1 < M < M_{\text{est}} := (r-1) \frac{\underline{a}}{\tilde{a}(0)} \left(\frac{2B \underline{a}^{\frac{r-1}{2-r}}}{\eta_0 \alpha} \beta - 1 \right) \quad (5.3)$$

then (5.2) satisfies **(A1)**–**(A3)**.

Proof. It is easy to check that, for all $p \in \mathbb{R}$ and $|\mathbf{D}| \geq 0$,

$$\eta_0 B^{r-2} (\varepsilon^2 + |\mathbf{D}|^2)^{\frac{r-2}{2}} \leq \eta_{M,B}(p, |\mathbf{D}|) \leq \eta_0 B^{r-2} M \frac{\tilde{a}(0)}{\underline{a}} (\varepsilon^2 + |\mathbf{D}|^2)^{\frac{r-2}{2}}.$$

Since $\partial_{|\mathbf{D}|} \eta_{M,B}(p, |\mathbf{D}|) |\mathbf{D}| \geq (r-2) \eta_{M,B}(p, |\mathbf{D}|)$, this conforms C_1 and C_2 in **(A1)**. For the least possible γ_0 that fulfills **(A2)** there holds

$$\gamma_0 \leq \eta_0 \alpha B^{r-4} (e^{2r-8} f^4 g^2 h^{2-r})^{\frac{1}{4}}, \quad \text{where}$$

$$e := B^{-2} (M^{-q} \tilde{a}(0)^{-q} + (1 - M^{-q}) \tilde{a}(p)^{-q}) + |\mathbf{D}|^2,$$

$$f := (1 - M^{-q}) \tilde{a}(p)^{-q},$$

$$g := |\mathbf{D}|^2,$$

$$h := \varepsilon^2 + |\mathbf{D}|^2 = B^{-2} \underline{a}^{-q} + |\mathbf{D}|^2.$$

We estimate that

$$e^{r-2}h^{2-r} \leq \max \left\{ 1, \underline{a}^{-q} (M^{-q}\tilde{a}(0)^{-q} + (1 - M^{-q})\tilde{a}(p)^{-q})^{-1} \right\}^{2-r},$$

$$e^{-4}f^2g^2 \leq 2^{-4}B^4, \quad e^{r-2}f^{2-r} \leq B^{2(2-r)} \quad \text{and} \quad f^r(e^{r-2}h^{2-r}) \leq \underline{a}^{-qr}.$$

This implies that

$$\gamma_0 \left(1 + \frac{C_2}{C_1} \right) \varepsilon^{\frac{r-2}{2}} \leq \frac{1}{2}\eta_0\alpha B^{-1}\underline{a}^{\frac{r-1}{r-2}} \left(1 + \frac{\tilde{a}(0)}{\underline{a}} \frac{M}{r-1} \right).$$

□

Note that for some parameters (e.g., for β or B too small or for α too large), the inequality (5.3) may not give any such M (since $M_{\text{est}} \leq 1$). The estimate M_{est} may not be optimal, however. We do not claim that **(A1)**–**(A3)** cannot be satisfied for some $M > M_{\text{est}}$. In the remaining of this section, we apply (5.2) to approximate the viscosities of the three reference liquids. We will report values of M (found by trial and error) for which **(A1)**–**(A3)** are certainly violated and compare these values with M_{est} . We will observe that (5.2) *fails to approximate* the pressure-thickening behavior for all those shear rates for which shear-thinning occurs. We will report the areas of pressures and shear rates where (5.2) approximates the viscosity of the reference liquids reasonably.

Approximation of reference liquids. Before applying the above approximation on the three reference models, we note that $a(p)$ is well-defined at some range $p \in (0, \bar{p})$ (where it was fitted to the experimental data), while it has inconvenient properties outside that interval: First, $a(p)$ given by (1.10) blows up at some finite $p > \bar{p}$. Note that this happens for pressure higher than about 3 GPa, while (1.10) is intended to describe (and was fitted to) the viscosity for pressures lower than around 1 GPa. The presented thesis aims at even lower pressures, as will become clear below.

Second, (1.9) has a singularity at some negative pressure (where $a(p)$ tends to zero). Remind that in reality, the negative pressures eventually lead to cavitation (see Section 1.1). We do not aim to discuss the models of cavitation here, we will simply extend $a(p)$ for negative pressures in a (mathematically) suitable way.

We obtain $\tilde{a}(p)$ which satisfies the assumptions of Lemma 19, for example by defining

$$\tilde{a}(p) := \begin{cases} \underline{a} + (a(0) - \underline{a}) \exp\left(\frac{a'(0)p}{a(0) - \underline{a}}\right), & p \leq 0, \\ a(p), & 0 \leq p \leq \bar{p}, \\ a(\bar{p}) \exp\left(\frac{a'(\bar{p})}{a(\bar{p})}(p - \bar{p})\right), & \bar{p} \leq p, \end{cases}$$

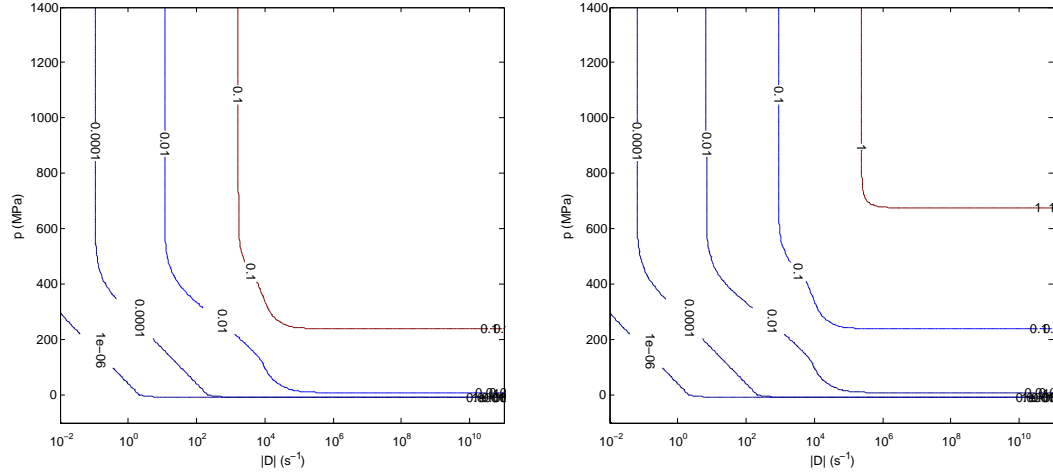
where \underline{a} is given such that $0 < \underline{a} < a(0)$, and \bar{p} is given large enough but below the singularity in (1.10). Note that

$$\sup_{p \in \mathbb{R}} \frac{\tilde{a}'(p)}{\tilde{a}(p)} \leq \sup_{p \in (0, \bar{p})} \frac{a'(p)}{a(p)}.$$

Using the above $\tilde{a}(p)$, we approximate the three reference liquids by the simple model (5.2). For given β , (5.3) provides an estimate M_{est} ensuring that **(A1)**–**(A3)** are satisfied for all $M < M_{\text{est}}$. We report the value of M_{est} for the reference liquids in Table 5.1, for parameters

	β	SQL $T = 40\text{ }^\circ\text{C}$	SQL $T = 100\text{ }^\circ\text{C}$	PGLY $T = 40\text{ }^\circ\text{C}$	PGLY $T = 100\text{ }^\circ\text{C}$	SQL+PIP $T = 40\text{ }^\circ\text{C}$	SQL+PIP $T = 100\text{ }^\circ\text{C}$
M_{est}	1	3.1	2.8	112	152	2845	2973
M_{over}	1	4.1	3.8	146	200	–	–
M_{est}	0.1	–	–	11	15	283	296
M_{over}	0.1	1.1	1.1	15	20	–	–

Table 5.1: Truncation parameters M for the simple example.



(a) Truncation parameter $M = 112$ ($= M_{\text{est}}$, $\beta = 1$).

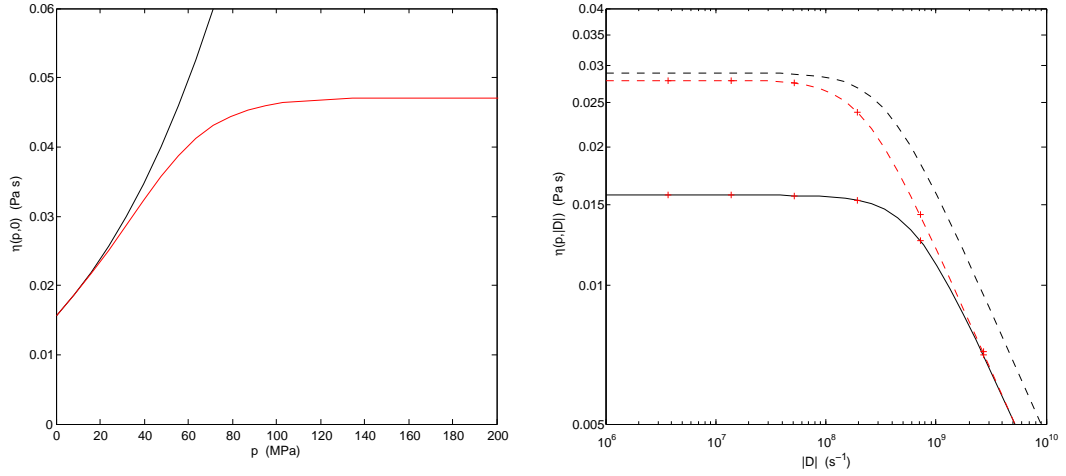
(b) Truncation parameter $M = 146$.

Figure 5.1: Contours of $I_{\mathbf{A3}}(p, |\mathbf{D}|)$ for PGLY, $T = 40\text{ }^\circ\text{C}$, approximated by (5.2).

$\underline{a} = 0.9a(0)$ and $p_b = 0$ (remind that $B = b(p_b)a(p_b)^{-q/2}$). Moreover, we report an approximate M_{over} (found by trial and error) for which we observed numerically that **(A1)**–**(A3)** are violated. For illustration see Figure 5.1, where contours of $I_{\mathbf{A3}}(p, |\mathbf{D}|)$ (see (5.1), with $\eta_{M,B}$ instead of η) are drawn for PGLY at $T = 40\text{ }^\circ\text{C}$ and for $M = M_{\text{est}}$ and $M = M_{\text{over}}$.

Table 5.1 shows that the values of the truncation parameter allowed for different fluids are quite different. For SQL, the upper limit for M is very low even in the most optimistic case that $\beta = 1$, while for $\beta = 0.1$ the approximation of (1.12) by (5.2) practically cannot be used. Figure 5.2a illustrates the viscosity dependence on pressure at low shear rates: $\eta(p, 0)$ (black line) and $\eta_{M,B}(p, 0)$ for $M = 3$ (red line) are shown. Figure 5.2b then depicts the dependence on the shear rate at two values of pressure: $p = 0$ (full lines) and $p = 30\text{ MPa}$ (dashed lines), again for the original model (black lines) and for (5.2) with $M = 3$ and $p_b = 0$ (red lines).

The values in Table 5.1 seems more auspicious for PGLY and SQL+PIP, for the latter fluid the author did not even observe violation of **(A3)** with $\beta = 0.1$. The reason is, however, rather unwelcome as is illustrated by Figure 5.3, where the reference viscosity $\eta(p, |\mathbf{D}|)$ for SQL+PIP fluid at $40\text{ }^\circ\text{C}$ (black lines) and its approximate $\eta_{M,B}(p, |\mathbf{D}|)$ with $M = 10^3$ and $p_b = 0$ (red lines) are drawn for $p = 0$ (full lines), $p = 50\text{ MPa}$ (dashed lines) and $p = 100\text{ MPa}$



(a) Pressure dependence at low shear rates. (b) Shear rate dependence, for $p = 0$ (full lines) and $p = 30$ MPa (dashed lines).

Figure 5.2: SQL at $T = 40$ °C, reference model (black) and (5.2) with $M = 3$ and $p_b = 0$ (red).

(dotted lines). We see that here the approximated viscosity is not primarily restricted due to the substitution of $a(p)$ by $A_M(p)$, but mainly due to the substitution of $b(p)a(p)^{-q/2}$ by a constant B . Indeed, (5.2) is unable to approximate the pressure-thickening behavior at those shear rates for which the shear-thinning occurs, as illustrated also by Figure 5.4, where for PGLY at 40 °C the original $\eta(p, |\mathbf{D}|)$ (black) and its approximation $\eta_{M,B}(p, |\mathbf{D}|)$ with $M = 100$ and with $p_b = 50$ MPa (red) or $p_b = 150$ MPa (blue) are shown, all for $p = 0$ (full line) and $p = 200$ MPa (dashed line).

In Figures 5.8–5.9, we report the ratio

$$\frac{\eta_{M,B}(p, |\mathbf{D}|)}{\eta(p, |\mathbf{D}|)}$$

for the reference liquids at $T = 40$ and 100 °C, for $p_b = 0$ and for selected values of M . Obviously, for pressures and shear rates where the ration is close to 1, the truncated model (5.2) is a reasonable approximation of the real fluid viscosity. The values of M are chosen in the examples such that **(A1)**–**(A3)** are satisfied for some $\beta \leq 1$. The figures illustrate in a different way what was commented on above. Let us admit as acceptable an approximation error of 5 percent, for example; i.e., let us seek for $\eta_{M,B}(p, |\mathbf{D}|)/\eta(p, |\mathbf{D}|) \geq 0.95$. For SQL, in the (optimistic) case $\beta = 0.9$, we see that only pressures at most around 25 MPa are allowed while $|\mathbf{D}(\mathbf{v})| < 10^8$ or 10^9 s $^{-1}$, where no shear-thinning occurs. For higher shear rates, pressures up to around 5 MPa seem to be included, but this is only here the variation due to pressure is less than the chosen 5 percent error. For SQL+PIP, much higher pressures are allowed for, but for very low shear rates only. Similar observation holds for PGLY.

Note that this inability to model pressure-thickening at higher shear rates is related to the simple approximation (5.2), but it is not necessarily attributed to the assumptions **(A1)**–**(A3)**

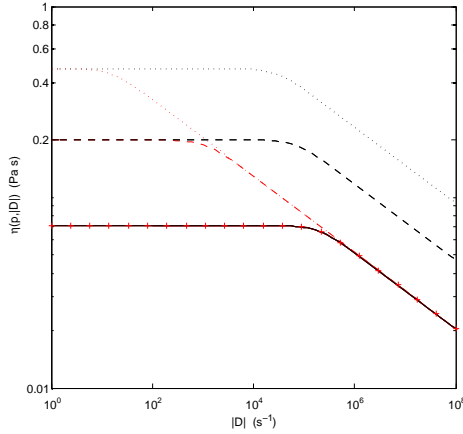


Figure 5.3: SQL+PIP at 40 °C, reference model (black) and (5.2) with $M = 10^3$ and $p_b = 0$ (red), for $p = 0, 50, 100$ MPa (full, dashed, dotted lines).

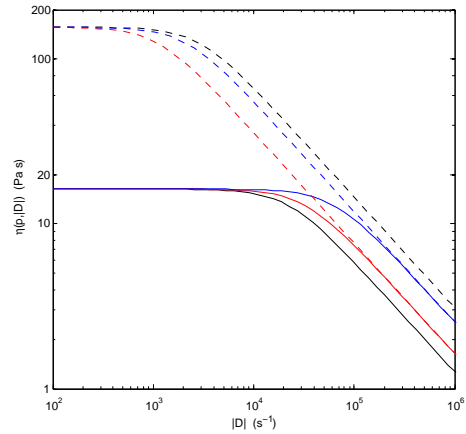


Figure 5.4: PGLY at 40 °C, reference model (black) and (5.2) with $M = 10^2$ and $p_b = 50$, 50 MPa (red, blue), for $p = 0, 200$ MPa (full, dashed).

themselves. One can imagine more general approximations, for example

$$\eta_{M, \tilde{B}}(p, |\mathbf{D}|) := \eta_0 \left(M^{-q} \tilde{a}(0)^{-q} + (1 - M^{-q}) \tilde{a}(p)^{-q} + \tilde{B}(p, |\mathbf{D}|)^2 |\mathbf{D}|^2 \right)^{\frac{r-2}{2}}, \quad q = \frac{2}{2-r},$$

where $\tilde{B}(p, |\mathbf{D}|) \rightarrow B$, for $|\mathbf{D}| \rightarrow +\infty$ and for all p .

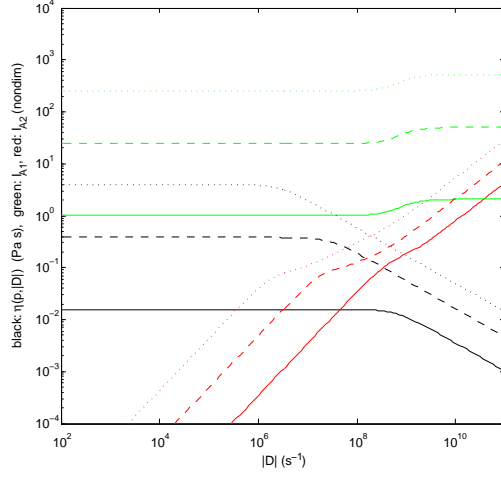
However, having in mind the observations in Figures 5.5–5.7 (b,d), the possible advantages of any such approximation will not surpass certain limits.

5.3 Relevance of condition (A4) for the reference lubricants

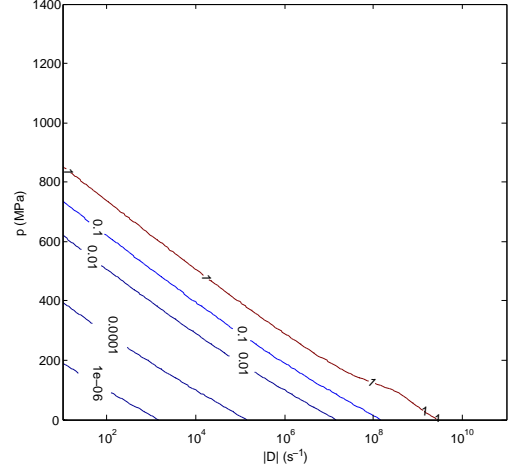
Similarly as in Section 5.1, it is obvious that the reference models do not satisfy (A4) for all pressures and shear rates, since the viscosity derivative with respect to pressure is unbounded with increasing pressure. It is also obvious that this assumption is implied by—and is less restrictive than—the assumptions (A1)–(A3). To view this quantitatively, we plot the values of

$$I_{(\mathbf{A4})}(p, |\mathbf{D}|) := \sup_{q \leq p, |Q| \leq |\mathbf{D}|} \{ |\partial_q \eta(q, Q)| Q \}$$

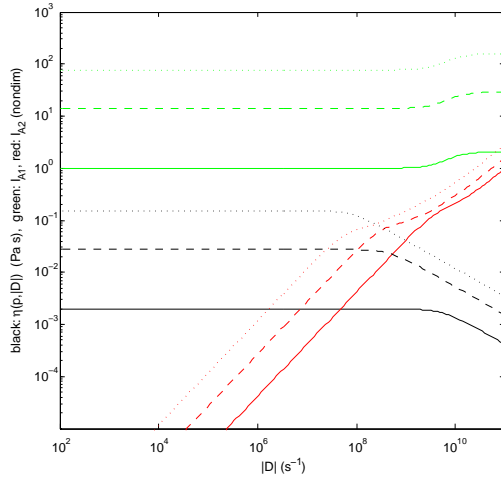
in Figure 5.10 for the three reference liquids at $T = 40$ and 100 °C, cf. Figures 5.5–5.7. According to experiments with the numerical method presented in Chapter 3, the line labeled by 1 divides the $(p, |\mathbf{D}|)$ -space into the upper-right part, where $I_{(\mathbf{A4})} \geq 1$ and the considered method certainly fails, and the lower-left part, where it was experienced to solve the discrete problem successfully.



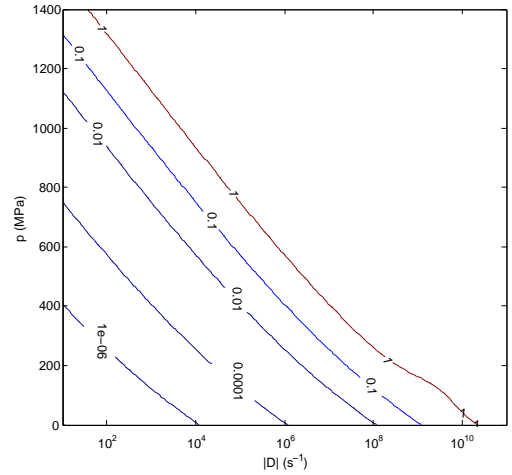
(a) Viscosity η , and $I_{(\mathbf{A}1)}$, $I_{(\mathbf{A}2)}$ for SQL, $T = 40$ °C.



(b) Contours of $I_{\mathbf{A}3}$ for SQL, $T = 40$ °C.

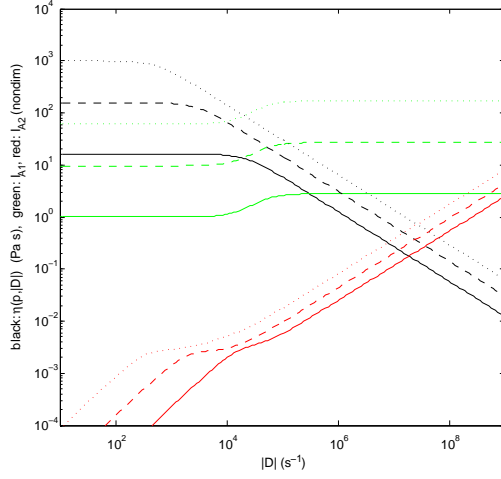


(c) Viscosity η , and $I_{(\mathbf{A}1)}$, $I_{(\mathbf{A}2)}$ for SQL, $T = 100$ °C.

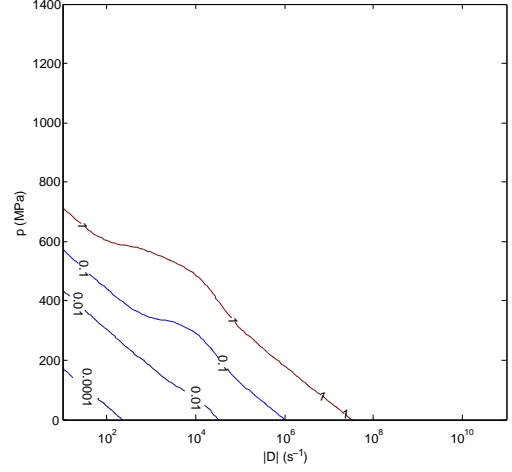


(d) Contours of $I_{\mathbf{A}3}$ for SQL, $T = 100$ °C.

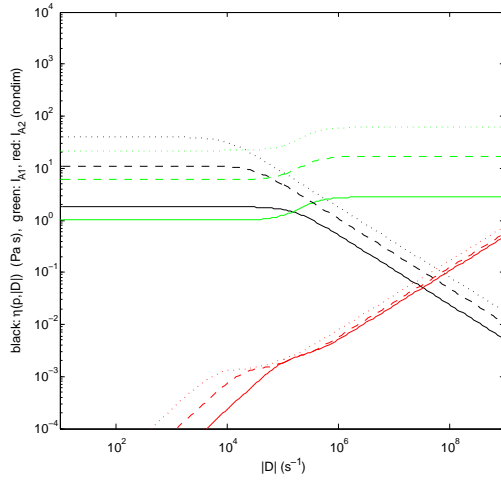
Figure 5.5: The viscosity, and local comparison with **(A1)**–**(A3)** for SQL, at $T = 40, 100$ °C. **Left (a,c):** Viscosity η (Pa s), and $I_{(\mathbf{A}1)}$, $I_{(\mathbf{A}2)}$ (black, green, red); for $p = 0, 200, 400$ MPa (full, dashed, dotted line); plotted dependence on $|\mathbf{D}(\mathbf{v})|$ (s^{-1} , in logarithmic scale). **Right (b,d):** Contours of $I_{\mathbf{A}3}$ (those less than 1); depending on $|\mathbf{D}(\mathbf{v})|$ (s^{-1} , in logarithmic scale) and p (MPa).



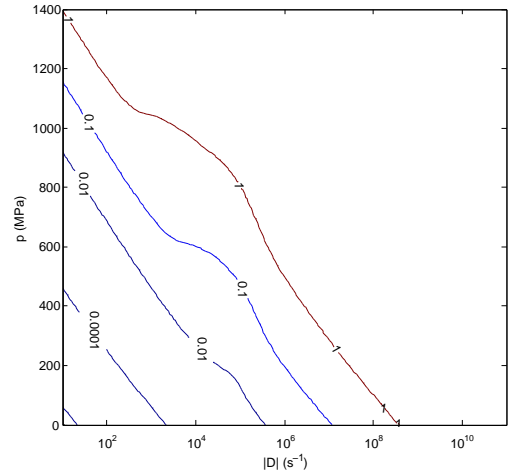
(a) Viscosity η , and $I_{(A1)}$, $I_{(A2)}$ for PGLY, $T = 40$ °C.



(b) Contours of I_{A3} for PGLY, $T = 40$ °C.

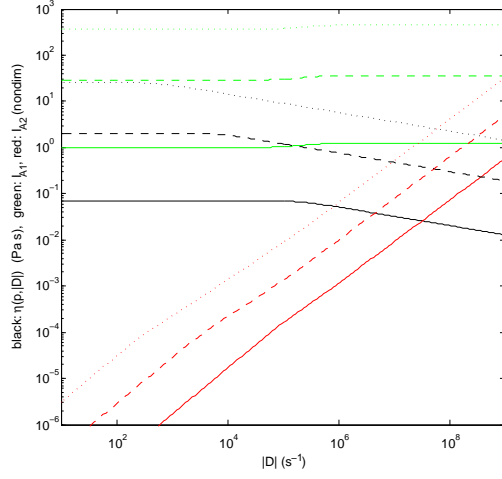


(c) Viscosity η , and $I_{(A1)}$, $I_{(A2)}$ for PGLY, $T = 100$ °C.

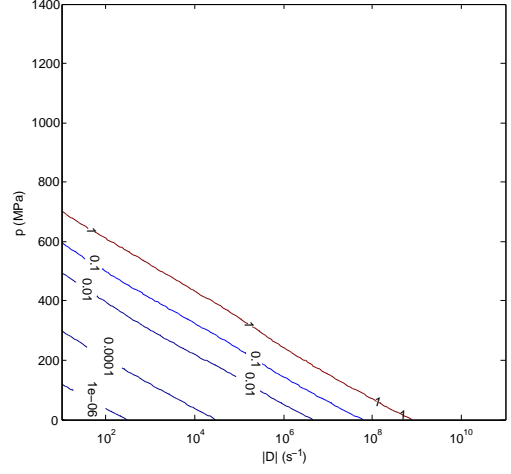


(d) Contours of I_{A3} for PGLY, $T = 100$ °C.

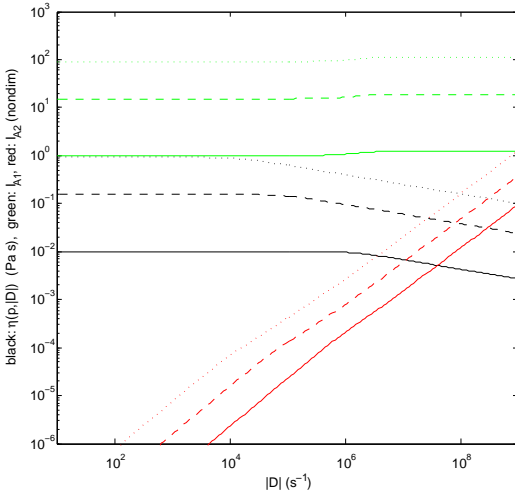
Figure 5.6: The viscosity, and local comparison with (A1)–(A3) for PGLY, at $T = 40, 100$ °C. **Left (a,c):** Viscosity η (Pa s), and $I_{(A1)}$, $I_{(A2)}$ (black, green, red); for $p = 0, 200, 400$ MPa (full, dashed, dotted line); plotted dependence on $|\mathbf{D}(\mathbf{v})|$ (s^{-1} , in logarithmic scale). **Right (b,d):** Contours of I_{A3} (those less than 1); depending on $|\mathbf{D}(\mathbf{v})|$ (s^{-1} , in logarithmic scale) and p (MPa).



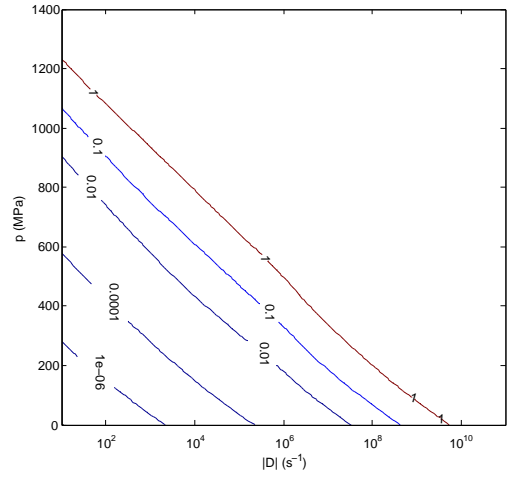
(a) η , and $I_{(\mathbf{A}1)}$, $I_{(\mathbf{A}2)}$ for SQL+PIP, $T = 40$ °C.



(b) Contours of $I_{\mathbf{A}3}$ for SQL+PIP, $T = 40$ °C.

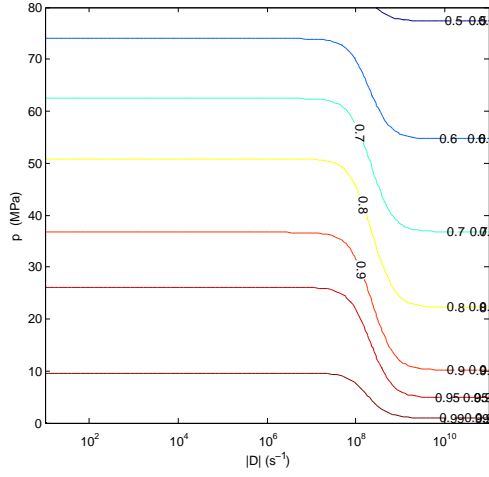


(c) η , and $I_{(\mathbf{A}1)}$, $I_{(\mathbf{A}2)}$ for SQL+PIP, $T = 100$ °C.

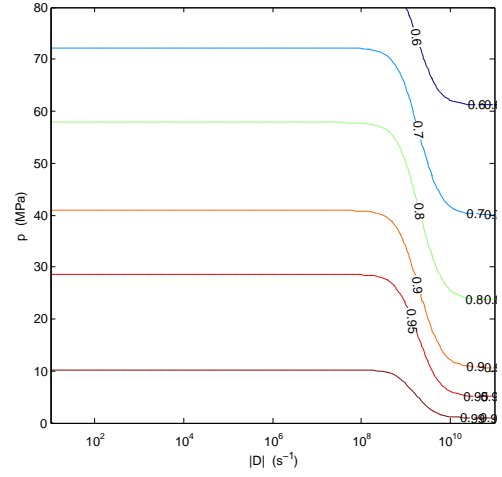


(d) Contours of $I_{\mathbf{A}3}$ for SQL+PIP, $T = 100$ °C.

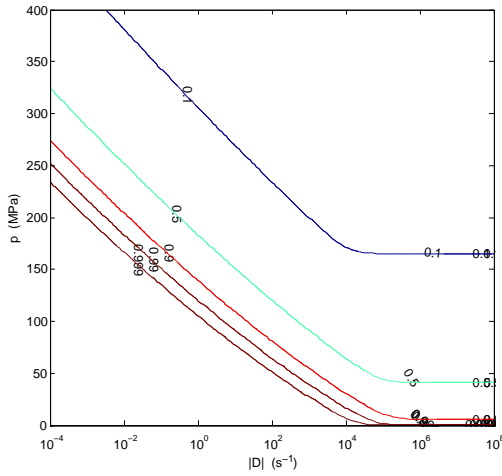
Figure 5.7: The viscosity, and local comparison with (A1)–(A3) for SQL+PIP, at $T = 40, 100$ °C. **Left (a,c):** Viscosity η (Pa s), and $I_{(\mathbf{A}1)}$, $I_{(\mathbf{A}2)}$ (black, green, red); for $p = 0, 200, 400$ MPa (full, dashed, dotted line); plotted dependence on $|\mathbf{D}(\mathbf{v})|$ (s^{-1} , in logarithmic scale). **Right (b,d):** Contours of $I_{\mathbf{A}3}$ (those less than 1); depending on $|\mathbf{D}(\mathbf{v})|$ (s^{-1} , in logarithmic scale) and p (MPa).



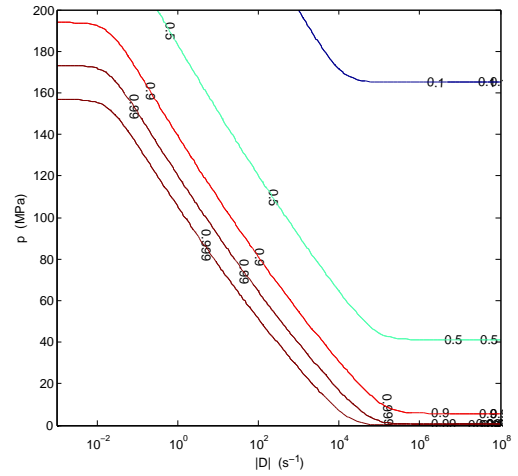
(a) SQL at 40 °C, $M = 2.5$
(satisfies (A1)–(A3) with $\beta = 0.9$)



(b) SQL at 100 °C, $M = 2.5$
(satisfies (A1)–(A3) with $\beta = 0.9$)

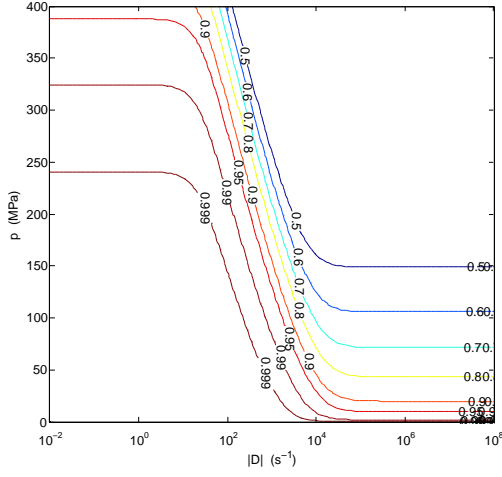


(c) SQL+PIP at 40 °C, $M \geq 100$
(satisfies (A1)–(A3) with $\beta = 0.04$)

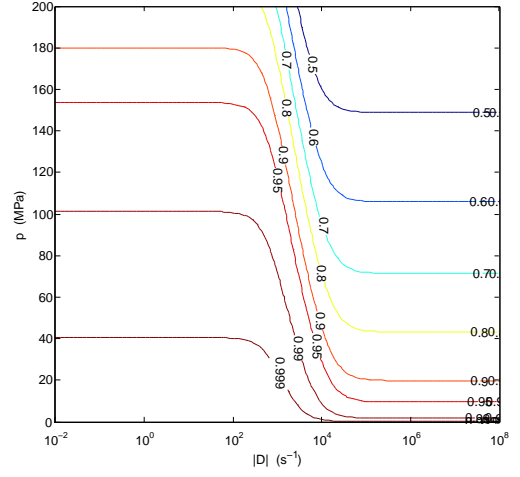


(d) SQL+PIP at 40 °C, $M = 25$
(satisfies (A1)–(A3) with $\beta = 0.01$)

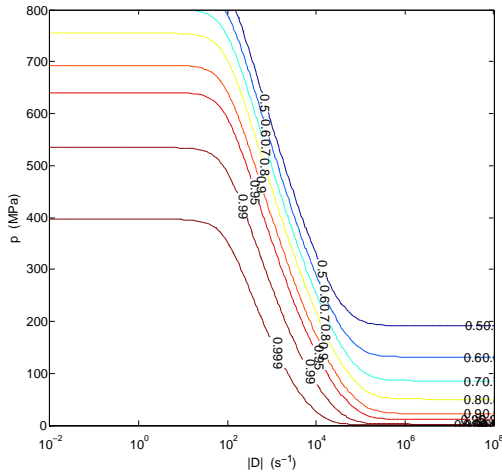
Figure 5.8: Contours of $\eta_{M,B}(p, |\mathbf{D}|)/\eta(p, |\mathbf{D}|)$ for SQL and SQL+PIP.



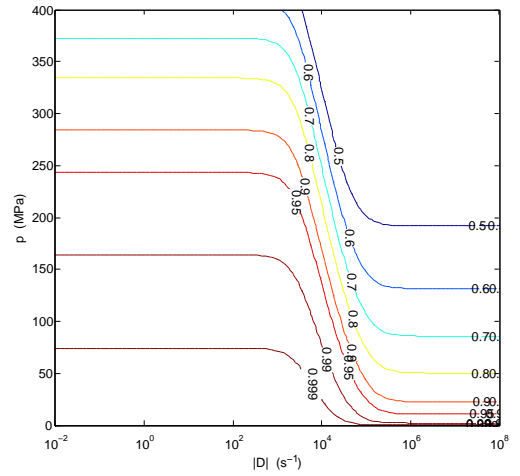
(a) PGLY at 40 °C, $M = 100$
(satisfies (A1)–(A3) with $\beta = 0.9$)



(b) PGLY at 40 °C, $M = 11$
(satisfies (A1)–(A3) with $\beta = 0.1$)

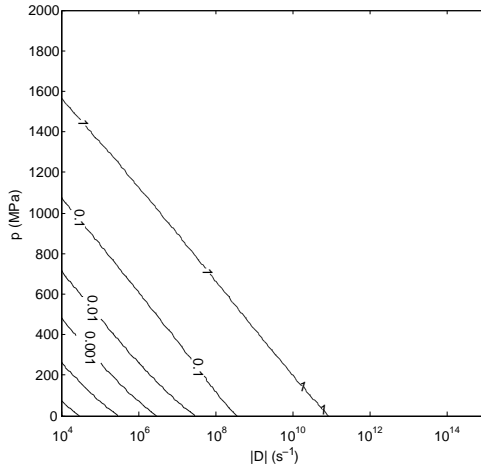


(c) PGLY at 100 °C, $M = 150$
(satisfies (A1)–(A3) with $\beta = 1.0$)

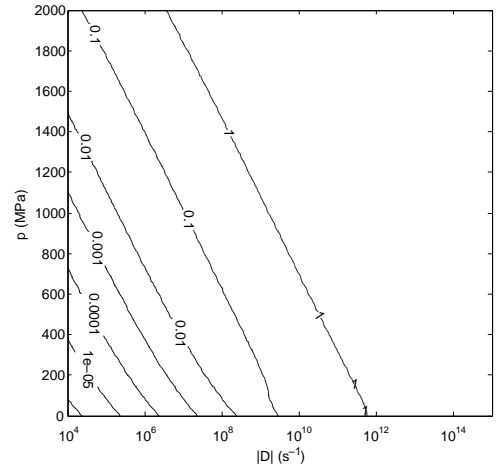


(d) PGLY at 100 °C, $M = 15$
(satisfies (A1)–(A3) with $\beta = 0.1$)

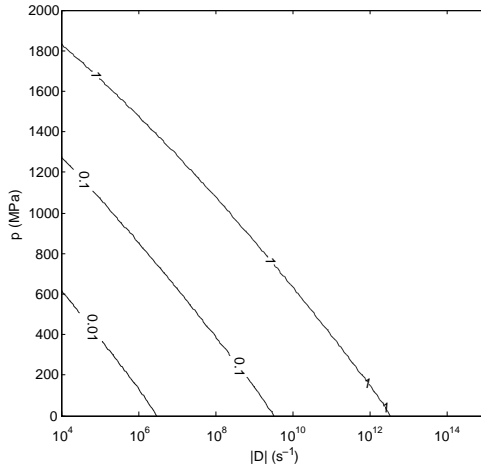
Figure 5.9: Contours of $\eta_{M,B}(p, |\mathbf{D}|)/\eta(p, |\mathbf{D}|)$ for PGLY.



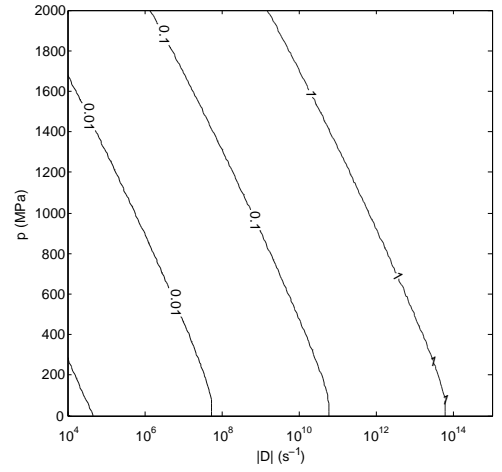
(a) Contours of I_{A4} for SQL, $T = 40$ °C.



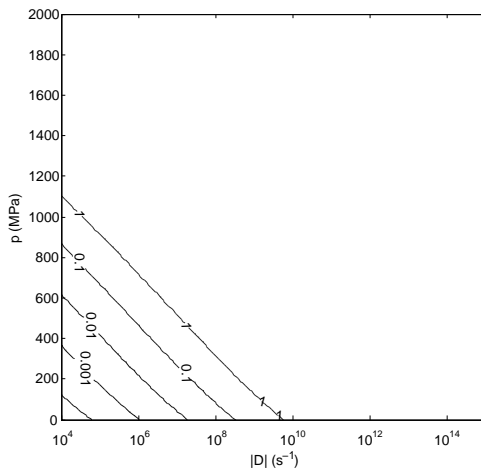
(b) Contours of I_{A4} for SQL, $T = 100$ °C.



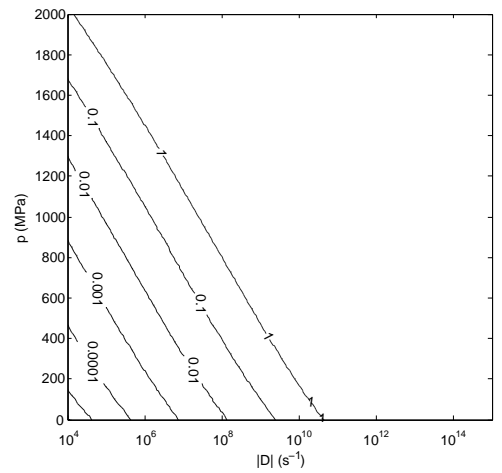
(c) Contours of I_{A4} for PGLY, $T = 40$ °C.



(d) Contours of I_{A4} for PGLY, $T = 100$ °C.



(e) Contours of I_{A4} for SQL+PIP, $T = 40$ °C.



(f) Contours of I_{A4} for SQL+PIP, $T = 100$ °C.

Figure 5.10: Contours of $I_{A4}(p, D)$ (those less than 1) for three reference liquids.

Chapter 6

Conclusion

The main results of the thesis have been presented in Chapter 2. We have studied the isothermal steady flow of a class of incompressible homogeneous fluids whose viscosity depends on pressure and shear rate. The results are based on the approach developed by Málek et al. (2002). In particular, the recent result by Franta et al. (2005) concerned with the steady flow subject to homogeneous Dirichlet boundary conditions has been generalized in the thesis.

The major improvement consists of including boundary conditions that appear in practical applications. In the flows subject to Dirichlet conditions on the entire boundary the level of pressure in the solution is not naturally determined, and it has to be fixed by an additional requirement (e.g., by prescribing the mean value of the pressure over the domain). Note that, in contrast to fluids whose viscosity does not depend on pressure, the level of pressure affects the entire solution of the problem if piezoviscous fluid is involved. Thus, we have been particularly interested in boundary conditions involving free inflow/outflow through the boundary and we have shown that they provide a natural way to determine the level of pressure in the solution uniquely.

A minor difference in the approach utilized in the provided proofs, compared to previous results, is related to how we accentuate the discrete approximations. In the previous studies the sequence of Galerkin approximations converged to a quasi-compressible approximation of the problem, and then the convergence of these quasi-compressible approximations to the “incompressible” solution of the problem has been shown on a continuous level. Motivated by the standard finite element method discretization, we have altered this procedure, showing that the discrete Galerkin approximations (satisfying the discrete incompressibility constraint) converge directly to the weak solution of the problem. Due to this slight modification, the role played by the (discrete) inf-sup conditions in the process has been revealed.

In the second part, we have addressed the numerical approximations. Using a finite element method implemented previously by J. Hron, and used successfully with a number of problems related to incompressible non-Newtonian fluids, we performed a set of experiments. One of our aims was to examine the behaviour of the numerical method when the assumptions required by the current theoretical results are not satisfied. In Chapter 3, we have observed that the numerical method fails once the changes of the viscosity due to the pressure are too rapid; moreover, we have experimentally identified the condition that seems to determine the failure. Note that the condition is somewhat weaker than the assumptions required to show the well-posedness; in fact, we did not observe any change of behaviour that could be linked to those assumptions.

The fluid models considered in the thesis are of great importance in engineering problems related to lubrication. Though our theoretical results may be applicable to other areas (such as in geology) our main concern has been hydrodynamic lubrication problems, in particular with the flow in journal bearings. In Chapter 4 we have illustrated the effects due to the pressure-thickening and shear-thinning on the flow in between parallel plates and on the flow in the journal bearing. We have shown a considerable sensitivity of the flow characteristics on the boundary conditions determining the pressure.

We have examined the relevance of the assumptions required by the theoretical results to the three reference lubricants recently characterized by Bair (2006). We have concluded that these accurate models satisfy our assumptions in certain ranges of pressures and shear rates, while outside these ranges the assumptions are inevitably violated. The ranges of parameters are quantified in Chapter 5.

Bibliography

- Amrouche, C. and Girault, V. (1994). Decomposition of vector-spaces and application of the Stokes problem in arbitrary dimension. *Czechoslovak Math. J.*, 44(1):109–140.
- Bair, S. (2006). Reference liquids for quantitative elastohydrodynamics: selection and rheological characterization. *Tribol. Lett.*, 22(2):197–206.
- Bair, S. and Gordon, P. (2006). Rheological challenges and opportunities for EHL. In Snidle, R. W. and Evans, H. P., editors, *IUTAM Symposium on Elastohydrodynamics and Micro-Elastohydrodynamics*, volume 134 of *Solid Mechanics And Its Applications*, pages 23–43. Springer.
- Bair, S., Khonsari, M., and Winer, W. O. (1998). High-pressure rheology of lubricants and limitations of the Reynolds equation. *Tribol. Int.*, 31(10):573–586.
- Bair, S. and Kottke, P. (2003). Pressure–viscosity relationship for elastohydrodynamics. *Tribol. Trans.*, 46:289–295.
- Bair, S., McCabe, C., and Cummings, P. T. (2002). Comparison of nonequilibrium molecular dynamics with experimental measurements in the nonlinear shear-thinning regime. *Phys. Rev. Lett.*, 88(5):058302.
- Ballal, B. Y. and Rivlin, R. S. (1976). Flow of a Newtonian fluid between eccentric rotating cylinders: inertial effects. *Arch. Ration. Mech. Anal.*, 62(3):237–294.
- Barus, C. (1893). Isothermals, isopiestic and isometrics relative to viscosity. *Amer. J. Sci.*, 45:87–96.
- Beavers, G. S. and Joseph, D. D. (1967). Boundary conditions at a naturally permeable wall. *J. Fluid Mech.*, 30:197–207.
- Bird, R. B., Armstrong, R. C., and Hassager, O. (1987). *Dynamics of Polymeric Liquids*. John Wiley & Sons.
- Bogovskii, M. E. (1980). Solutions of some vector analysis problems connected with operators div and grad (in Russian). *Trudy Sem. S. L. Soboleva*, 80(1):5–40.
- Bramley, R. and Wang, X. (1995). SPLIB: A library of iterative methods for sparse linear system. Technical Report IN 47405, Indiana University–Bloomington.
- Bridgman, P. W. (1931). *The Physics of High Pressure*. MacMillan, New York.
- Brindley, J., Elliot, L., and McKay, J. T. (1983). The role of cavitation in whirl instability in a rotor bearing. *ASME J. Appl. Mech.*, 50:877–890.
- Bulíček, M. and Fišerová, V. (2009). Existence theory for steady flows of fluids with pressure and shear rate dependent viscosity, for low values of the power-law index. *Z. Anal. Anwend.*, 28(3):349–371.
- Bulíček, M., Málek, J., and Rajagopal, K. R. (2007). Navier’s slip and evolutionary Navier–Stokes-like systems with pressure and shear-rate dependent viscosity. *Indiana Univ. Math. J.*, 56(1):51–85.

- Bulíček, M., Málek, J., and Rajagopal, K. R. (2009a). Analysis of the flows of incompressible fluids with pressure dependent viscosity fulfilling $\nu(p, \cdot) \rightarrow +\infty$ as $p \rightarrow +\infty$. *Czechoslovak Math. J.*, 59(2):503–528.
- Bulíček, M., Málek, J., and Rajagopal, K. R. (2009b). Mathematical analysis of unsteady flows of fluids with pressure, shear-rate and temperature dependent material moduli that slip at solid boundaries. *SIAM J. Math. Anal.*, 41(2):665–707.
- Carreau, P. J. (1968). PhD thesis, University of Wisconsin, Madison.
- Carreau, P. J. (1972). Rheological equations from molecular network theories. *T. Soc. Rheol.*, 16:99–127.
- Davies, T. A. (2004). UMFPACK version 4.3 user guide. Technical Report REP-2004-349, University of Florida, (<http://www.cise.ufl.edu/research/sparse/umfpack>).
- Doolittle, A. K. (1951). Studies in Newtonian flow 2. The dependence of the viscosity of liquids on free-space. *J. Appl. Phys.*, 22(12):1471–1475.
- Dowson, D. and Higginson, G. R. (1966). *Elastohydrodynamic Lubrication, The Fundamentals of Roller and Gear Lubrication*. Pergamon, Oxford.
- Duffing, G. (1924). Attempt at the friction of solid boundaries (in German). *Z. Angew. Math. Me.*, 4:296–314.
- Dymond, J. H. and Malhotra, R. (1988). The Tait equation—100 years on. *Int. J. Thermophys.*, 9(6):941–951.
- Feireisl, E. (2004). *Dynamics of viscous compressible fluids*, volume 26 of *Oxford Lecture Series in Mathematics and Its Applications*. Oxford Univ. Press.
- Feireisl, E. (2007). Mathematical theory of compressible, viscous, and heat conducting fluids. *Comput. Math. Appl.*, 53:461–490.
- Ferry, J. D. (1980). *Viscoelastic properties of polymers*. Wiley, New York, 3rd edition.
- Franta, M., Málek, J., and Rajagopal, K. R. (2005). On steady flows of fluids with pressure- and shear-dependent viscosities. *Proc. R. Soc. A*, 461(2055):651–670.
- Gazzola, F. (1997). A note on the evolution of Navier-Stokes equations with a pressure-dependent viscosity. *Z. Angew. Math. Phys.*, 48:760–773.
- Gazzola, F. and Secchi, P. (1998). Some results about stationary Navier-Stokes equations with a pressure-dependent viscosity. In Salvi, R., editor, *Navier-Stokes equations: theory and numerical methods (Varenna, 1997)*, volume 388 of *Pitman Res. Notes Math. Ser.*, pages 31–37. Longman, Harlow.
- Granick, S., Zhu, Y. X., and Lee, H. (2003). Slippery questions about complex fluids flowing past solids. *Nat. Mater.*, 2(4):221–227.
- Gresho, P. and Sani, R. (2000). *Incompressible flow and the finite element method.*, volume 2: Isothermal laminar flow. John Wiley & Sons Ltd.

- Gwynllwyw, D. R., Davies, A. R., and Phillips, T. N. (1996a). A moving spectral element approach to the dynamically loaded journal bearing problem. *J. Comput. Phys.*, 123(2):476–494.
- Gwynllwyw, D. R., Davies, A. R., and Phillips, T. N. (1996b). On the effects of a piezoviscous lubricant on the dynamics of a journal bearing. *Journal of Rheology*, 40(6):1239–1266.
- Gwynllwyw, D. R. and Phillips, T. N. (1996). Preconditioned iterative methods for unsteady non-Newtonian flow between eccentrically rotating cylinders. *SIAM J. Sci. Comput.*, 17(6):1369–1394.
- Gwynllwyw, D. R. and Phillips, T. N. (2005). Some issues regarding spectral element meshes for moving journal bearing systems. *Int. J. Numer. Meth. Fluids*, 48:423–454.
- Haslinger, J. and Stebel, J. (2011). Shape optimization for Navier–Stokes equations with algebraic turbulence model: Numerical analysis and computation. *Appl. Math. Comput.*, 63(2):277–308.
- Heywood, J. G., Rannacher, R., and Turek, S. (1996). Artificial boundaries and flux and pressure conditions for the incompressible Navier–Stokes equations. *Int. J. Numer. Meth. Fluids*, 22(5):325–352.
- Hirn, A., Lanzendörfer, M., and Stebel, J. (2010). Finite element approximations of flow of fluids with shear rate and pressure dependent viscosity. *IMA Journal of Numerical Analysis*, submitted for publication.
- Hron, J. (2001). *Fluid structure interaction with applications in biomechanics*. PhD thesis, Charles University, Prague, Faculty of Mathematics and Physics.
- Hron, J., Málek, J., Nečas, J., and Rajagopal, K. R. (2003). Numerical simulations and global existence of solutions of two-dimensional flows of fluids with pressure- and shear-dependent viscosities. *Math. Comput. Simulation*, 61(3-6):297–315. MODELLING 2001 (Pilsen).
- Hron, J., Málek, J., Průša, V., and Rajagopal, K. R. (2011). Further remarks on simple flows of fluids with pressure-dependent viscosities. *Nonlinear Anal. Real World Appl.*, 12(1):394–402.
- Hron, J., Málek, J., and Rajagopal, K. R. (2001). Simple flows of fluids with pressure-dependent viscosities. *Proc. R. Soc. Lond. Ser. A Math. Phys. Eng. Sci.*, 457(2011):1603–1622.
- Hutton, J. F., Jones, B., and Bates, T. W. (1983). Effects of isotropic pressure on the high temperature high shear viscosity of motor oils. *S. A. E.*, Paper No. 830030:1–11.
- Jones, I. P. (1973). Low Reynolds number flow past a porous spherical shell. *Proc. Camb. Philos. Soc.*, 73:231–238.
- Kamal, M. M. (1966). Separation in flow between eccentric rotating cylinders. *J. Basic Eng.—T ASME*, 88:717–724.
- Kelley, C. T. (2003). *Solving nonlinear equations with Newton’s method*. SIAM.
- Lanzendörfer, M. (2009). On steady inner flows of an incompressible fluid with the viscosity depending on the pressure and the shear rate. *Nonlinear Anal.—Real*, 10(4):1943–1954.

- Lanzendörfer, M. and Stebel, J. (2011a). On a mathematical model of journal bearing lubrication. *Math. Comput. Simulat.* In print.
- Lanzendörfer, M. and Stebel, J. (2011b). On pressure boundary conditions for steady flows of incompressible fluids with pressure and shear rate dependent viscosities. *Appl. Math.–Czech*, 56(3):265–285.
- Li, X. K., Davies, A. R., and Phillips, T. N. (2000a). A transient thermal analysis for dynamically loaded bearings. *Comput. Fluids*, 29(7):749–790.
- Li, X. K., Gwynllyw, D. R., Davies, A. R., and Phillips, T. N. (1999). Three-dimensional effects in dynamically loaded journal bearings. *Int. J. Numer. Meth. Fluids*, 29(3):311–341.
- Li, X. K., Gwynllyw, D. R., Davies, A. R., and Phillips, T. N. (2000b). On the influence of lubricant properties on the dynamics of two-dimensional journal bearings. *J. Non-Newtonian Fluid Mech.*, 93:29–59.
- Málek, J., Nečas, J., and Rajagopal, K. R. (2002). Global analysis of the flows of fluids with pressure-dependent viscosities. *Arch. Ration. Mech. Anal.*, 165(3):243–269.
- Málek, J., Nečas, J., Rokyta, M., and Růžička, M. (1996). *Weak and measure-valued solutions to evolutionary PDEs*. Chapman & Hall, London.
- Málek, J. and Rajagopal, K. R. (2006). *Handbook of Differential Equations: Evolutionary equations*, volume 2, chapter 5. Mathematical issues concerning the Navier–Stokes equations and some of its generalizations, pages 371–459. Elsevier/North-Holland, Amsterdam.
- Málek, J. and Rajagopal, K. R. (2007). *Handbook of Mathematical Fluid Dynamics*, volume 4, chapter 7. Mathematical properties of the solutions to the equations governing the flow of fluids with pressure and shear rate dependent viscosities, pages 407–444. Elsevier/North-Holland, Amsterdam.
- Málek, J. and Rajagopal, K. R. (2010). Compressible generalized Newtonian fluids. *Z. Angew. Math. Phys.*, 61:1097–1110.
- Murnaghan, F. D. (1944). The compressibility of media under extreme pressures. *Proc. Natl. Acad. Sci. U. S. A.*, 30(9):244–247.
- Neto, C., Evans, D. R., Bonaccorso, E., Butt, H. J., and Craig, V. S. J. (2005). Boundary slip in Newtonian liquids: a review of experimental studies. *Rep. Prog. Phys.*, 68(12):2859–2897.
- Nield, D. A. (2009). The Beavers–Joseph boundary condition and related matters: A historical and critical note. *Transp. Porous Med.*, 78(3):537–540.
- Novotný, A. and Straškraba, I. (2004). *Introduction to the Mathematical Theory of Compressible Flow*, volume 27 of *Oxford Lecture Series in Mathematics and its Applications*. Oxford Univ. Press, New York.
- Oseen, C. W. (1927). *Hydrodynamik*. Akademische Verlagsgesellschaft M.B.H., Leipzig.
- Rajagopal, K. R. (2006). On implicit constitutive theories for fluids. *J. Fluid Mech.*, 550:243–249.
- Rajagopal, K. R. and Szeri, A. Z. (2003). On an inconsistency in the derivation of the equations of elastohydrodynamic lubrication. *Proc. R. Soc. A*, 459(2039):2771–2786.

- Reissner, H. (1935). Planar and spatial currents of incompressible, inertia-free liquids between excentric, relative rotating cylinder layers (in German). *Z. Anal. Anwend.*, 15:81–87.
- Renardy, M. (1986). Some remarks on the Navier–Stokes equations with a pressure-dependent viscosity. *Comm. Part. Diff. Eq.*, 11:779–793.
- Repin, S. I. (2008). *A posteriori estimates for partial differential equations*, volume 4 of *Radon Series on Computational and Applied Mathematics*. Walter de Gruyter, New York.
- Reynolds, O. (1886). On the theory of lubrication and its application to Mr. Beauchamp Tower’s experiments, including an experimental determination of the viscosity of olive oil. *Phil. Trans. R. Soc. Lond.*, 177:157–234.
- Saffman, P. (1971). On the boundary condition at the surface of a porous medium. *Studies appl. Math.*, 50:93–101.
- Sani, R. L., Gresho, P. M., Lee, R. L., and Griffiths, D. F. (1981). The cause and cure of the spurious pressures generated by certain FEM solutions of the incompressible Navier–Stokes equations. *Int. J. Numer. Methods Fluids*, 1:17–43 (Part I), 171–204 (Part II).
- Szeri, A. Z. (1998). *Fluid Film Lubrication: Theory and Design*. Cambridge University Press.
- Yasuda, K. (1979). *Investigation of the analogies between viscometric and linear viscoelastic properties of polystyrene fluids*. PhD thesis, Massachusetts Institute of Technology, Cambridge.